AD-A063 922 ROCKWELL INTERNATIONAL THOUSAND OAKS CALIF SCIENCE --ETC F/G 11/6
ELECTROCHEMICAL STUDIES OF ATMOSPHERIC CORROSION.(U)
JAN 79 F B MANSFELD N00014-75-C-0788
UNCLASSIFIED SC5030-7FR NL

1 OF 2
AD A063822

LEVEL II

12

14 SC5030.7FR

COPY NO. 18

ELECTROCHEMICAL STUDIES OF ATMOSPHERIC CORROSION.

9 FINAL REPORT • 1 Apr 75-29 Dec 78,

Contract No. N00014-75-C-0788

For Period 04/01/75 through 12/29/78

15 N00014-75-C-0788

Submitted to:

Director, Metallurgy Programs
Material Sciences Division
Office of Naval Research
800 North Quincy Street
Arlington, Virginia 22217

12 141 p.

11 Jan 79

Prepared by:

10 Florian B. Mansfeld

"This research was sponsored by the Office of Naval Research under Contract No. N00014-75-C-0788."

Rockwell International
Science Center

JOB

389 949

20 01 20 175

Unclassified

SECURITY CLASSIFICATION OF THIS PAGE (When Data Entered)

REPORT DOCUMENTATION PAGE		READ INSTRUCTIONS BEFORE COMPLETING FORM
1. REPORT NUMBER	2. GOVT ACCESSION NO.	3. RECIPIENT'S CATALOG NUMBER
4. TITLE (and Subtitle) Electrochemical Studies of Atmospheric Corrosion		5. TYPE OF REPORT & PERIOD COVERED Final Report 6. PERFORMING ORG. REPORT NUMBER SC5030.7FR
7. AUTHOR(s) Florian Mansfeld		8. CONTRACT OR GRANT NUMBER(s) N00014-75-C-0788
9. PERFORMING ORGANIZATION NAME AND ADDRESS Rockwell International Science Center 1049 Camino Dos Rios Thousand Oaks, CA. 91360		10. PROGRAM ELEMENT, PROJECT, TASK AREA & WORK UNIT NUMBERS 471
11. CONTROLLING OFFICE NAME AND ADDRESS Office of Naval Research Material Sciences Div. 800 North Quincy St., Arlington, Virginia 22217		12. REPORT DATE January 1979 13. NUMBER OF PAGES 135 + 58
14. MONITORING AGENCY NAME & ADDRESS(if different from Controlling Office)		15. SECURITY CLASS. (of this report) Unclassified 15a. DECLASSIFICATION/DOWNGRADING SCHEDULE

16. DISTRIBUTION STATEMENT (of this Report)

Approved for Public Release; distribution unlimited

17. DISTRIBUTION STATEMENT (of the abstract entered in Block 20, if different from Report)

18. SUPPLEMENTARY NOTES

Final Report consists of two parts; Task 6 (Selected Bibliography of Atmospheric Corrosion) has been issued separately.

19. KEY WORDS (Continue on reverse side if necessary and identify by block number)

Atmospheric corrosion, time-of-wetness, corrosion rates, polarization resistance, thin layer electrolytes, pollutants, relative humidity, vapor phase inhibitors, surface analysis, corrosion product chemistry, steel, zinc, weight loss, electrochemical techniques

20. ABSTRACT (Continue on reverse side if necessary and identify by block number)

Electrochemical studies of atmospheric corrosion phenomena have been performed over a 42 months period. The kinetics of corrosion reactions occurring under thin electrolyte layers (100-1000 μm) have been studied for steel, zinc, Cu and Al by recording potentiodynamic polarization curves using a modified atmospheric corrosion monitor (ACM). Normal Tafel behavior was observed, the limiting current for oxygen reduction increased linearly with inverse film thickness. Similar experiments in which corrosion kinetics were determined

DD FORM 1 JAN 73 1473 EDITION OF 1 NOV 65 IS OBSOLETE

Unclassified

SECURITY CLASSIFICATION OF THIS PAGE (When Data Entered)

microns

20.

from polarization resistance measurements using the CORFIT computer program showed that with decreasing film thickness the corrosion reaction becomes charge transfer controlled. Laboratory and outdoor exposure tests have shown that corrosion rates increase drastically when the electrolyte layers become very thin during the drying out process at RH < 100%. This phenomenon has been studied in detail by evaluating the effects of corrosion product chemistry, RH and SO_2. For these studies a two-electrode ACM has been used to which a potential difference ΔE = 30 mV was applied, the polarity of which was reversed every 50 sec. The electrochemical results have been analyzed in terms of total electricity flow during the drying-out period. The inhibiting effects of $NaNO_2$ and dichan, a vapor phase inhibitor, have been evaluated also in this manner briefly with the result that inhibition is satisfactory in chloride but not in sulfate environments. This effect was confirmed in weight loss experiments under thin electrolyte layers, in which the electrolyte was allowed to dry out at relative humidities RH < 100%. These experiments showed that corrosion rates are much higher - at least for neutral environments - under thin layers than during immersion in bulk electrolytes. For steel an accelerating effect of additions of 1 ppm SO_2 to air was observed, while for zinc SO_2 had an inhibiting effect in acid chloride media reducing corrosion rates to those observed in acid or neutral sulfate media.

A comparison of corrosion rates obtained under identical conditions in weight loss and electrochemical experiments has been carried out for steel and zinc as a function of RH and electrolyte concentration. It has been determined that the electrochemical data underestimate corrosion rates most likely due to resistive effects and uncertainties in the conversion from polarization resistance to corrosion rate data. This problem makes the electrochemical technique a semi-quantitative tool in laboratory studies, which is, however, still very useful in indicating fast changes in corrosion behavior when one of the parameters which determine atmospheric corrosion kinetics is changed. Based on the comparison of weight loss and electrochemical data a "cell factor" can be determined which can be used to correct the electrochemical data obtained in outdoor exposure.

The ACMs have been used extensively to monitor atmospheric corrosion behavior in outdoor exposure. On the Science Center roof, ACM data, RH and temperature have been monitored simultaneously for almost three years. In St. Louis, Mo. where an exposure program was conducted for the EPA, ACMs were also exposed at up to four test sites. Time-of-wetness data have been determined for both locations, which show large fluctuations with the time of the year. For the Science Center roof, time-of-wetness corresponds closely to the time for which RH ≥80%. The corrosion current has also been determined as a function of RH for four months in 1978 by evaluating the statistical distribution of RH and log I_g as a function of time. A log log dependence of the corrosion current on RH seems to be indicated.

In the final phase of this project surface analyses have been carried out for 4130 steel and zinc which had been corroding under thin electrolyte layers. These scanning Auger microprobe (SAM) analyses have shown that sulfide inclusions in the steel act as nucleation sites for corrosion of the steel. When SO_2 was present in the air, sulfate was observed on the steel and zinc which acted as nucleation sites for corrosion in the case of steel. For zinc, nucleation sites were not observed in either case. The SAM data are especially valuable since they show the distribution of sulfur compounds over the surface

20. - continued

During the course of this program, the more important papers on basic aspects of atmospheric corrosion have been collected. A report has been prepared which lists these papers in a chronological sequence with the title, name of authors and abstract if provided by the authors. A total number of 171 papers has been listed.

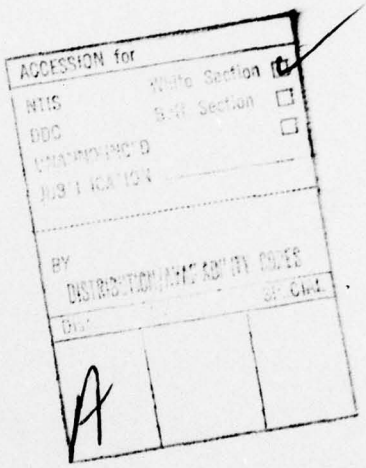

TABLE OF CONTENTS

ABSTRACT

Electrochemical studies of atmospheric corrosion phenomena have been performed over a 42 months period. The kinetics of corrosion reactions occurring under thin electrolyte layers (100-1000 μm) have been studied for steel, zinc, Cu and Al by recording potentiodynamic polarization curves using a modified atmospheric corrosion monitor (ACM). Normal Tafel behavior was observed, the limiting current for oxygen reduction increased linearly with inverse film thickness. Similar experiments in which corrosion kinetics were determined from polarization resistance measurements using the CORFIT computer program showed that with decreasing film thickness the corrosion reaction becomes charge transfer controlled. Laboratory and outdoor exposure tests have shown that corrosion rates increase drastically when the electrolyte layers become very thin during the drying out process at RH < 100%. This phenomenon has been studied in detail by evaluating the effects of corrosion product chemistry, RH and SO_2. For these studies a two-electrode ACM has been used to which a potential difference ΔE = 30 mV was applied, the polarity of which was reversed every 50 sec. The electrochemical results have been analyzed in terms of total electricity flow during the drying-out period. The inhibiting effects of $NaNO_2$ and dichan, a vapor phase inhibitor, have been evaluated also in this manner briefly with the result that inhibition is satisfactory in chloride but not in sulfate environments. This effect was confirmed in weight loss experiments under thin electrolyte layers, in which the electrolyte was allowed to dry out at relative humidities RH < 100%. These experiments showed that corrosion rates are much higher - at least for neutral environments - under thin layers than during immersion in bulk electrolytes. For steel an accelerating effect of additions of 1 ppm SO_2 to air was observed, while for zinc

SO_2 had an inhibiting effect in acid chloride media reducing corrosion rates to those observed in acid or neutral sulfate media.

A comparison of corrosion rates obtained under identical conditions in weight loss and electrochemical experiments has been carried out for steel and zinc as a function of RH and electrolyte concentration. It has been determined that the electrochemical data underestimate corrosion rates most likely due to resistive effects and uncertainties in the conversion from polarization resistance to corrosion rate data. This problem makes the electrochemical technique a semi-quantitative tool in laboratory studies, which is, however, still very useful in indicating fast changes in corrosion behavior when one of the parameters which determine atmospheric corrosion kinetics is changed. Based on the comparison of weight loss and electrochemical data a "cell factor" can be determined which can be used to correct the electrochemical data obtained in outdoor exposure.

The ACMs have been used extensively to monitor atmospheric corrosion behavior in outdoor exposure. On the Science Center roof, ACM data, RH and temperature have been monitored simultaneously for almost three years. In St. Louis, Mo., where an exposure program was conducted for the EPA, ACMs were also exposed at up to four test sites. Time-of-wetness data have been determined for both locations, which show large fluctuations with the time of the year. For the Science Center roof, time-of-wetness corresponds closely to the time for which RH$\geq$80%. The corrosion current has also been determined as a function of RH for four months in 1978 by evaluating the statistical distribution of RH and log I_g as a function of time. A log log dependence of the corrosion current on RH seems to be indicated.

In the final phase of this project surface analyses have been carried out for 4130 steel and zinc which had been corroding under thin electrolyte layers. These scanning Auger microprobe (SAM) analyses have shown that sulfide inclusions in the steel act as nucleation sites for corrosion of the steel. When SO_2 was present in the air, sulfate was observed on the steel and zinc which acted as nucleation sites for corrosion in the case of steel. For zinc, nucleation sites were not observed in either case. The SAM data are especially valuable since they show the distribution of sulfur compounds over the surface of the test samples after exposure to air + SO_2.

During the course of this program, the more important papers on basic aspects of atmospheric corrosion have been collected. A report has been prepared which lists these papers in a chronological sequence with the title, name of authors and abstract if provided by the authors. A total number of 171 papers has been listed.

I. INTRODUCTION

This report summarizes work performed over a 42 months period under contract with the Office of Naval Research in the area of atmospheric corrosion. Despite its great importance as a corrosion mechanism which can lead to catastrophic failure of airplanes, bridges, electronic equipment, etc. comparatively little basic research has been carried out which evaluates atmospheric corrosion phenomena. A large number of exposure tests over long time periods have been carried out, in the United States for example by various ASTM groups, and much work has been devoted to studies of organic coatings which are used to protect metals from atmospheric corrosion. Uhlig (1) has estimated that about $1.25 billion annually are spent on corrosion protection by paints and lacquers to which an average cost for labor of application equalling two or three times the cost of the paint has to be added. While field tests provide reliable information concerning the corrosion behavior of a given metal at a given test site, these tests have the disadvantage that they take a long time and are difficult to interpret in terms of the influence of the many atmospheric variables on the observed corrosion behavior.

It has been recognized for a long time that atmospheric corrosion is of electrochemical nature,and Rosenfeld (2), Evans (3), Barton (4) and Kaesche (5) among others have made attempts to describe the electrochemical reactions occurring under atmospheric corrosion conditions. The nature of the atmospheric corrosion process presents an experimental problem which makes such studies much more complicated than the normal electrochemical corrosion studies. The electrolyte layers encountered under atmospheric corrosion conditions are usually very thin and subject to changes when moisture condensates or evaporates.

The presence and chemical composition of corrosion products is likely to play an important role since they favor condensation at relative humidites (RH) less than 100%. Gaseous pollutants can also be of major importance although only SO_2 has been considered in most exposure studies as an accelerating factor. The characteristic feature of the atmospheric corrosion process is the discontinuous nature of corrosion which can only occur when electrolyte is present due to condensation from precipitation, dew, fog, etc. The total corrosion loss K can be expressed as:

$$K = \sum_{1}^{n} r_{1-n} \tau_{1-n}$$

where r is the average corrosion rate during the time-of-wetness τ. The task to be carried out in monitoring the kinetics of atmospheric corrosion and evaluating the effects of different constituents of the atmosphere on the corrosion behavior, is therefore, the continuous determination of r and τ. A large part of this project was devoted to this problem.

The success with electrochemical corrosion cells - the atmospheric corrosion monitor (ACM) (6) - in monitoring the time-of-wetness in outdoor exposure (7) led to the proposal to develop an electrochemical approach to basic studies of atmospheric corrosion phenomena.

The proposed program included an investigation of corrosion kinetics under thin electrolyte layers (Task 1) with the purpose of determining whether the relationships between potential and current which have been

developed for exposure to bulk solutions are valid under atmospheric corrosion conditions. It was necessary to develop a new experimental approach for this task in which atmospheric parameters such as RH, SO_2 level, etc. were also to be varied. In Task 2 these effects as well as the influence of electrolyte and corrosion product chemistry were to be studied. Task 3 proposed to carry out weight loss experiments in the laboratory under conditions which simulate atmospheric corrosion conditions. Electrochemical corrosion rate measurements were to be carried out under identical conditions and the results compared in order to determine whether the polarization resistance measurements can be used as a quantitative measure of corrosion rates in laboratory and outdoor exposure. An extension of the previous efforts on monitoring of atmospheric corrosion phenomena was proposed in Task 4 with the aim of improving the experimental technique and determining the relationship between RH, time-of-wetness and corrosion rates. Since corrosion products play an important role in condensation of electrolytes, time-of-wetness and carrosion rates, it was proposed to perform surface analyses of corrosion products formed on steel and zinc under conditions similar to those used in the weight loss experiments and to determine the location of initiation sites for corrosion as well as the distribution of compounds such as sulfur and chlorine (Task 5).

Since a large number of publications dealing with atmospheric corrosion phenomen was expected to be collected during the duration of the proposed research, it was suggested to issue as part of this final report a selected bibliography of atmospheric corrosion.

C. Experimental Results and Discussion

Description of Experimental Methods

Under this contract a number of electrochemical methods have been evaluated for use in studies of atmospheric corrosion phenomena in the laboratory and in outdoor exposure. The design of the atmospheric corrosion monitor (ACM) (Fig. 1) had been completed before this effort was started (6). Various modifications were then made in the fabrication of the ACM and in the design for two- and three-electrode systems. The basic principle of the ACM was first discussed by Tomashov (8), and Kucera and Mattson (9). A description of the ACMs built in this laboratory has been given earlier in two publications (6,10).

In most cases, ten plates (0.06 cm thick) each of Cu and steel or zinc are arranged in a holder in a way that adjacent dissimilar metals were separated by mylar spaces (0.006 cm thick) leading to a sequence: metal A - space - metal B - space - metal A (6). All plates of metal A are electrically connected as are all plates of metal B. The whole arrangement is cast in epoxy and then mechanically polished on one side to expose the cross-section of the plates. The total exposed geometric area of each type of metal was about 4.6 cm^2 (ten plates).

For the case of a diffusion controlled corrosion reaction which can be assumed to occur in neutral, aerated solutions, the galvanic current I_g flowing between the two groups of dissimilar metal plates represents the corrosion current I_{corr} (10):

$$I_g = I_{corr} \qquad (1)$$

The recording of the ACM signal represents, therefore, a continuous record of the instantaneous corrosion rate of the anode in the ACM (steel, zinc). For monitoring of atmospheric exposure data it would be desirable to obtain the total electricity flow by integration in addition to the time dependence of I_g. However, since no simple, inexpensive integration system with con-

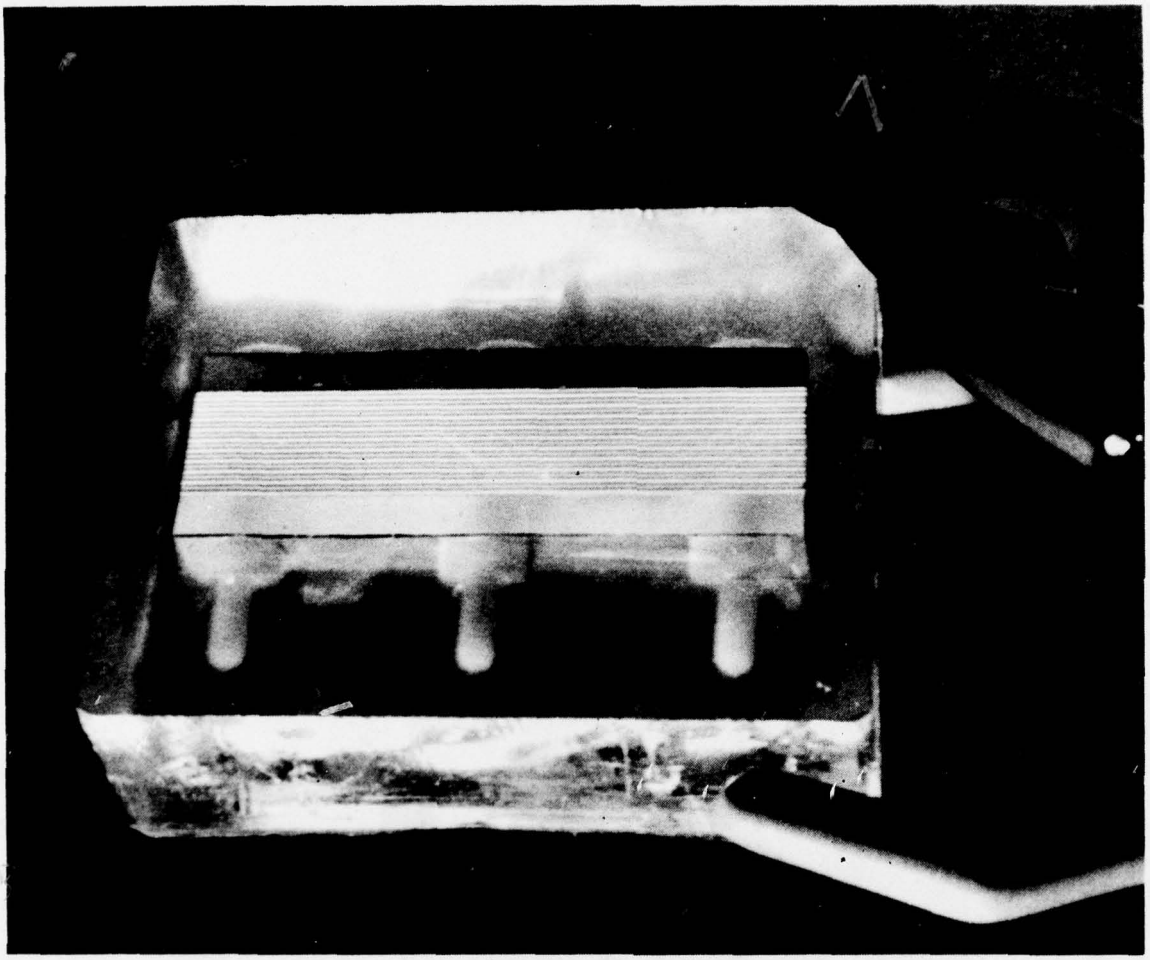

Fig. 1 Atmospheric corrosion monitor (ACM).

tinuous display was available, only I_g was recorded in outdoor exposure tests. Since I_g changes over many orders of magnitude between dry and wet conditions, the galvanic current as measured with a zero resistance ammeter (ZRA) was fed into a logarithmic converter, the output of which was recorded on a strip chart recorder.

For laboratory experiments, it was of interest to measure the corrosion rate of a metal under thin layers of electrolyte using the polarization resistance technique for two- and three-metal electrode systems (11). Only one type of metal was used in this arrangement, alternating plates serving as members of one of the electrodes. Usually a total of ten plates was used for both systems. For the two-metal electrode system, a potential pulse ΔE = 30 mV was applied using a potentiostat and a function generator. After 50 sec the polarity of ΔE was reversed in order to avoid constant polarization of one group of plates as anodes or cathodes. Using the polarization resistance principle the corrosion current I_{corr} can be calculated from the current I_{30} measured at ΔE = 30 mV according to:

$$I_{corr} = \frac{2B}{\Delta E} I_{30} = kI_{30} \qquad (2)$$

where B is a combination of Tafel slopes:

$$B = \frac{b_a b_c}{2.303(b_a+b_c)} \qquad (3)$$

For this type of measurement, the Tafel slopes are not measured in the same experiment. Assumptions have to be made, therefore, concerning the most likely values of the Tafel slopes. For diffusion controlled processes, $b_c \rightarrow \infty$ and

$$B = \frac{b_a}{2.303} \qquad (4)$$

Theoretical values of b_a range from about 30 mV to about 120 mV (11). For an exact determination of corrosion rates and evaluation of corrosion kinetics under changing atmospheric conditions, it is necessary to obtain the Tafel

slopes at the same time as the polarization resistance. This approach is made possible through use of the computer program CORFIT (12) by which potentiodynamic polarization curves (2mV/sec) obtained in a potential region of ±30 mV from the corrosion potential are analyzed. The polarization resistance R_p, the Tafel slopes b_a and b_c and the corrosion current I_{corr} are obtained simultaneously. The ACM was modified for this approach to contain four plates each serving as working and counter electrode and two plates as reference electrode. 4130 steel, Cu, zinc and Al 6061 were studied under the conditions described in Task 1.

For most experiments the ACMs were wet polished down to 600 SiC paper, rinsed with dist. H_2O and dried. The resistance between the different groups of plates was measured and the ACM was judged acceptable if 1 MΩ was exceeded. For most experiments the ACM was placed in a glass cell through which humid air or other gases such as argon or nitrogen are flowing at selected relative humidities (RH). The RH could be varied by mixing dry and wet air using precision flow meters. Additions of gaseous pollutants could be made in the same manner. For the studies reported here SO_2 was added at 0.1 and 1.0 ppm levels. The flow rate of the gas through the cell was 2ℓ/min. The gas mixing system was calibrated by measuring the RH in the test cell and the flow rate and SO_2 concentration at the exit side of the cell. Provisions were made for electrical connection of the ACM leads to the electronic equipment through the glass cell.

For typical experiments a thin layer of electrolyte was placed on a freshly polished ACM which had been positioned horizontally in the glass cell. The electrochemical measurement was carried out until the surface layer had dried out or until a certain test procedure had been carried out. For some cases rust powder was placed on ACM surfaces and the response variations of RH and/or SO_2 additions measured.

A description of certain details of the experimental techniques including a unique weight loss technique under thin electrolyte layers is given in the tasks in which they were applied.

Task 1. Kinetics of Corrosion Reactions Under Thin Electrolyte Films

While electrochemical corrosion studies are usually carried out in bulk solutions with small samples which have been carefully cleaned, it is characteristic for atmospheric corrosion that only small amounts of electrolyte are present and only at certain times and that the corrosion product chemistry plays a dominant role. In order to evaluate the kinetics of atmospheric corrosion, a different experimental approach has to be used, therefore, which takes into account the fact that corrosion takes place under thin electrolyte layers, the thickness of which can be time dependent, and that the metal surfaces to be studied are in most cases covered with corrosion products. In addition, the chemical composition of the atmosphere in contact with the electrolyte might change due to different levels of gaseous pollutants.

A first attempt has been made to develop an experimental approach for the study of atmospheric corrosion under carefully controlled conditions in the laboratory. A study of the literature (13) has shown that only very few thin layer studies which simulate atmospheric corrosion phenomenon have been published. Rosenfeld and his co-workers have been very active in this field and an account of this work is given in Rosenfeld's book. (2).

In the studies conducted during the first year of this contract it became evident that a number of experimental problems have to be solved before electrochemical studies of the kinetics of corrosion reactions can be carried out under thin layers of electrolytes (1000-100 μm). After evaluating the approach of Rosenfeld and co-workers (2), who used rather complicated arrangements of test, counter and reference electrodes, it was decided that a modified version of the ACM would be best suited for electrochemical corrosion studies under thin layers. The ten metal plates of an ACM were connected in a way that the inner two plates serve as reference electrode, the outer four plates

were used as counter electrode and the four plates between reference and counter electrode served as working electrode. The advantages of this very simple arrangement are that all three electrodes are located in the same plane, which avoids the problems often encountered in other attempts to study corrosion behavior under thin layers (14).

In the first series of experiments (15) layers of 0.1N NaCl or 0.1N Na_2SO_4 were deposited on steel, zinc, Cu and Al samples in thicknesses of 1000, 700, 400 and 100 μm exposed to laboratory air (RH = 30-50%). After a few minutes at the open circuit potential a potentiodynamic sweep (2mV/sec) was carried out either in the anodic or cathodic direction. From the anodic curve the anodic Tafel slope was determined and the corrosion current I_{corr} obtained by extrapolation to the corrosion potential. From the cathodic curve the limiting current I_L for oxygen reduction was determined. These data were compared with data for metals totally immersed in bulk electrolyte. Figure 2 shows the anodic curves, while Fig. 3 shows the cathodic curves obtained for 4130 steel. Tafel behavior is observed even at 100 μm film thickness, the anodic Tafel slope seems to decrease slightly with film thickness (Fig. 2). These findings are in contrast with those of Rosenfeld et al (2) who reported "anomalous anodic polarization curves". Their results were probably due to experimental problems related to the fast increase of the current with potential observed in Fig. 2. Also listed in Fig. 2 are the corrosion d.c. i_{corr}, which are higher in Na_2SO_4 than in NaCl except at 1000 μm. For comparison Fig. 4 shows the results obtained for iron in bulk electrolytes. As also observed for Cu, the rate of the anodic reaction is slower in NaCl than in Na_2SO_4.

The cathodic polarization curves in Fig. 3 show an increase of the limiting current I_L with decreasing film thickness. The limiting c.d. i_L

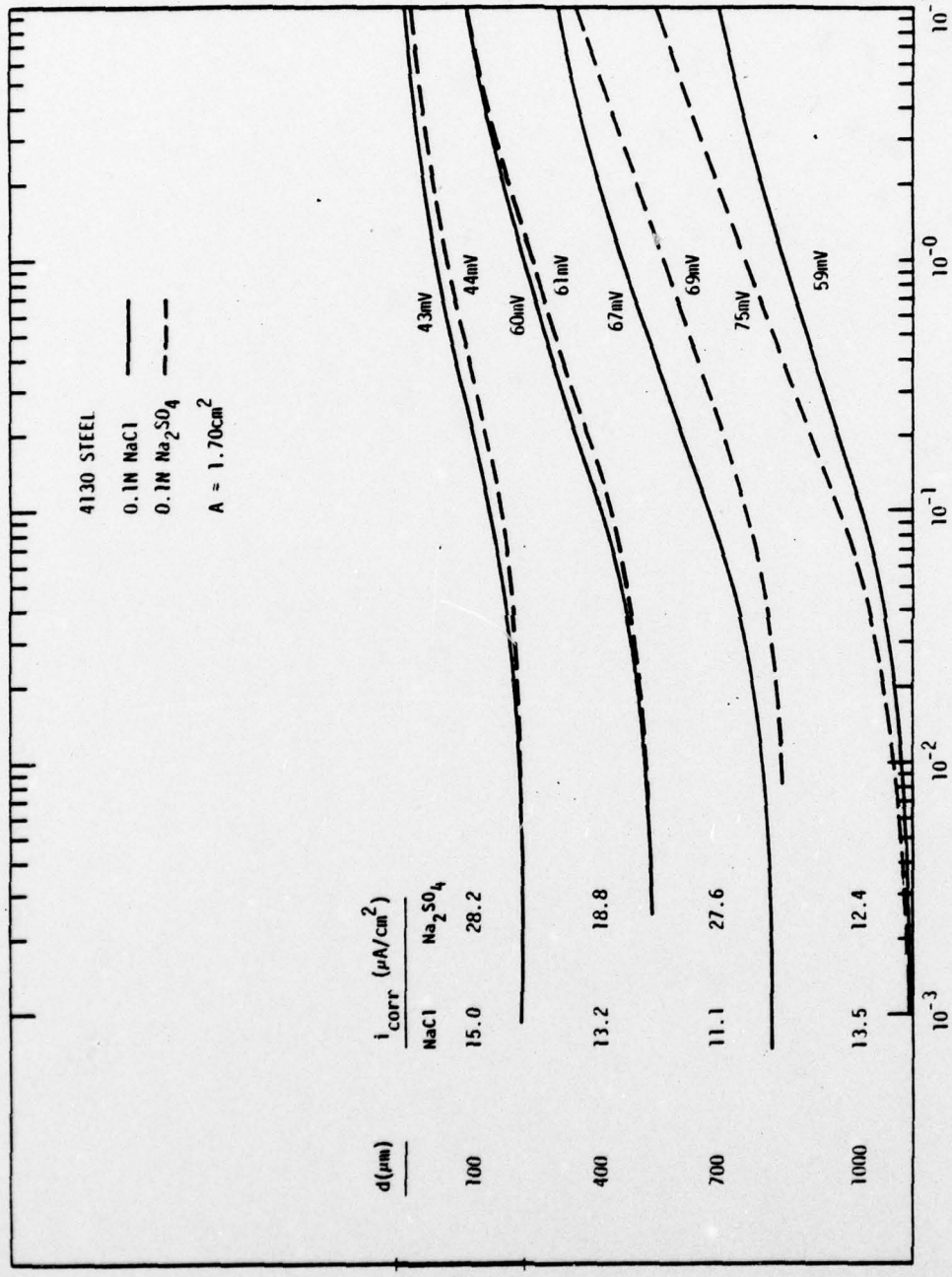

Fig. 2 Anodic potentiodynamic polarization curves for 4130 steel under thin layers of electrolyte.

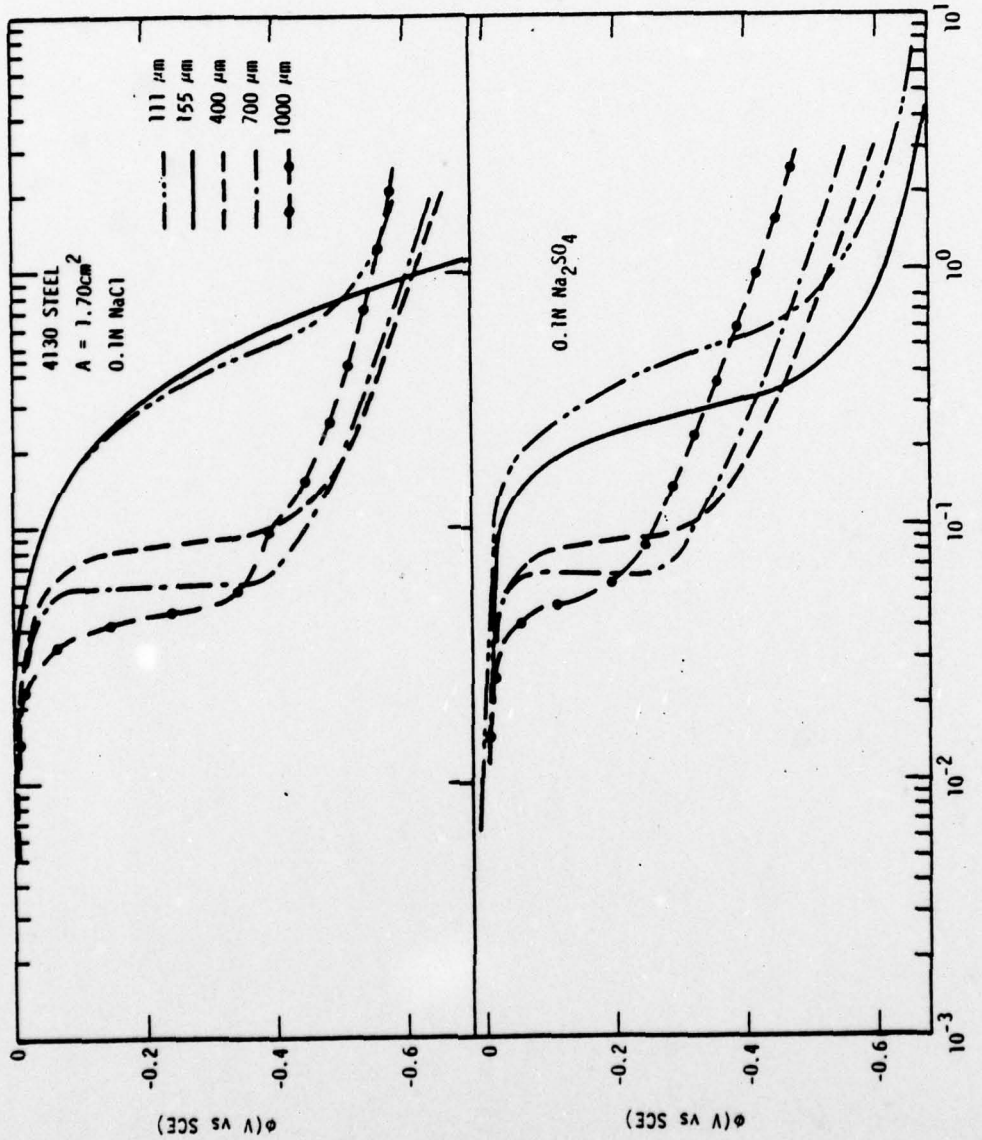

Fig. 3 Cathodic potentiodynamic polarization curves for 4130 steel under thin layers of electrolyte.

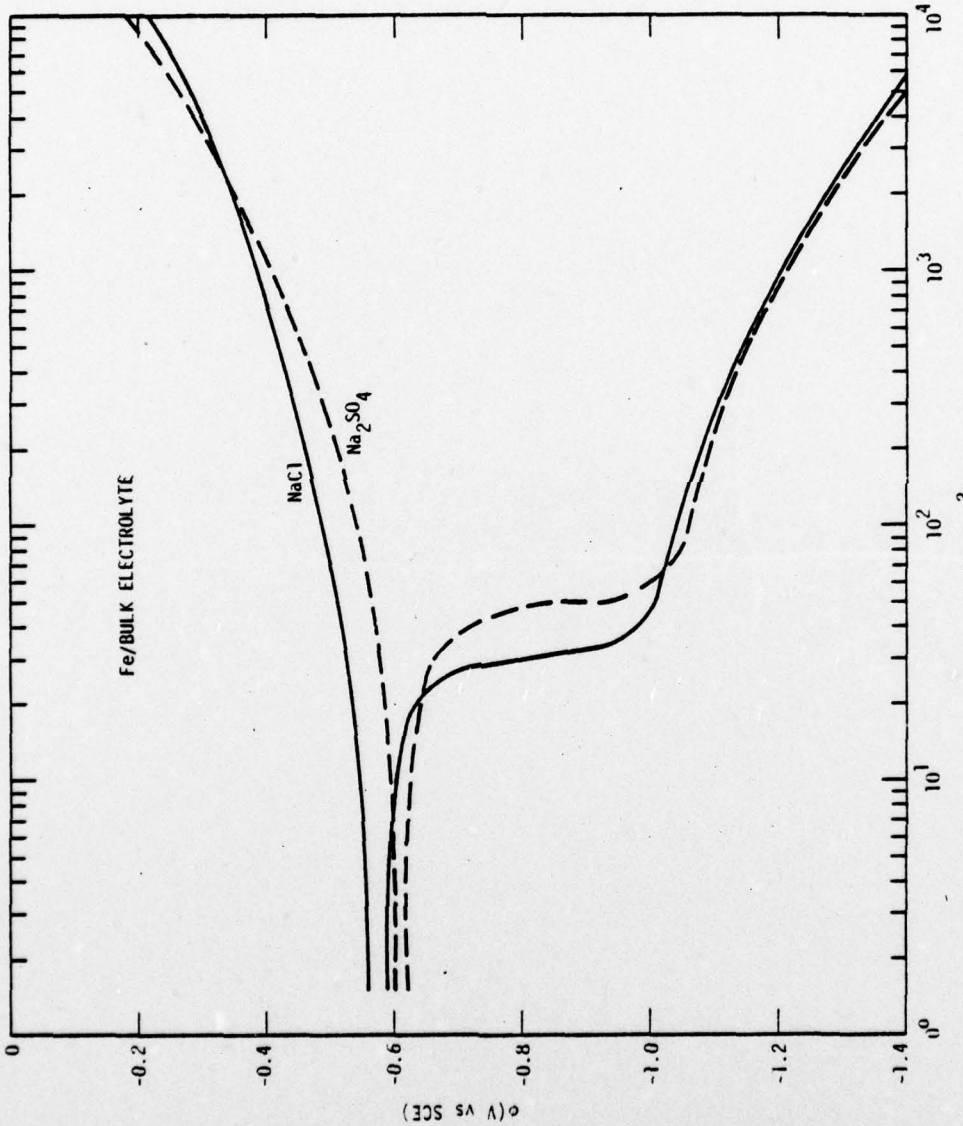

Fig. 4 Anodic and cathodic potentiodynamic polarization curves for iron in bulk electrolytes.

is inversely proportional to the thickness of the diffusion layer:

$$i_L = nFD \frac{C_o}{\delta} \qquad (5)$$

where n = 4, since four electrons are exchanged per molecule of oxygen. If one assumes $D = 1.9 \cdot 10^{-5}$ cm^2/sec for the diffusion coefficient of oxygen in 0.1N NaCl at room temperature and $C_o = 2.52 \times 10^{-7}$ mole/cm^3 for oxygen solubility, then one obtains (2):

$$i_L \delta = 1.91 \times 10^{-6} \text{ (A/cm)} \qquad (6)$$

In Fig. 5 the limiting c.d. i_L is plotted vs. the inverse film thickness d for Cu, 4130 steel and Al 6061 in 0.1N NaCl and 0.1N Na_2SO_4. Straight line relationships are observed with a slope which is close to the one calculated in Eq. 6 except for the Al 6061, for which a much lower slope is observed probably due to the presence of the oxide film. At lower thicknesses (d = 155 or 110 μm) deviations from the straight lines are observed in Fig. 5. It is likely that these very thin films evaporate when applied to the metal surface leading to an even thinner film at the time of the measurement. It will be also noticed that the shape of the cathodic polarization curves in Fig. 3 has changes for the lower d-values which makes determination of i_L more difficult. The results in Figs. 3 and 5indicate that for $d < 1000$ μm the diffusion layer thickness corresponds to the electrolyte thickness. With decreasing electrolyte layer thickness a pronounced increase of the rate of oxygen reduction occurs which can lead to similar increases of corrosion rates provided that the corrosion reaction remains diffusion controlled even at the lower d-values. The drying-out experiments discussed below have always shown a drastic increase of the galvanic current during the time period when the visible electrolyte layer disappeared, which corresponds to a thinning of the film.

Rockwell International
Science Center

SC5030.7FR

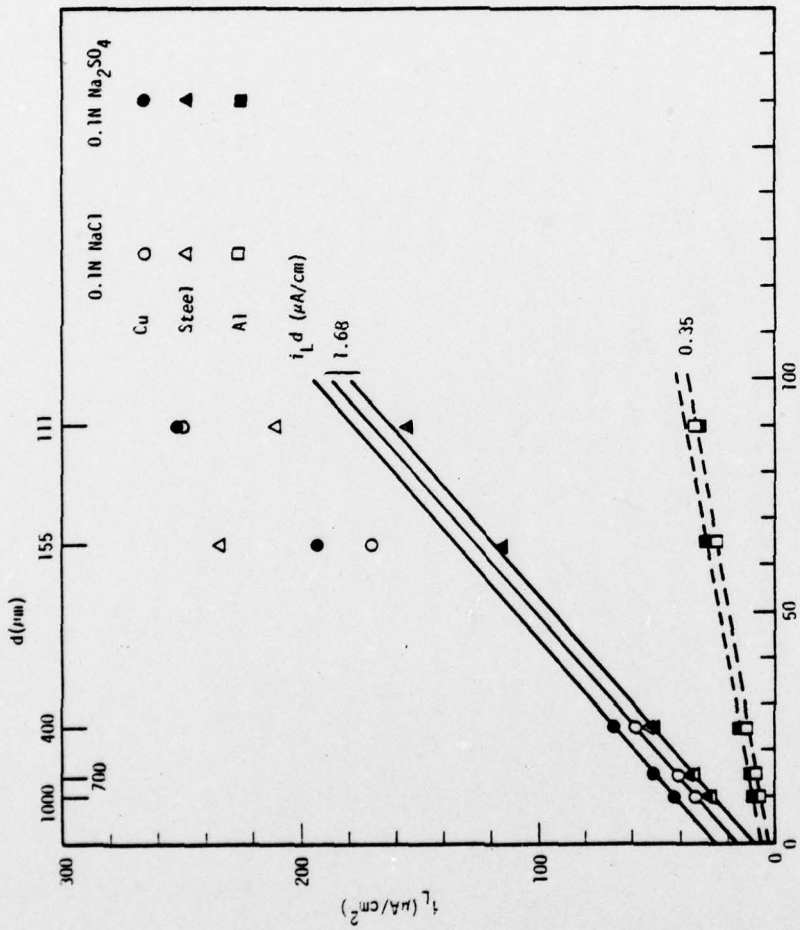

Fig. 5 Plot of limiting c.d. i_L for oxygen diffusion as a function of inverse electrolyte thickness d^{-1} for Cu, 4130 steel and Al 6061.

While the polarization curves for steel (Figs. 2-4), Cu, Al and Zn showed the general polarization behavior as a function of film thickness, it was also of interest to investigate the corrosion kinetics as a function of time simulating the drying-out process and also in the presence of pollutants such as SO_2. For these purposes, the recording of polarization curves such as shown in Figs. 2-4 is not suitable since the measuring process alters the nature of the test electrode surface and contaminates the electrolyte with corrosion products and reaction products from the counter electrode. The corrosion c.d. i_{corr} and the Tafel slopes b_a and b_c were, therefore, determined from polarization curves obtained within ± 30 mV from the corrosion potential Φ_{corr}, thereby avoiding excessive polarization. These curves were then analyzed with the computer program CORFIT (12). Figure 6 shows as an example the inverse polarization resistance R_p^{-1}, the corrosion current I_{corr}, the Tafel slopes and the constant B. Corrosion current and R_p are related by:

$$I_{corr} = \frac{b_a b_c}{2.3(b_a+b_c)} \cdot \frac{1}{R_p} = \frac{B}{R_p} \qquad (7)$$

The evaluation with the CORFIT program provides the error of each parameter which is also shown in Fig. 6. The electrode area was 1.70 cm^2. The results in Fig. 6 show that the cathodic Tafel slope b_c decrease significantly during the time of the experiment while the electrolyte, which is exposed to laboratory air, dries out. This finding indicates that the corrosion mechanism changes from diffusion control ($b_c \rightarrow \infty$) at the beginning of the experiment to charge transfer control (b_c = 40-120 mV) as the electrolyte layer becomes thinner. The anodic Tafel slope b_a, on the other hand, decreases only slightly during the time of the experiment. Similar results were observed in many

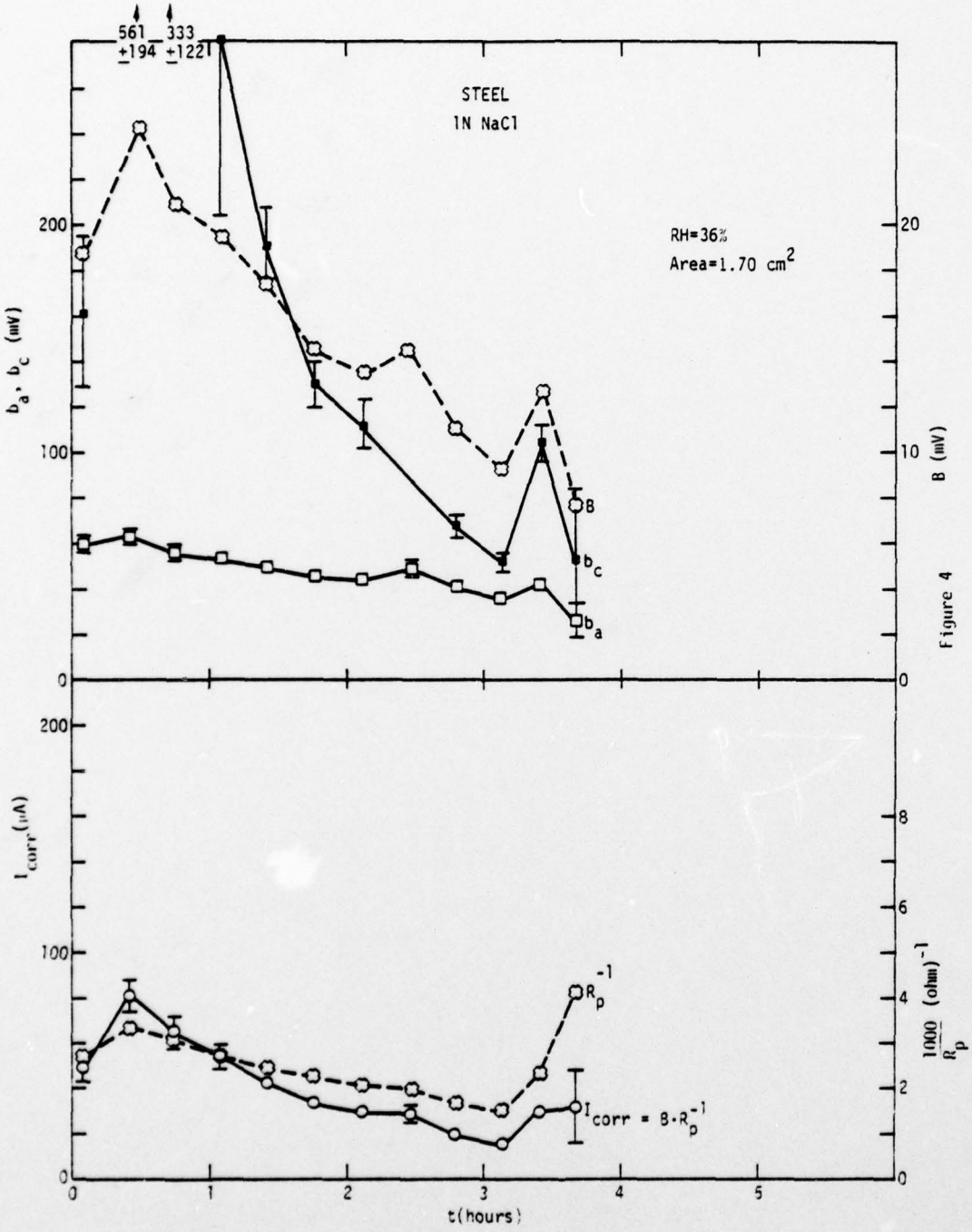

Figure 4

Fig. 6 Corrosion parameters of 4130 steel during drying-out of a 1N NaCl electrolyte layer (1100 μm).

experiments with steel in NaCl or Na_2SO_4. The corrosion current density decreased slightly during the experiment shown in Fig. 6 from about 50$\mu A/cm^2$ which is in the range of the values obtained by Tafel extrapolation (Fig. 2). The sharp increase of the limiting current observed during drying out in ACM experiments (see below) and indirectly in the results of Fig. 5 could not be followed entirely in these measurements because the potentiostat becomes unstable when the electrolyte layers become too thin.

A comparison of the corrosion c.d. obtained for 4130 steel from the polarization curves in Fig. 2 and from the experiment of Fig. 6 with the changes of the limiting c.d. i_L for oxygen diffusion and the changes of the cathodic Tafel slope b_c during thinning of the electrolyte suggests that while the electrolyte film becomes thinner the corrosion mechanism changes from diffusion control ($b_c \rightarrow \infty$, $i_{corr} = i_L$) to charge transfer control ($b_c \leq 120$ mV, $i_{corr} < i_L$). For this case the anodic and cathodic Tafel lines intersect at a current which is smaller than the limiting current. While the limiting c.d. i_L increase to 190-230 $\mu A/cm^2$ when a film thickness of 100 μm is reached, the corrosion c.d. i_{corr} observed are in general below 80 $\mu A/cm^2$ even at the time when the electrolyte film is evaporating.

Further studies involved the comparison of the galvanic current I_g measured with Cu/steel ACM and the corrosion current I_{corr} obtained with a three-electrode steel ACM. The theory of galvanic corrosion shows that for a diffusion controlled process the galvanic c.d. i_g equals the limiting c.d. for diffusion i_L, which in turn equals the corrosion c.d. i_{corr}:

$$i_g = i_L = i_{corr}. \qquad (8)$$

Experimental proof for Eq. 8 was provided in the experiment of Fig. 7, in which i_g as determined from a Cu/steel ACM and i_{corr} as determined from a steel ACM are compared. Both devices were covered with a layer of 0.1N NaCl

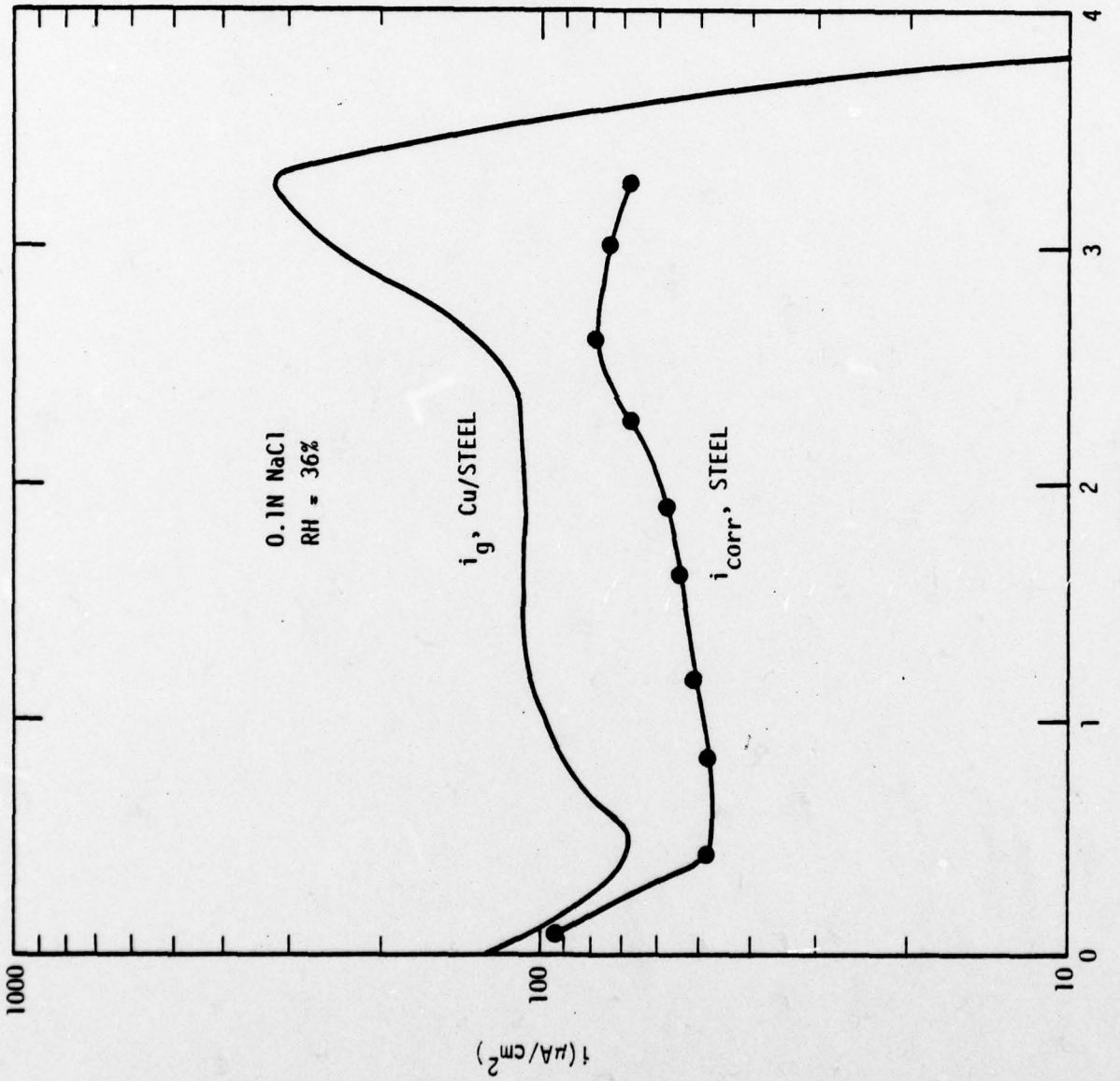

Fig. 7 Comparison of Cu/steel and all-steel ACM data under 0.1N NaCl at RH = 36%.

and exposed to laboratory air at RH = 36%. Fig. 7 shows similar behavior within a factor of two of the two measured quantities which confirms the assumption that measurements made with a Cu/steel ACM represent the corrosion rate of steel. Due to instabilities experienced with the potentiostatic three-electrode system the drying-out period could not be followed with the modified all-steel ACM.

The experiments conducted during the first and second year of this contract did not show any definite effects of SO_2 on corrosion of steel covered with thin layers of NaCl, Na_2SO_4 or with artificial rust which was clean or doped with chloride or sulfates (10). In order to investigate this phenomenon in more detail the corrosion kinetics of steel covered with 0.1N or 1.0N NaCl or Na_2SO_4 were studied as described above starting with an electrolyte thickness of about 1000 μm (15). In the presence of 1 ppm SO_2, which was added to humid air (RH = 38%) in the gas mixing system developed under this contract, the corrosion kinetics were very similar to those observed in the absence of SO_2 (Fig. 6). The cathodic Tafel slope b_c showed the same decrease with time while the electrolyte dried out; the corrosion c.d. was slightly higher in the presence of SO_2. The results for 0.1N NaCl and 0.1N Na_2SO_4 are summarized in Figs. 8a and b, which contain also data for bulk electrolytes free of SO_2. When the experimental polarization curves for bulk solutions through which SO_2 had been bubbled prior to the recording of the polarization curve were analyzed with the CORFIT - program, analytical solutions were obtained which included negative b_c-values. Since Tafel slopes are by definition positive one has to assume that the presence of SO_2 gas in the bulk electrolyte has altered the corrosion kinetics in a way that the simple exponential relationship between potential and current was no longer valid.

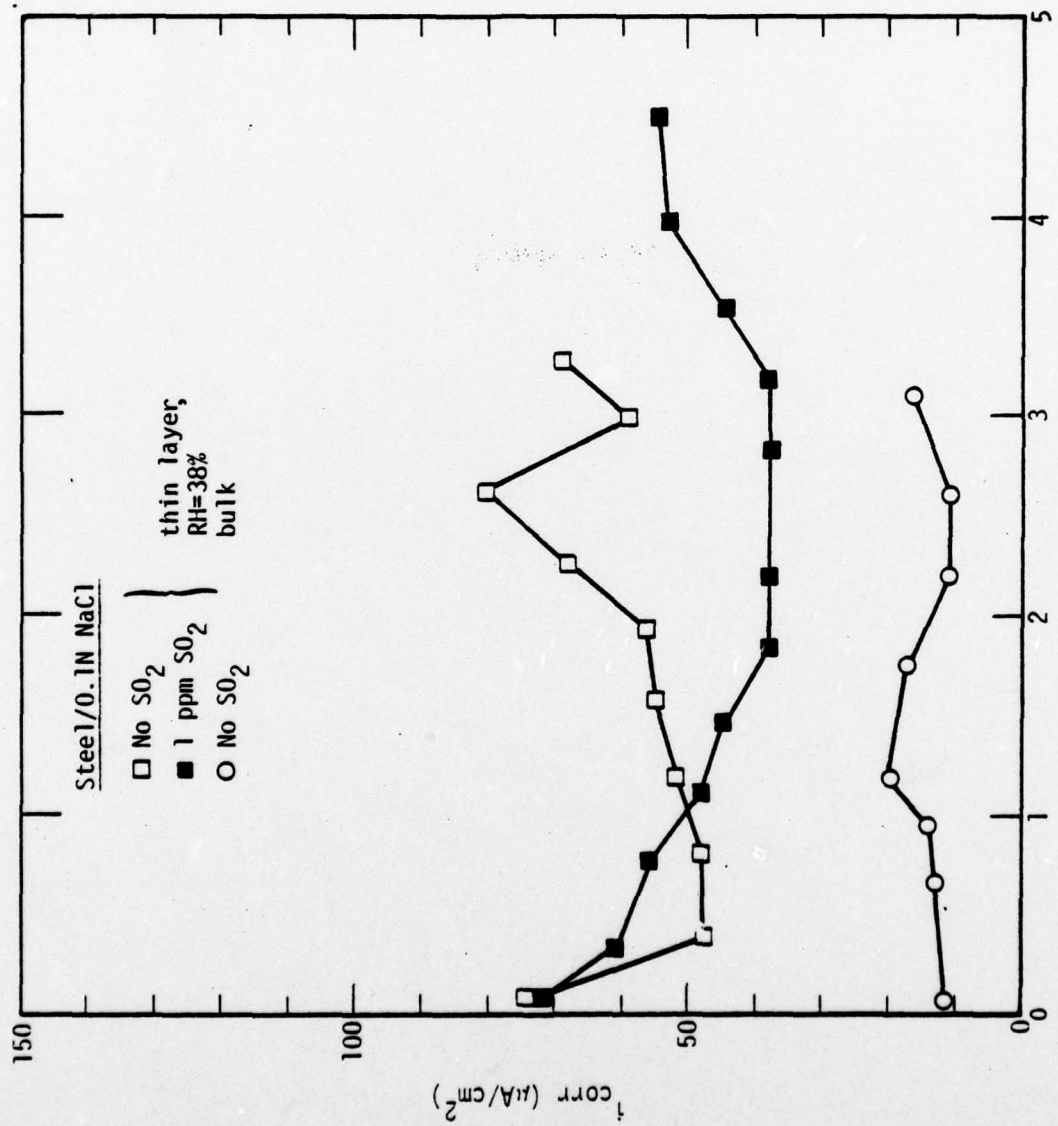

Fig. 8a Corrosion parameters of 4130 steel in thin layers and bulk electrolyte 0.1N NaCl (Fig. 8a) or 0.1N Na_2SO_4 (Fig. 8b) in the absence and presence of SO_2.

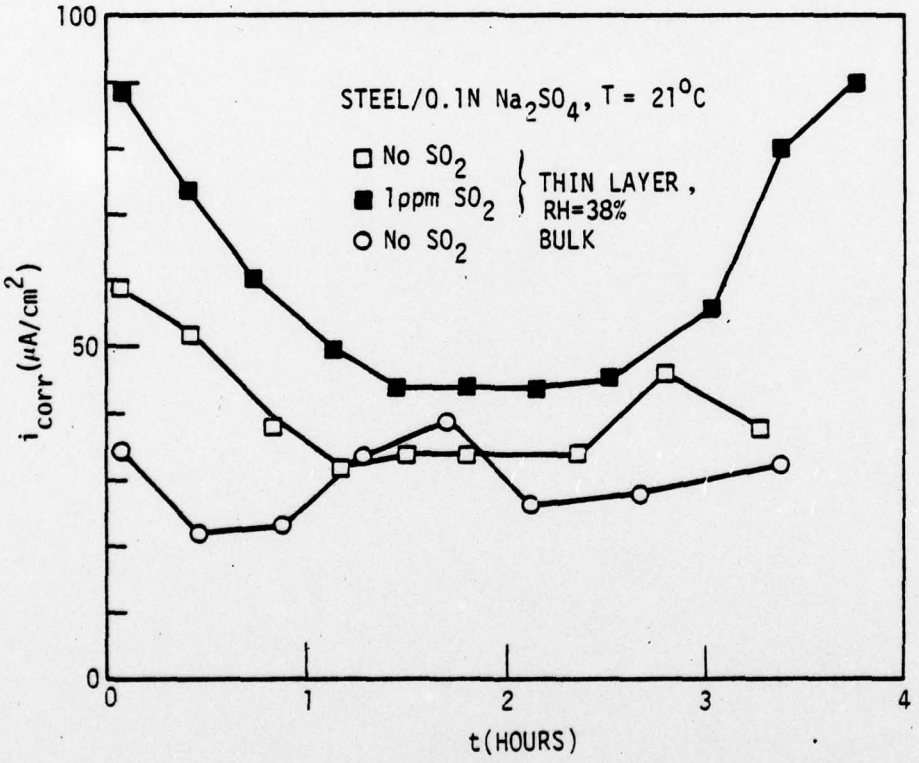

Fig. 8b Corrosion parameters of 4130 steel in thin layers and bulk electrolyte 0.1N NaCl (Fig. 8a) or 0.1N Na_2SO_4 (Fig. 8b) in the absence and presence of SO_2.

In 0.1N NaCl (Fig. 8a) the corrosion c.d. i_{corr} is higher in thin layer electrolytes than in the bulk and after about one hour, i_{corr} is lower in the presence of SO_2. On the other hand, in 0.1N Na_2SO_4 (Fig. 8b) i_{corr} is always higher in the presence of SO_2. The corrosion parameters (i_{corr}, b_a, b_c) for 4130 steel (thin layers) and iron (bulk) after 2 hours exposure are listed in Table I. Except for 0.1N NaCl the corrosion c.d. i_{corr} is always somewhat higher in the presence of SO_2. The anodic Tafel slope b_a seems to be lower in the presence of SO_2. The cathodic Tafel slope b_c has values in bulk electrolyte which are characteristic of diffusion control while in thin layers the b_c-values are found to decrease with time and assume values which are characteristic of charge transfer control as discussed above. The values of i_{corr} stay much lower ($i_{corr} < 60\ \mu A/cm^2$) than one would expect from the i_L-values of Fig. 5 for $d < 400\ \mu m$ which confirms that the corrosion reaction becomes charge transfer controlled as the electrolyte layer becomes thinner. The small immediate effect of SO_2 was surprising; however, weight loss measurements carried out under identical conditions (see below) confirmed that at low RH (fast drying out) the effect of SO_2 is very small.

Further experiments related to the corrosion kinetics of atmospheric corrosion followed the results of Zinevich et al (16) who have studied the kinetics of corrosion on iron and zinc in moist environments using thin metal films on glass substrates. The corrosion rate was calculated from the changes of the electrical resistance of the current carrying layer, the potential was measured by pressing the bridge for the $Cu/CuSO_4$ reference electrode tightly against the metal surface. The authors concluded that passivation phenomena occur in a moist atmosphere and that the protective properties of the passivating layers are determined by the RH and the concentration of activators such as SO_2 and chlorides in the environment. In order to study the reactions occurring under the conditions used throughout

TABLE I. CORROSION PARAMETERS IN THIN LAYERS (4130 STEEL) AND BULK ELECTROLYTE (IRON) AFTER 2 HOURS

	$i_{corr}(\mu A/cm^2)$	b_a(mV)	b_c(mV)
0.1N NaCl	59	80	158
0.1N NaCl + 1 ppm SO_2	38	36	246
0.1N NaCl (Bulk)	14	80	885
1N NaCl	18	44	117
1N NaCl + 1 ppm SO_2	37	33	63
1N NaCl (Bulk)	25	81	340
0.1N Na_2SO_4	34	55	190
0.1N Na_2SO_4 + 1 ppm SO_2	44	34	240
0.1N Na_2SO_4 (Bulk)	30	74	571
1N Na_2SO_4	15	42	84
1N Na_2SO_4 + 1 ppm SO_2	25	65	104
1N Na_2SO_4 (Bulk)	10	46	445

this project, potential and pH measurements were carried out using microelectrodes (Microelectrodes, Inc.) positioned on the surfaces of one-metal or galvanic ACMs. The galvanic current I_g or the current I_{-30} measured when a potential difference $\Delta E = \pm 30mV$ was applied between metal plates arranged in an ACM as a two-electrode system (for a detailed description see Task 2) were recorded continuously as were pH and potential E. The results are shown in Fig. 9 for steel and Fig.10 for zinc. The current-time curves under thin layers of 0.01N NaCl (Figs. 9a and 10a) and 0.01N Na_2SO_4 (Figs. 9b and 10b) are characterized by a maximum which occurs shortly before the surface dries out at RH = 49 ± 1% (laboratory air). For steel and Cu/steel the potential becomes more negative while corrosion proceeds, with lower values in Na_2SO_4. For the steel ACM the corrosion potential E_{corr} becomes more positive when the current maximum occurs while for Cu/steel the galvanic potential E_g levels off. For the four experiments in Fig. 9 the pH decreased slowly from initial values around 7.5 to final values around 5. When the surface dried out as evidenced by a drop to very low currents, potential and pH measurement became very difficult for the experiments in Fig. 9. The potential became much more positive, while the pH dropped to lower values. Integration of the current-time traces resulted in the charge data shown in Fig. 9, which will be discussed in more detail in Task 2.

For zinc maxima for the current (I_g, I_{-30}) and minimum for the potential (E_g, E_{corr}) are also observed (Figs 10a and b). When the surface has dried out, the potential seems to shift drastically in the positive direction accompanied by a drop of the pH except for Cu/Zn in 0.01N Na_2SO_4 (Fig. 10b) where the pH seems to increase. However, due to the uncertainties of potential and pH measurements at the time when the surface is just drying out, the sharp changes indicated at the end of the runs in Figs. 9 and 10 might not reflect real effects.

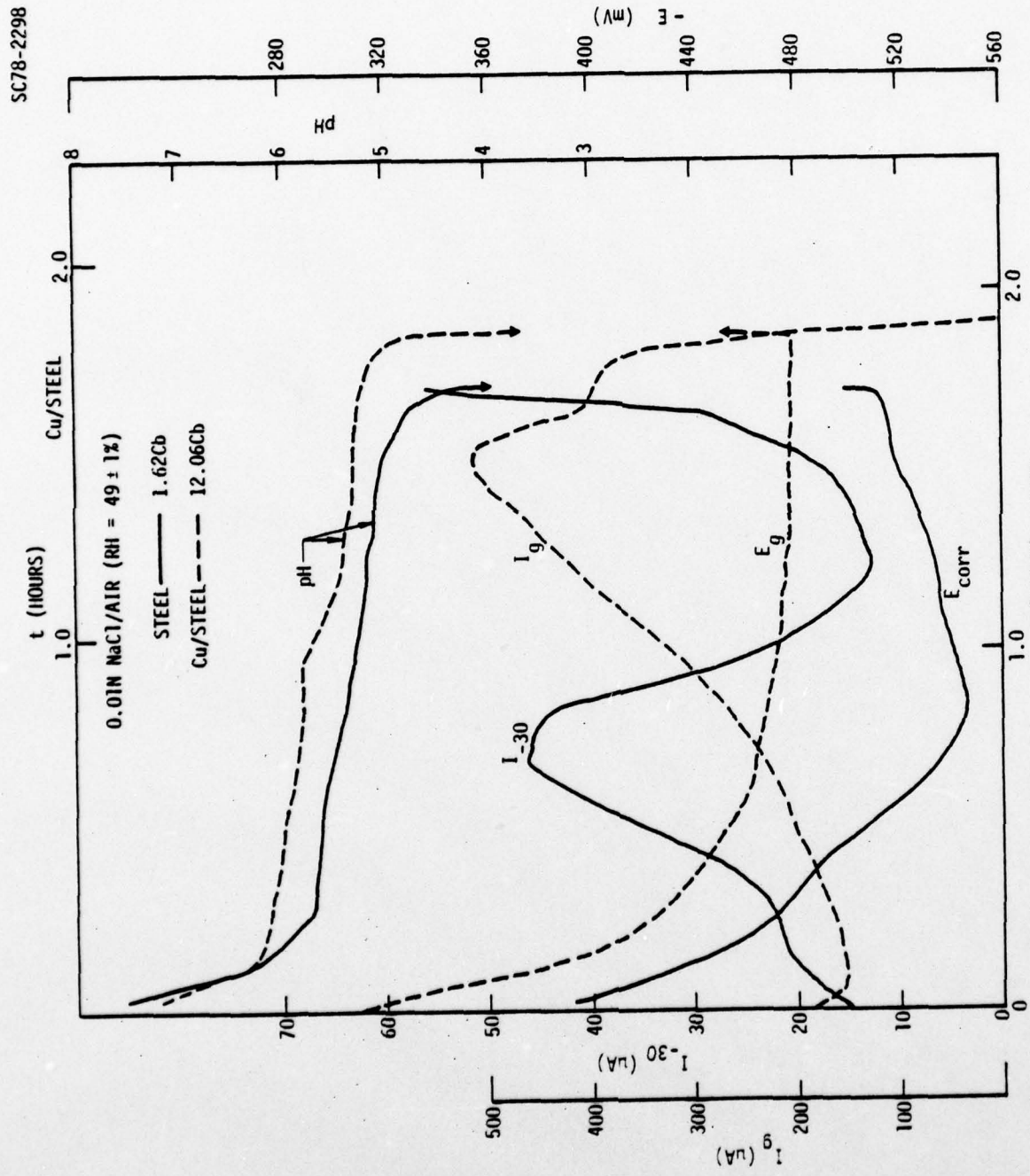

Fig. 9a Time dependence of potential, current and pH for steel (E_{corr}, I_{-30}) and Cu/steel (E_g, I_g) ACMs drying out in air at RH = 49±1% under a 0.5 mm layer of 0.01 NaCl (Fig. 9a) and 0.01N Na_2SO_4 (Fig. 9b).

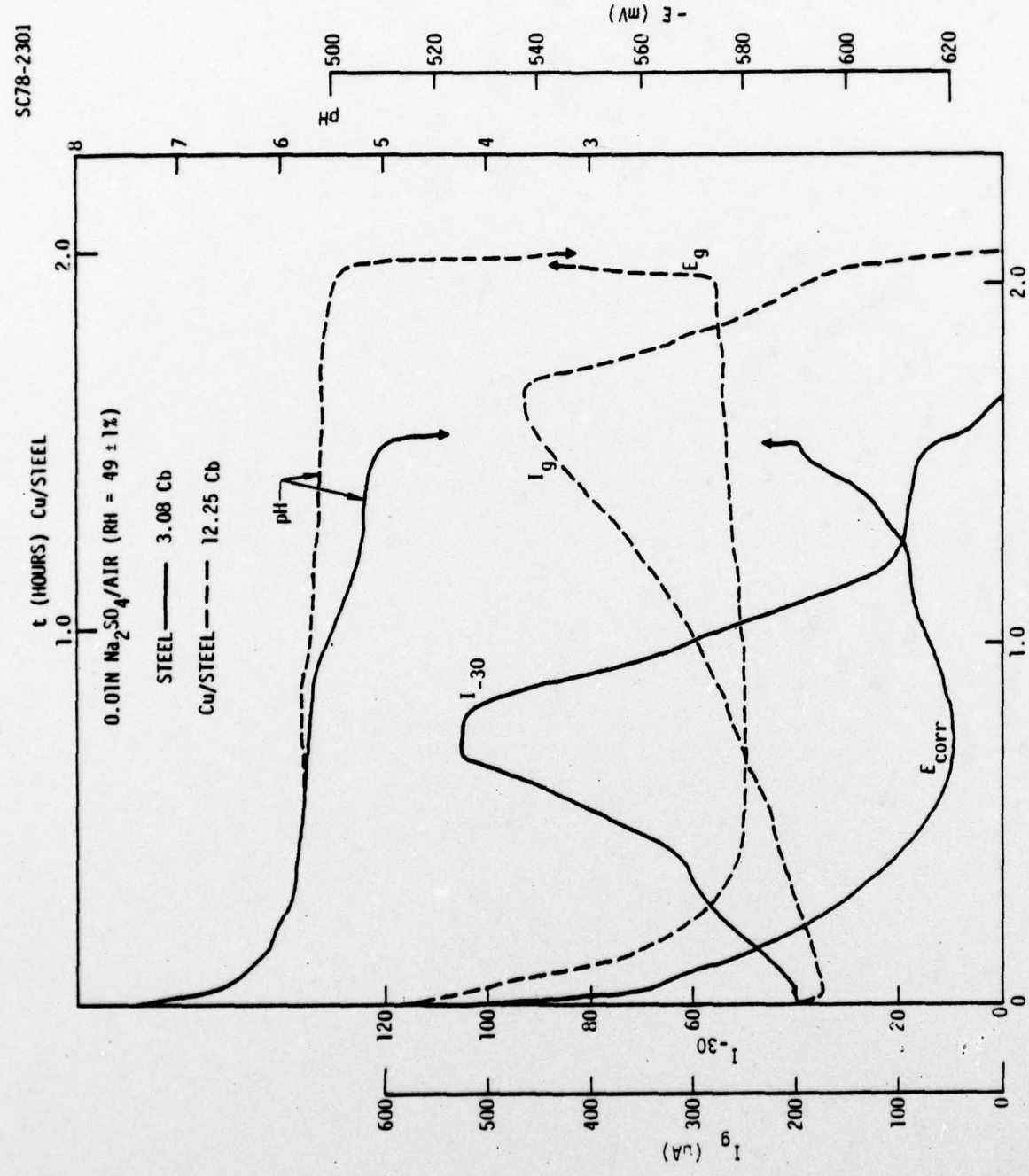

Fig. 9b Time dependence of potential, current and pH for steel (E_{corr}, I_{-30}) and Cu/steel (E_g, I_g) ACMs drying out in air at RH = 49±1% under a 0.5 mm layer of 0.01 NaCl (Fig. 9a) and 0.01N Na_2SO_4 (Fig. 9b).

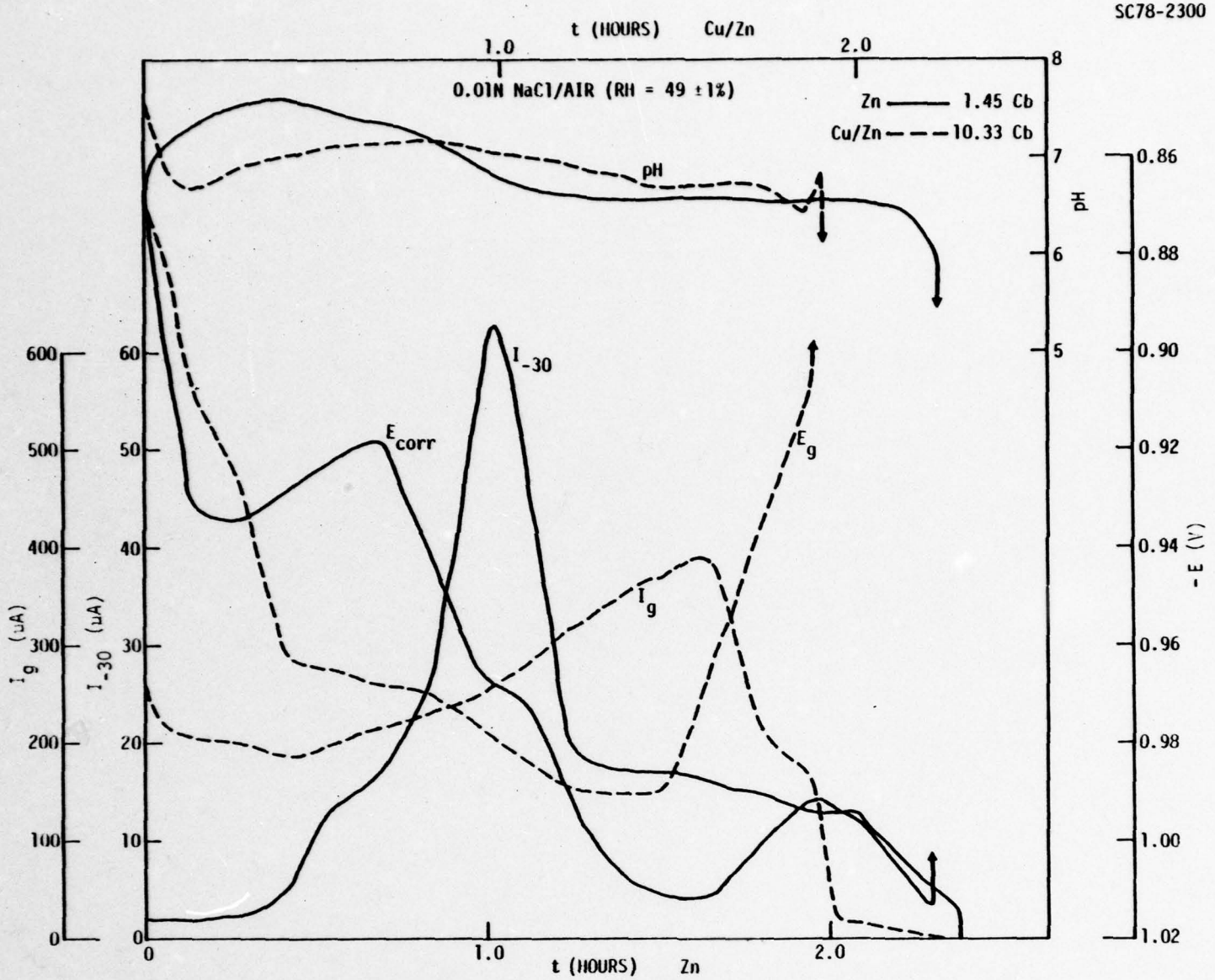

Fig.10a Time dependence of potential, current and pH for zinc (E_{corr}, I_{-30}) and Cu/Zn (E_g, I_g) ACMs drying out in air at RH = 49±1% under a 0.5 mm layer of 0.01N NaCl (Fig. 10a) and 0.01N Na_2SO_4 (Fig. 10b).

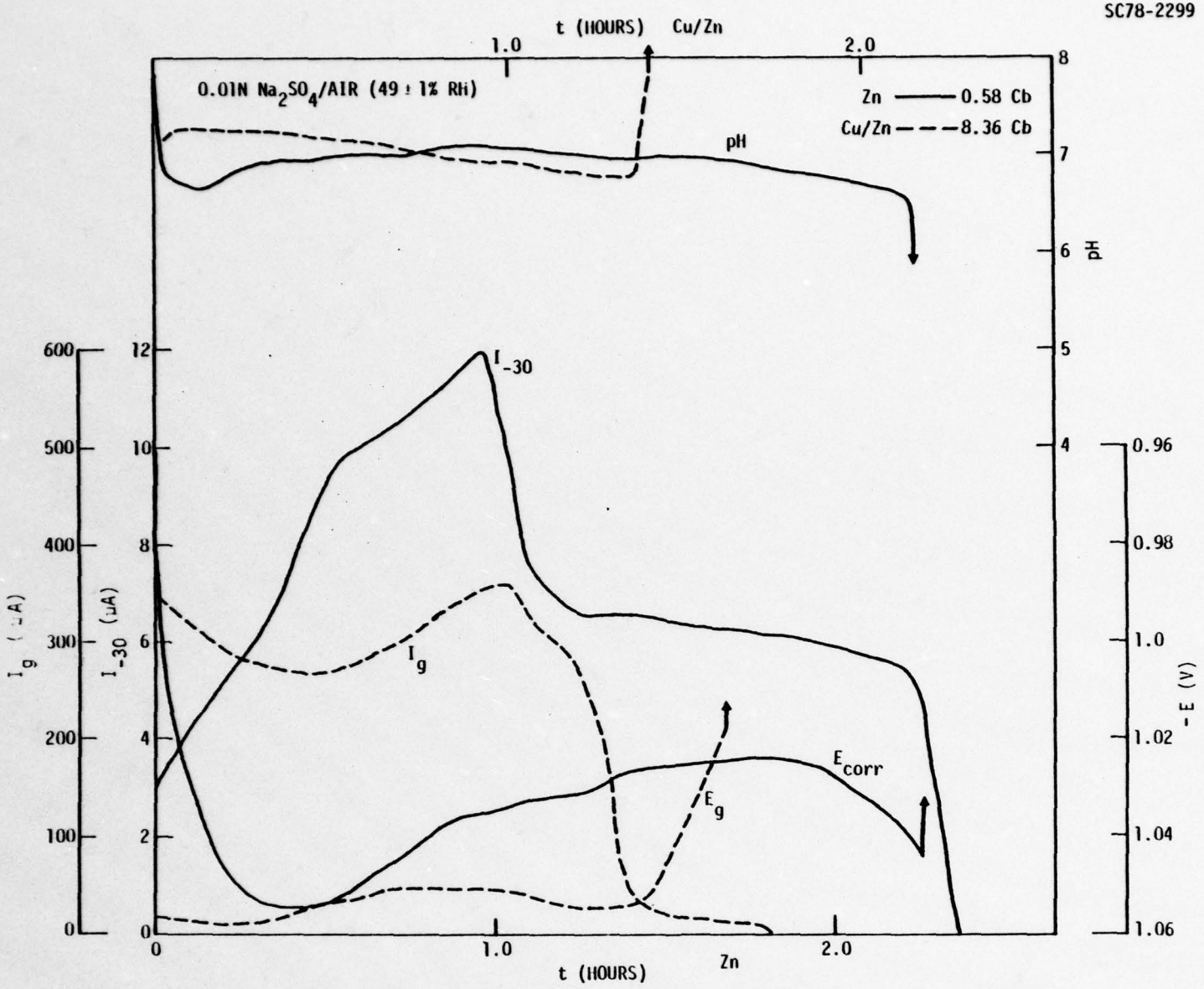

Fig.10b Time dependence of potential, current and pH for zinc (E_{corr}, I_{-30}) and Cu/Zn (E_g, I_g) ACMs drying out in air at RH = 49±1% under a 0.5 mm layer of 0.01N NaCl (Fig. 10a) and 0.01N Na_2SO_4 (Fig. 10b).

The results of these types of kinetic studies have not given indications of passivation to occur in the time for which electrolyte was present and corrosion occurred. Measurements of surface pH showed a slight decrease of pH to about 5 for steel and Cu/steel and about 6.5 for zinc and Cu/Zn. The possibility that passivation occurs towards the end of the corrosion process when the electrolyte layer disappears cannot be excluded based on the potential measurements. Further studies in the presence of SO_2 would be interesting with regards to the resulting potential and pH effects. In order to compare the present results more closely with those obtained by Zinevich et al (16) measurements should also be carried out between RH = 75 and 100%. The Russian authors used this range and distinguished between unactivated surfaces (pure adsorbed moisture films) and surfaces activated with chloride ions. Passivation occurred in all cases, although to different extents.

Task 2. The Effects of Electrolyte and Corrosion Product Composition, Pollutants and Relative Humidity

In this taks, which was active throughout the entire program period, various environmental effects were evaluated in the laboratory under conditions which were designed to simulate atmospheric corrosion phenomena. Initially the dependence of the "critical relative humidity" RH_{crit} on the chemical composition of corrosion product layers was evaluated and correlations between corrosion rates and RH determined as a function of rust composition. The effects of surface electrolyte composition, RH and presence of SO_2 were studied next for Cu, steel, zinc and Al 6061 using polarization resistance measurements. The effects of $NaNO_2$ and dichan, a compound proposed as vapor phase inhibitor, were studied in the same manner.

a. The Effect of Corrosion Product Chemistry on Atmospheric Corrosion Rates

A number of authors have presented results which suggest that atmospheric corrosion rates depend on the chemical composition of the corrosion product (17,18). Weight loss measurements have been used exclusively. In order to understand better the effects of corrosion product chemistry on RH_{crit} and atmospheric corrosion rates, a number of experiments with Cu/Zn, and Cu/steel ACMs have been performed as a function of humidity (10). Rust was produced in the laboratory (19), which was then doped with various impurities for a total of 2.5 w/o. This rust mixture was placed on a freshly polished ACM which was exposed in a glass cell through which air at different RH with and without SO_2 (0.1 - 1.0 ppm) was flowing at a rate of 2 ℓ/min. In one set of experiments the ACM was first exposed to RH = 38% for 2h, the RH was then

raised to a higher level for 2h and again returned to RH = 38%. Figure 11 shows the response for clean rust (Fig.11a) and rust doped with NaCl (Fig.11b).

The response to a change in RH is almost immediately, which demonstrates the sensitivity of ACMs to changes in atmospheric conditions. Different time dependence at constant RH is observed for clean rust and rust doped with NaCl: for clean rust I_g reaches a maximum after 30 min. and then decays, while for rust doped with NaCl I_g increases continuously except for RH = 51%. At the highest RH-value the current is more than 100 times higher in the doped rust than in the clean rust, which shows again the tremendous effect of pollutants on atmospheric corrosion behavior observed earlier.

The I_g values recorded after 2 hours at a given RH have been plotted in Fig. 12 for clean and doped rust in air and in air + 1 ppm SO_2. A linear relationship is observed in all cases which can be described as:

$$\log I_g = a + b \cdot RH, \tag{9}$$

where the slope b depends on the rust composition and probably also on the gaseous environment. If the constant a is chosen to represent $\log I_g$ at the critical humidity RH_{crit}

$$a = \log I_g^{crit}, \tag{10}$$

Eq. 9 can be rewritten as:

$$\log I_g = a + b\left(\frac{RH-RH_{crit}}{100}\right). \tag{11}$$

Eq. 11 can be transformed into Eq. 12:

$$\log I_g = \log I_g^{crit} + b'\left(\frac{RH-RH_{crit}}{100-RH_{crit}}\right) \tag{12}$$

where b' represents the normalized I_g-value at RH = 100%:

$$b' = \left(\log \frac{I_g}{I_g^{crit}}\right)_{RH = 100\%} \tag{13}$$

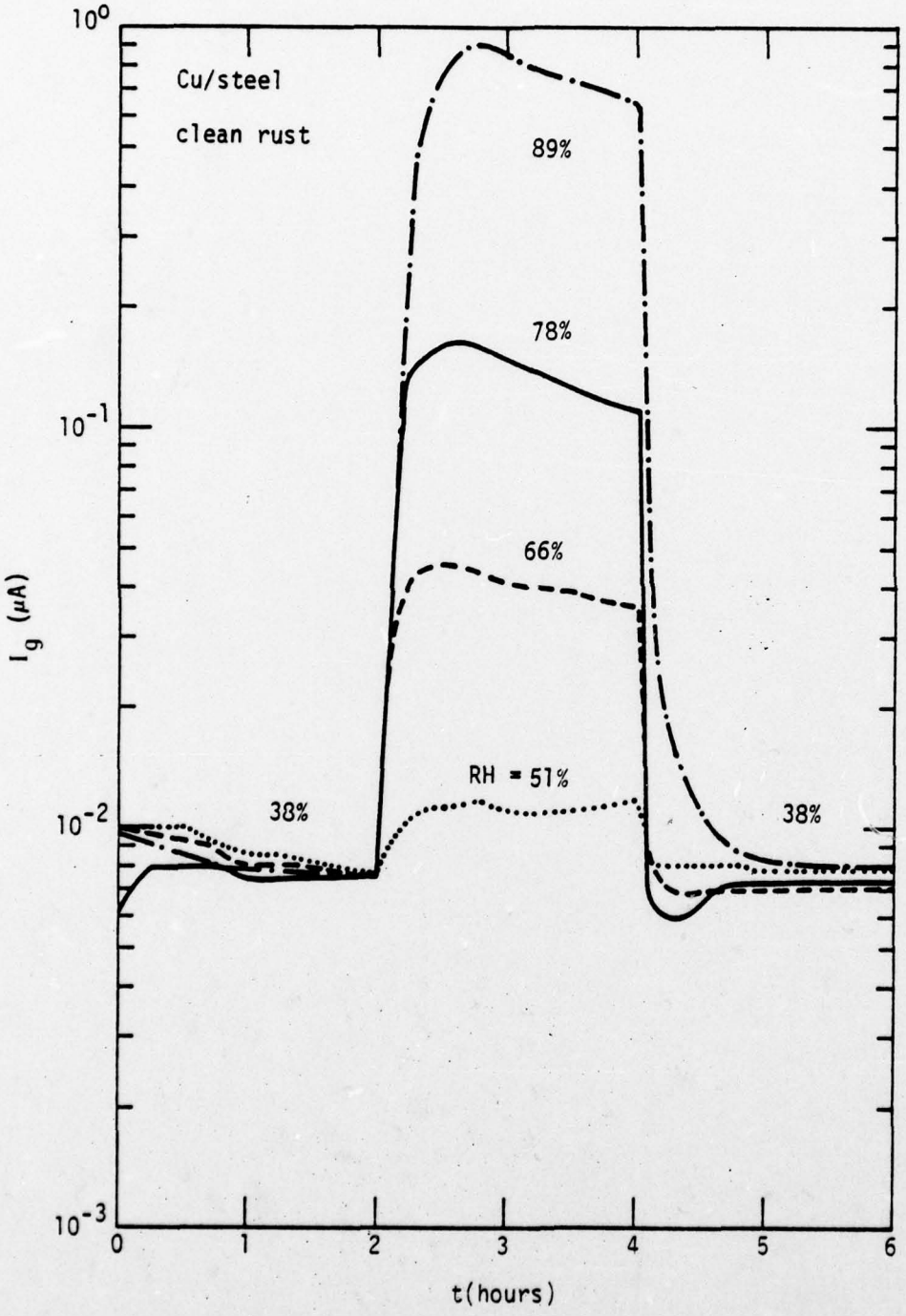

Fig. 11a Time dependence of galvanic current for Cu/steel ACM covered with clean rust (Fig.11a) and not doped with 2.5 w/a NaCl (Fig.11b) at different RH.

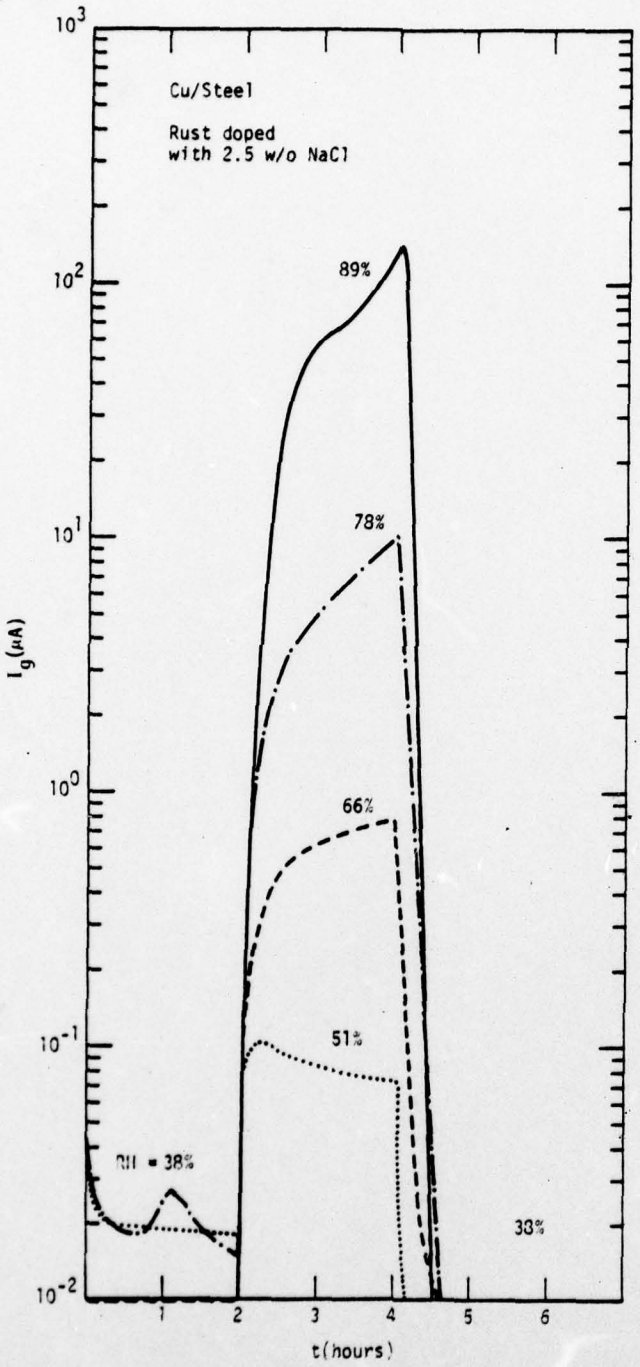

Fig. 11b Time dependence of galvanic current for Cu/steel ACM covered with clean rust (Fig.11a) and not doped with 2.5 w/a NaCl (Fig.11b) at different RH.

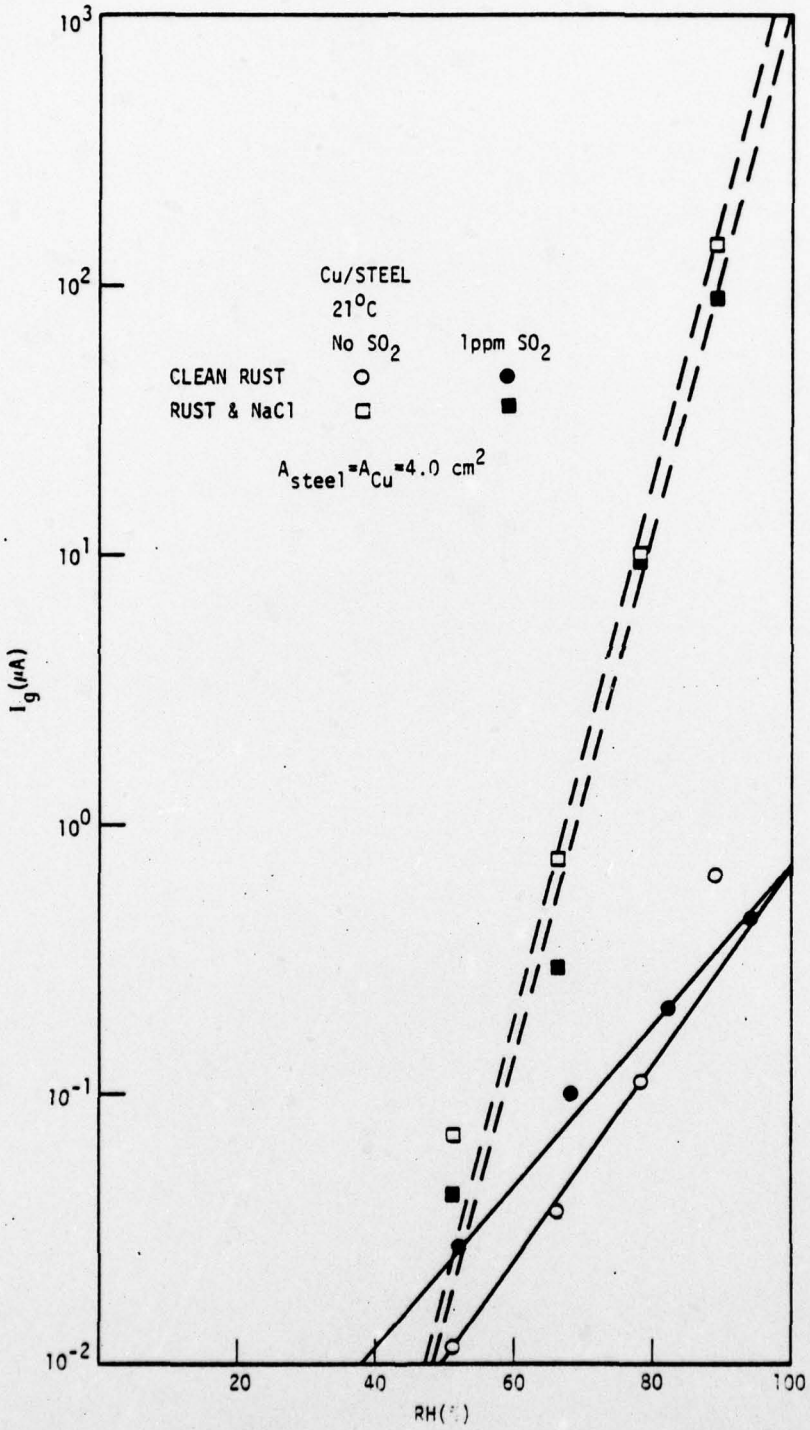

Fig. 12 RH-dependence of galvanic current for Cu/steel ACM after 2h (data from Fig.11).

The constants b (Eq. 9) and b' (Eq. 13) are related by:

$$b' = b\left(\frac{100-RH_{crit}}{100}\right) \qquad (14)$$

For the experiments shown in Fig. 11 it is assumed that RH_{crit} corresponds to RH at I_g = 0.01 μA which corresponds to 0.0025 $\mu A/cm^2$. The constant b' is characteristic of the surface reactivity and the environment. The much higher b'-values for rust containing NaCl show the accelerating effect of this pollutant. The effect of SO_2 is found to be very small. In further experiments a number of different salts were added to rust and the response of the rust covered ACM determined. The galvanic current I_g was measured at four different RH levels (51, 66, 77 and 88%) for a total of eight hours (Fig.13). In all cases, I_g is higher for doped rust than for clean rust indicating the important role which pollutants play in condensation of electrolyte from the atmosphere. Chloride ions lead to higher currents at all RH levels, but it will be noticed that the nature of the chloride compounds affects the current. NaCl + NH_4Cl leads to higher current flow than $FeCl_3 \cdot 6H_2O$ + NH_4Cl, which produces more current flow than $FeCl_3 \cdot 6H_2O$. The addition of Na_2SO_4 to rust leads to more corrosion than addition of $FeSO_4 \cdot 7H_2O$ + $(NH_4)_2SO_4$ or $FeSO_4 \cdot 7H_2O$, which is somewhat surprising considering the role usually attributed to ferrous sulfate.

At the highest RH studied, the spread of I_g-values reaches almost three orders of magnitude showing the tremendous effect of impurities in corrosion products on condensation, electrolyte conductivity and corrosion rates. If one assumes that the ACM surfaces in Fig.13 become wet and corrosion starts for RH $\geq$ 0.1 μA, one finds from Fig.13 that contaminants in rust shift RH_{crit} from about 72% for pure rust to about 55% for contaminated rust. A unique RH_{crit} which is often assumed to be close to 80% for steel does, therefore, not exist. RH_{crit} will probably be much lower near sea-

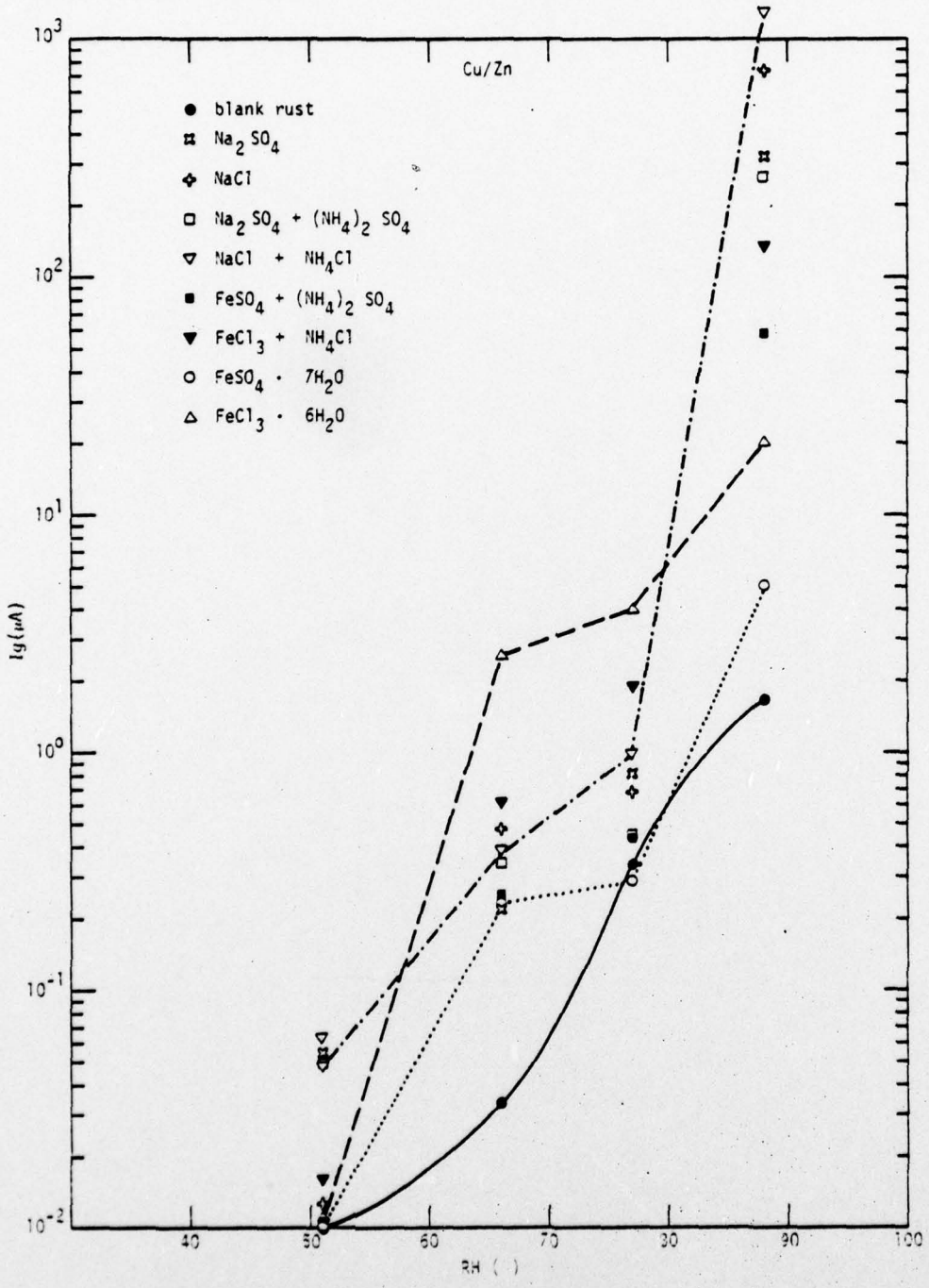

Fig. 13 RH-dependence of galvanic current for Cu/Zinc ACM covered with clean and doped rust.

coasts than in other locations. The effect of chlorides is most likely not due to its special corrosivity but to its lowering of RH_{crit} and consequently higher time-of-wetness.

b. The Use of Polarization Resistance Measurements to Study the Effects of Relative Humidity and SO_2.

The studies discussed above had not shown a clear effect of SO_2, but had clearly documented the tremendous importance of RH. In order to measure instantaneous corrosion rates in a better defined manner, an experimental approach differing from the previous use of galvanic couples (Cu/steel or Cu/Zn) was used to monitor corrosion rates. In order to measure the corrosion rate of a certain metal the previously used atmospheric corrosion monitor (ACM) was modified to consist of only one material. Ten metal plates were used in the modified ACM separated by mylar spacers and electrically connected as a two-electrode system in a manner that of two adjacent plates one would be the anode and one the cathode. A similar approach is being used by Kucera (9) who applies a constant voltage of 100 mV between the two sets of plates. It is, however, not possible to determine with any accuracy the corrosion current from the current measured at 100 mV polarization. In addition, permanent polarization of each set of plates with a fixed polarity might lead to constant irreversible changes of the test samples which in turn might obscure the effects to be studied. The corrosion current measurement was, therefore, carried out in our experiments with a 30 mV pulse applied potentiostatically for 50 sec. after which the polarity of the pulse was reversed. In this manner, corrosion currents are monitored using the polarization resistance concept for a two-electrode system (11). The corrosion current I_{corr} can be calculated from the measured current I at potential pulse ΔE as:

$$I_{corr} = 2B \frac{I}{\Delta E} = kI, \qquad (15)$$

provided B is constant during the experiment. As shown earlier (11) the parameter B, which is a combination of Tafel slopes:

$$B = \frac{b_a b_c}{2.303(b_a+b_c)} \qquad (16)$$

is a function of time, material and environment, and corrosion currents can be calculated only as an approximation with the use of Eq.15. For a diffusion controlled process ($b_c \rightarrow \infty$), $B = \frac{b_a}{2.303}$ and values for B between 10 and 60 mV can be expected. The constant k will, therefore, have values between 0.7 and 4.0.

Typical results are shown in Fig.14 for a 4130 steel ACM which was covered with a layer of 0.01N Na_2SO_4 (initial thickness was 0.55 mm) and allowed to dry out in air + 1 ppm SO_2 in a glass cell at RH = 30%, room temperature. When the measured current had decreased below 0.1μA, RH was increased to RH = 60% using a mixture of dry and wet air at a flow rate of 2ℓ/min. to which SO_2 was added in the desired concentration. After one hour RH was changed again to 90% and then changed to 60% and 30% for one hour each. The results in Fig.14 show that, in general, the positive and negative pulse lead to similar current flow, which indicates that no irreversible changes have occurred during an anodic or cathodic pulse. The current changes very rapidly following a change of RH to higher or lower values.

α. Results in neutral environments

In this series of experiments solutions of 0.01N NaCl or Na_2SO_4 were applied and RH varied in the sequence 30-60-90-60-30% in air, air + 1 ppm SO_2, N_2, and N_2 + 1 ppm SO_2. In this manner it was expected to detect changes in the response to changing RH of corrosion product films

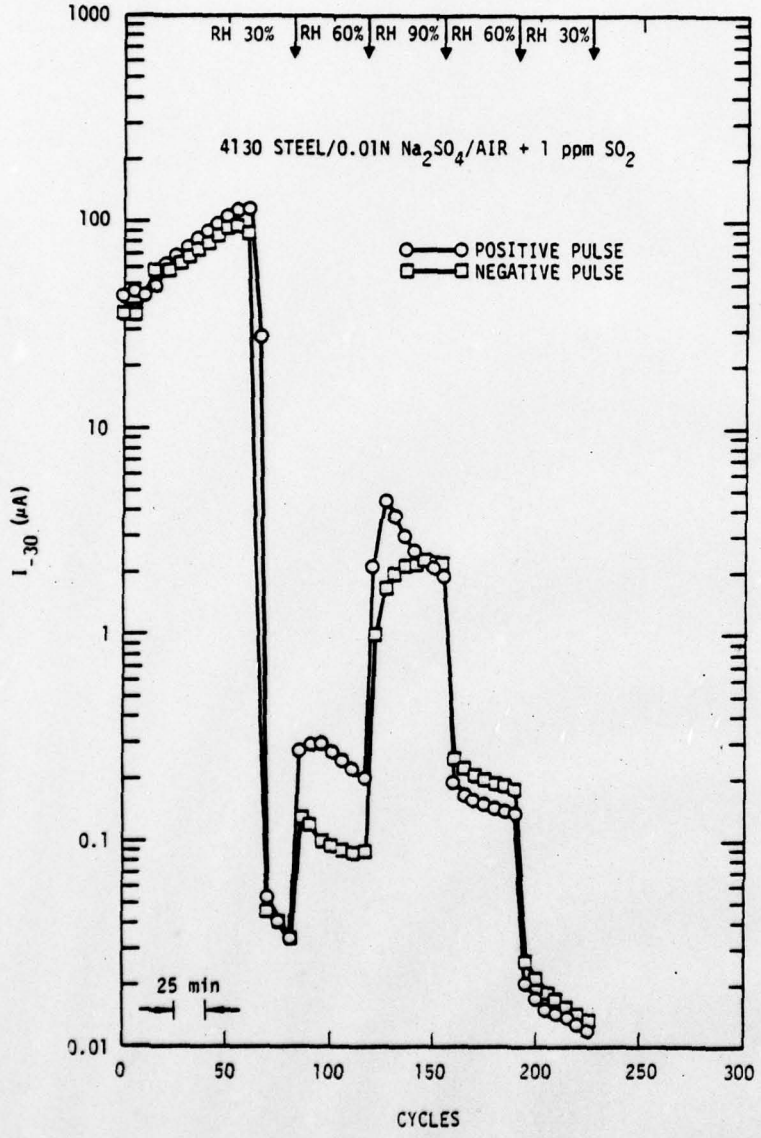

Fig. 14 Corrosion current measurements for 4130 steel with the potential-pulse method.

formed under different atmospheres on different metals. Figure 15 shows results obtained under NaCl for 4130 steel in air (Fig.15a) and N_2 (Fig.15b). During the drying-out period (RH = 30%) higher currents are observed for steel in air and air + 1 ppm SO_2 than in N_2 and N_2 + 1 ppm SO_2, the time until the surface is dried out ($I < 0.1\mu A$) is also longer for air and air + 1 ppm SO_2. These trends continue throughout the experiment. Addition of SO_2 at the 1 ppm level does not seem to increase the current. During the whole experiment the currents were in fact higher for air than for air + SO_2. When RH was increased to 90%, the current was the highest in air followed by air + SO_2, N_2, and N_2+SO_2. At the final RH value (30%) the current in air and air + SO_2 was more than a factor of ten higher than in N_2 and N_2+SO_2.

A different behavior is observed for Cu (Fig. 16), where in the drying-out period the highest currents are observed for air + SO_2 (Fig.16a) and N_2+SO_2 (Fig.16b), which suggests that SO_2 acts as a depolarizer. The maximum current in air during drying-out is about a factor of ten lower for Cu than for steel. When RH is increased from 30% to 60%, significant current flow is observed only for air and air + SO_2. At RH = 90% the highest currents are recorded in air and air + SO_2.

Similar results have been obtained in 0.01N Na_2SO_4 as shown in Table II(Cu), Table III(4130 steel) and Table IV , which lists the results for Zinc (99.9%). Tables II-IV contain the time t_{dry} until a surface has dried out at RH = 30%, the maximum current I_{max}^{30} at RH = 30%, the current I_{dry}^{30} recorded when the surface has dried out and the amount of electricity Q_{dry} which had been flowing in the drying-out period. I_{max}^{60} and I_{max}^{90} are the maximum currents measured at RH = 60% and 90%, $I_{dry}^{30,f}$ is the current recorded at the end of the experiment. Current values are for a negative (-30 mV) pulse.

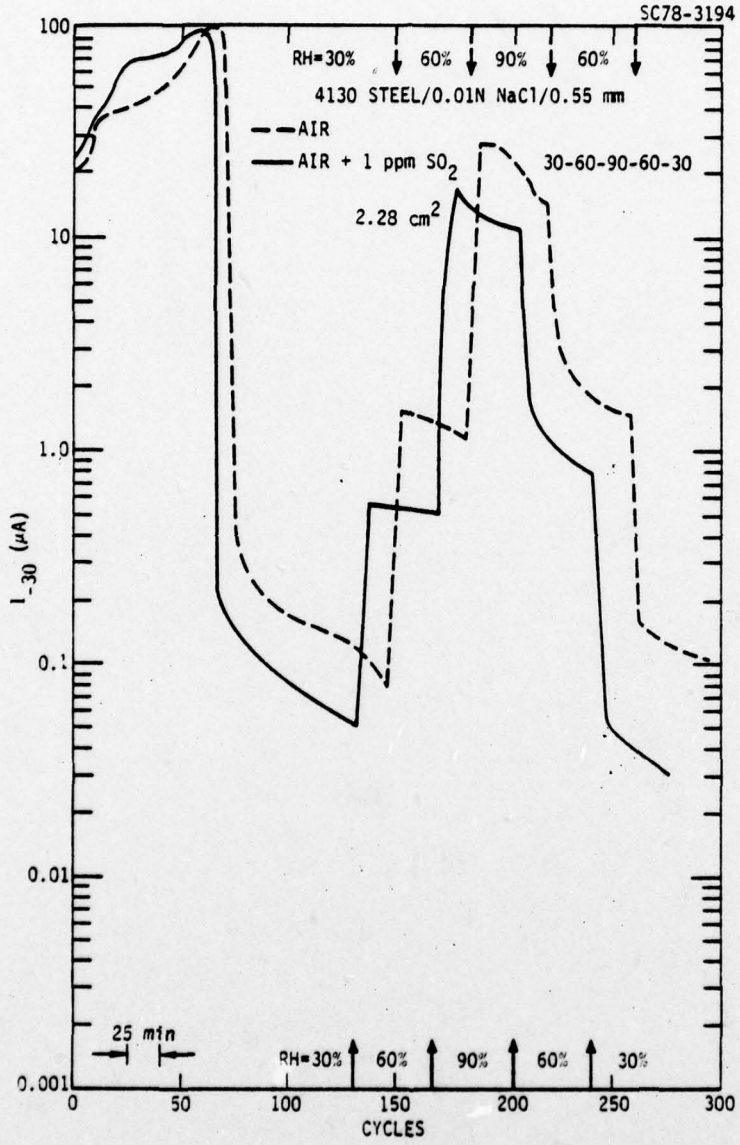

Fig. 15a Current at ± 30 mV for 4130 steel initially covered with a 0.55 mm layer of 0.01N NaCl in different atmospheres.

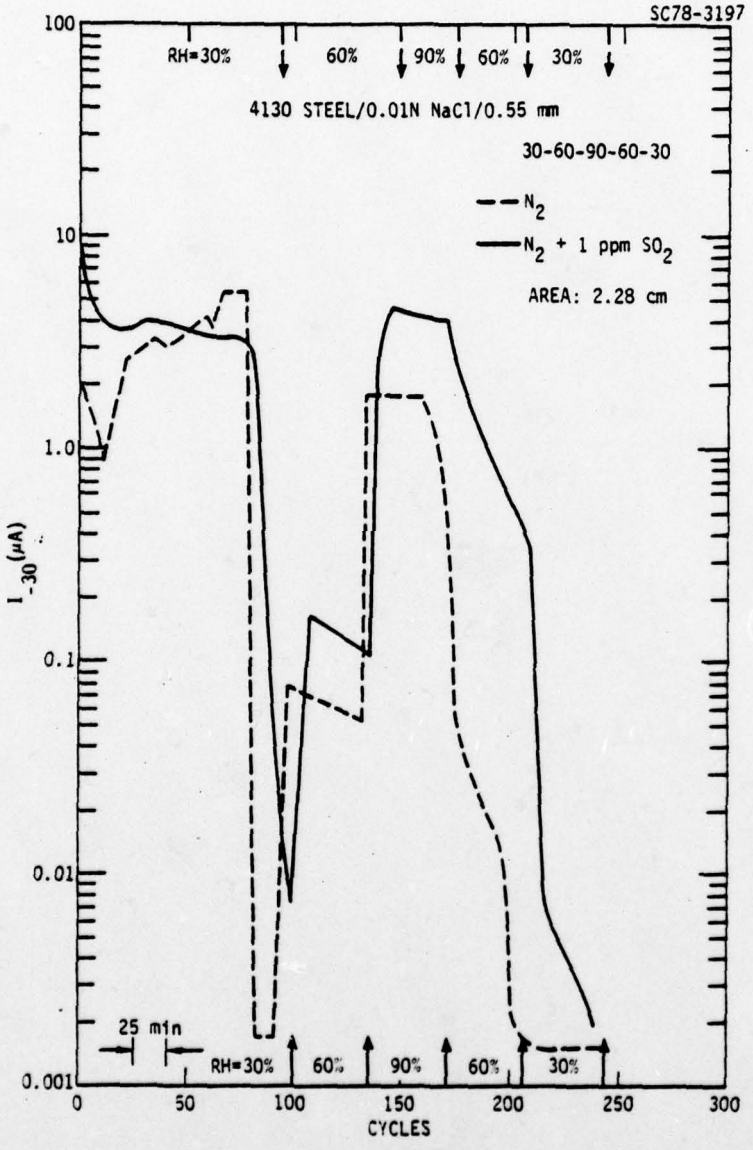

Fig. 15b Current at ± 30 mV for 4130 steel initially covered with a 0.55 mm layer of 0.01N NaCl in different atmospheres.

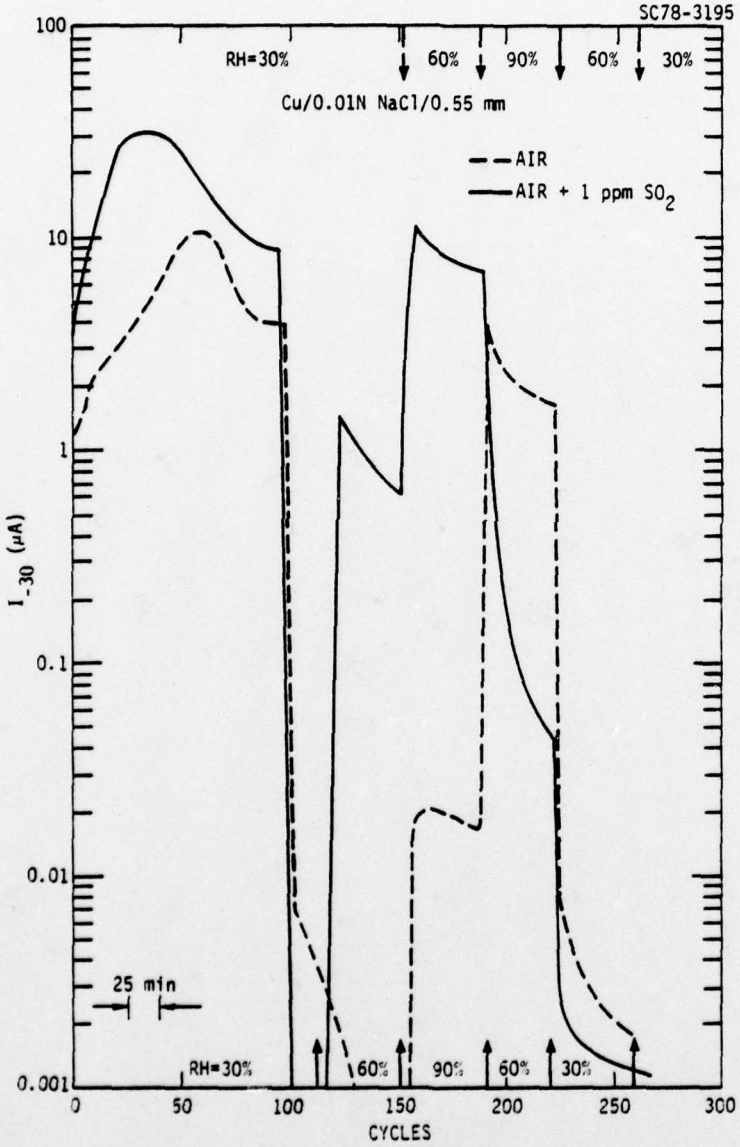

Fig. 16a Current at ± 30 mV for Cu/steel initially covered with a 0.55 mm layer of 0.01N NaCl in different atmospheres.

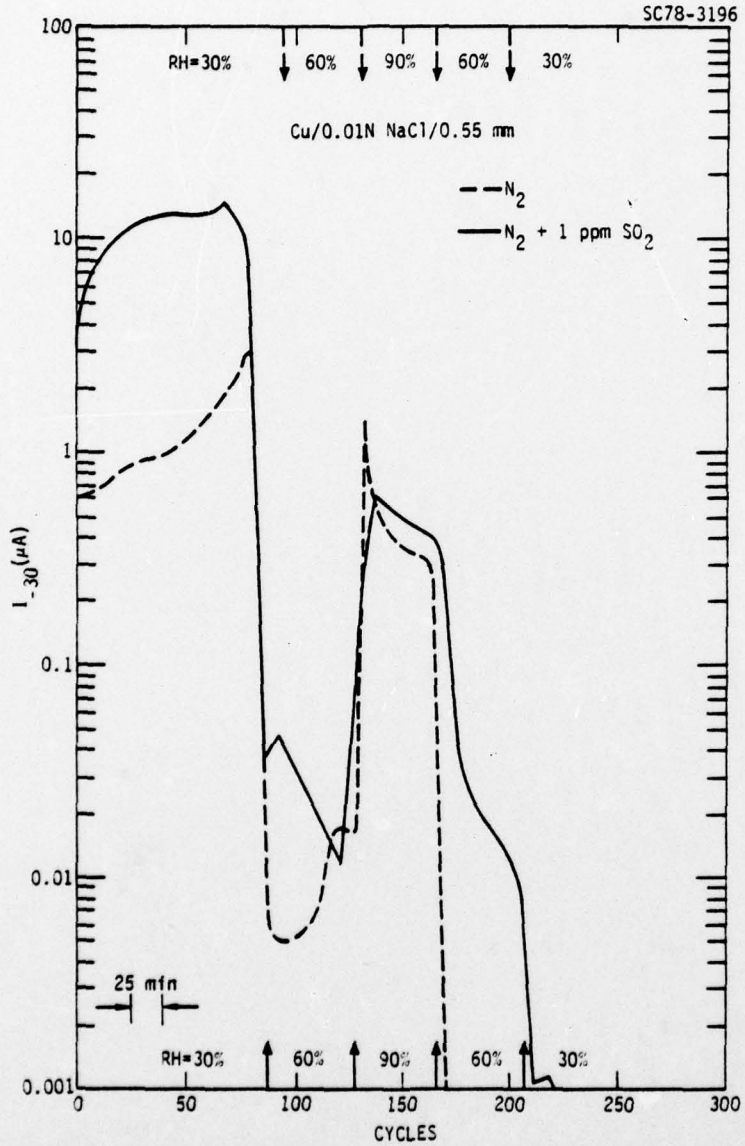

Fig. 16b Current at ± 30 mV for Cu/steel initially covered with a 0.55 mm layer of 0.01N NaCl in different atmospheres.

In order to further evaluate the effects of SO_2, experiments were performed in which the surface was allowed to dry out at RH = 30% in air or N_2, RH was then raised to 90% for one hour and then 0.1 ppm SO_2 was added to the gas stream. After one hour the SO_2 concentration was increased to 1.0 ppm followed by one hour at RH = 90% and one hour at RH = 30% without SO_2. Only small effects were observed for steel and Cu. A small increase of the current was found for steel when the SO_2 concentration was raised to 1.0 ppm. However, the overall trend during the time at RH = 90% was a decrease of the corrosion current independent of SO_2 additions. For Cu/NaCl in air the corrosion current increased when 0.1 ppm SO_2 and 1.0 ppm SO_2 were added. In the latter case the current reached a maximum and then decreased again. In N_2 no effect of SO_2 additions was observed for Cu, steel or zinc as can be seen in Tables II-IV by comparing the different I_{max}^{90} values. An interesting feature was observed when RH was lowered again to 30% for Cu/NaCl in air. The corrosion current did not decrease as is usually observed, which might be a result of modifications of the corrosion product film produced at high RH in the presence of SO_2. This film was black, while films formed in air were similar to copper oxide films. A more detailed study of the effect would be interesting.

The results obtained for zinc (Table IV) were similar to those for Cu and 4130 steel. For all three metals higher corrosion currents were obtained at RH = 90% in NaCl solutions than in Na_2SO_4 despite the fact that the currents during the drying-out period were rather similar. This behavior is similar to that observed for steel surfaces covered with rust containing chlorides (10) or Cu/steel ACMs covered with $FeCl_3$ solutions. The effect of sulfate additions was much smaller in these experiments (10) (see above).

β. Results in acid environments

A number of experiments were carried out in 0.01N HCl and 0.01N H_2SO_4 in air or N_2 in order to evaluate the effect of acidification of the electrolyte during atmospheric exposure. The results are listed in Tables II-IV. During the drying-out period much higher currents were observed in air than in N_2, during the period of changing RH the differences between air and N_2 become much smaller. For Cu a much higher current flow is observed for HCl in air or N_2 during the drying-out period than for NaCl. The current flow and the total Cbs are higher for Cu than for steel. When RH is raised to 90% significant current flow occurs in air but not in N_2. For HCl and H_2SO_4 more electricity was flowing during the drying-out period for Cu in N_2 environment, while in the following stages of the experiment, corrosion was more pronounced in air.

For zinc in HCl/air the current suddenly increased sharply during the drying-out period. This behavior was due to shortening of the plates of the sensor by a solid layer of corrosion products which were formed at high rates in the acid environments.

γ. The effect of SO_2 additions on the drying-out process.

Due to the importance of the drying process of thin layers, the effect of SO_2 on corrosion under thin layers drying-out under various environmental conditions was studied in more detail for steel and zinc under 0.01N NaCl or Na_2SO_4 in air or N_2 containing 0.1 or 1.0 ppm SO_2. The results for steel are shown on a linear scale suitable for integration for air (Fig.17 a) and N_2 (Fig.17 b). In air increasing SO_2 contents increase the corrosion rate of steel to a small extent. In N_2, however, no acceleration due to SO_2 is observed and corrosion rates are more than a factor of ten lower. This result shows that a reaction which involves direct reduction of SO_2 is unlikely.

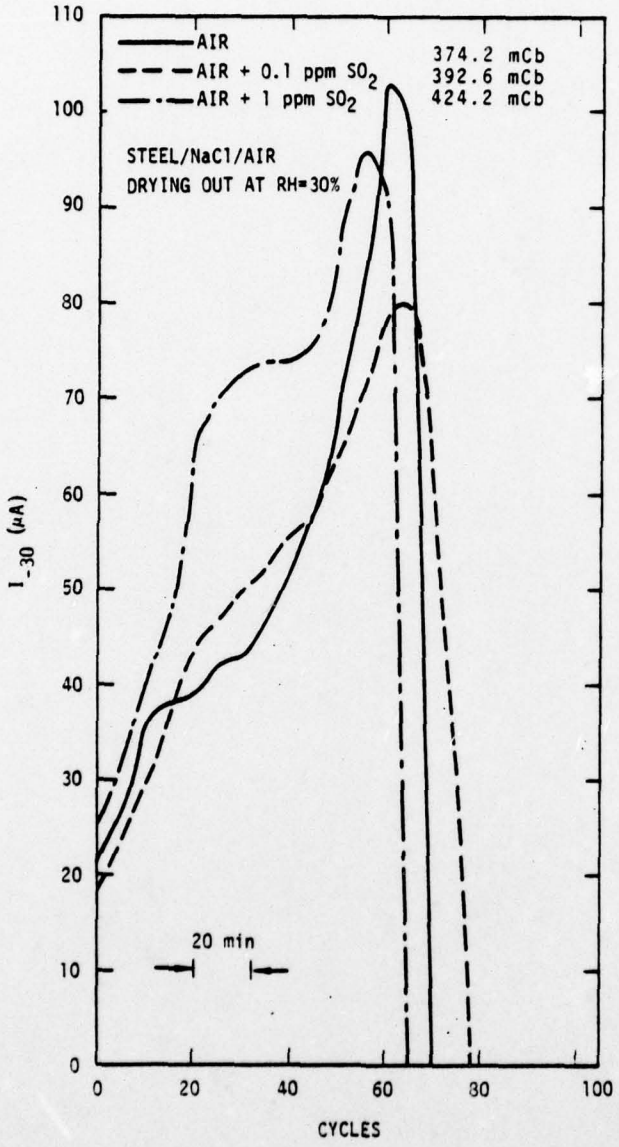

Fig. 17a Current flow for 4130 steel under 0.01N NaCl drying out at RH = 30% in air (Fig.17a) and N_2 (Fig.17b) atmospheres.

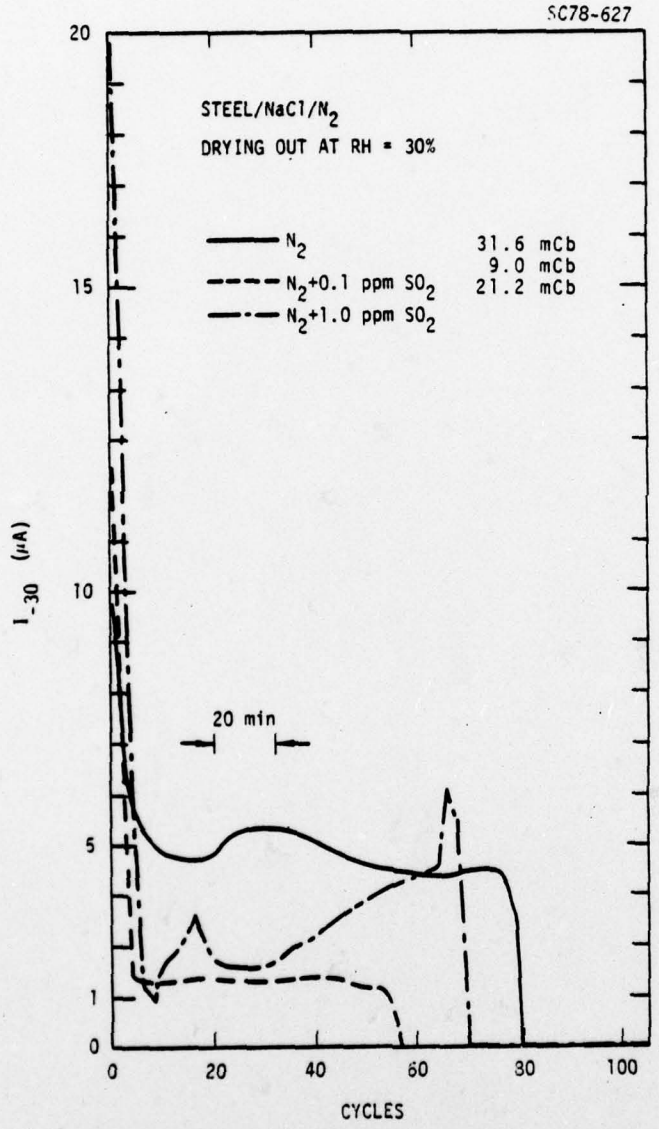

Fig. 17b Current flow for 4130 steel under 0.01N NaCl drying out at RH = 30% in air (Fig. 17a) and N_2 (Fig. 17b) atmospheres.

The observed lack of an effect of SO_2 might be explained by assuming that oxygen is needed for SO_2 to form sulfates which accelerate corrosion rates. Similar results have been obtained for 4130 steel in Na_2SO_4.

For zinc (Table IV it is more difficult to determine the effects of SO_2 on the drying-out process. In both NaCl and Na_2SO_4 the total Cb (Q_{dry}) are lower in air + SO_2 than in air. In NaCl a higher Q_{dry} value is measured for N_2+SO_2 than for N_2, while in Na_2SO_4 corrosion appears to be higher in N_2 and N_2+SO_2 than in air or air + SO_2. The weight loss data obtained for zinc (see below) show that corrosion is faster in N_2+SO_2 than in N_2, but indicate that corrosion rates in air and air + SO_2 are higher than N_2 or N_2+SO_2.

c. Electrochemical Evaluation of Vapor Phase Inhibitors

Vapor phase inhibitors (VPI) show promise in protection of materials from atmospheric corrosion. The materials which have been shown to be useful are of organic nature and contain oxidizing agents such as NO_2^- or compounds which absorb strongly. Useful VPIs have to have a vapor pressure hign enougn to make evaporation and absorption on metal surfaces or dissolution in surface films possible and low enough to prevent early loss of the VPI material.

Time and funding restraints limited this task to some preliminary studies which involved $NaNO_2$ and dichan (dicyclohexylamine nitrite) dissolved in 0.01N NaCl or Na_2SO_4. Potentiodynamic polarization curves have shown that both $NaNO_2$ and dichan not only act as oxidizing agents but also produce a passivation effect which is more pronounced in Na_2SO_4 than in NaCl, $NaNO_2$ being more effective than dichan.

Further experiments were carried out using Cu/steel ACMs which were covered with thin layers of $NaNO_2$ or dichan in the standard manner. In the absence of inhibitor the galvanic current is high and rusting occurs

TABLE II. Corrosion Current Measurements $(I_{-30}(\mu A))/Cu$

Solution/Atmosphere	t_{dry}(min)	Q_{dry}(mCb)	I^{30}_{max}	I^{30}_{dry}	I^{60}_{max}	I^{90}_{max}	$I^{30,f}_{dry}$
NaCl/air	250	54.2	10.5	$2.3 \cdot 10^{-4}$	$2.3 \cdot 10^{-2}$	3.8	$1 \cdot 10^{-4}$
NaCl/air + 1 ppm SO_2	187	170.3	31	$1 \cdot 10^{-4}$	1.5	11.5	$1.2 \cdot 10^{-3}$
NaCl/N_2	152	11.0	31	$4.7 \cdot 10^{-4}$	$2.0 \cdot 10^{-2}$	1.45	$1 \cdot 10^{-4}$
NaCl/N_2 + 1 ppm SO_2	142	92.6	16	$3.8 \cdot 10^{-2}$	$4.7 \cdot 10^{-2}$	0.70	$1 \cdot 10^{-4}$
Na_2SO_4/air	197	39.5	1.95	$1 \cdot 10^{-4}$	$1 \cdot 10^{-4}$	0.12	$1 \cdot 10^{-4}$
Na_2SO_4/air + 1 ppm SO_2	167	447.6	89	$1 \cdot 10^{-4}$	$1 \cdot 10^{-4}$	0.42	$1 \cdot 10^{-4}$
Na_2SO_4/N_2	172	16.9	0.81	$1 \cdot 10^{-4}$	$4.7 \cdot 10^{-4}$	1.15	$2.2 \cdot 10^{-4}$
Na_2SO_4/N_2 + 1 ppm SO_2	108	25.0	3.3	$1 \cdot 10^{-4}$	$2.3 \cdot 10^{-4}$	0.39	$4.0 \cdot 10^{-4}$
HCl/air	183	111.5	185	0.10	0.14	1.7	$3.2 \cdot 10^{-3}$
HCl/N_2	142	140.5	195	$4.3 \cdot 10^{-4}$	$2.4 \cdot 10^{-4}$	0.15	$4.3 \cdot 10^{-3}$
H_2SO_4/air	155	103.4	180	$1.5 \cdot 10^{-4}$	0.10	0.24	
H_2SO_4/N_2	108	140.8	220	0.01	0.024	0.14	$5.0 \cdot 10^{-3}$

TABLE II. continued

	t_{dry}(min)	Q_{dry}(mCb)	I^{30}_{max}	I^{30}_{dry}	I^{90}_{max}	$I^{90,0.1}_{max}$	$I^{90,1.0}_{max}$	I^{90}_{f}
NaCl/air	233	42.9	12.5	$1 \cdot 10^{-4}$	4.3	2.25	2.9	1.35
$NaCl/N_2$	163	15.5	3.6	$2.2 \cdot 10^{-3}$	0.59	0.51	0.32	0.092
Na_2SO_4/air	217	19.3	2.6	$1.4 \cdot 10^{-3}$	0.52	0.30	0.17	0.050
Na_2SO_4/N_2	145	5.0	0.68	$1 \cdot 10^{-4}$	0.39	0.088	0.09	0.096

Note: Concentration of all solutions is 0.01N
Initial solution layer thickness is 0.55 mm
A pulse of ± 30 mV is applied for 50 sec followed by reversal of polarity
All currents are in μA, total exposed area is 4.56 cm^2

TABLE III . Corrosion Current Measurements ($I_{-30}(\mu A)$)/4130 Steel

Solution/Atmosphere	t_{dry}(min)	Q_{dry}(mCb)	I^{30}_{max}	I^{30}_{dry}	I^{60}_{max}	I^{90}_{max}	$I^{30,f}_{dry}$
NaCl/air	242	383.9	103	0.073	1.5	2.8	1.15
NaCl/air + 1 ppm SO_2	218	421.7	96	0.053	0.58	17.5	0.032
NaCl/N_2	163	31.4	8.6	0.0078	0.19	4.6	0.0021
NaCl/N_2 + 1 ppm SO_2	133	27.4	5.8	0.0018	0.082	1.95	0.0016
Na_2SO_4/air	168	485.5	115	0.057	0.30	3.5	0.038
Na_2SO_4/air + 1 ppm SO_2	135	460.5	97	0.033	0.135	2.3	0.014
Na_2SO_4/N_2	188	37.1	10.5	0.0026	0.11	4.2	0.001
Na_2SO_4/N_2 + 1 ppm SO_2	117	21.8	6.6	0.0018	0.0039	2.4	0.002
HCl/air	157	350.0	68	0.03	2.2	6.1	0.012
HCl/N_2	200	25.8	9.6	0.03	1.6	2.75	0.009
H_2SO_4/air	152	601.6	97	0.01	0.08	1.2	0.022
H_2SO_4/N_2	125	9.9	45	0.0004	0.0004	0.002	0.0005

	t_{dry}(min)	Q_{dry}(mCb)	I^{30}_{max}	I^{30}_{dry}	I^{90}_{max}	$I^{90,0.1}_{max}$	$I^{90,1.0}_{max}$	I^{90}_{f}
NaCl/air	185	389.5	113	0.085	40	21	17.5	9.0
NaCl/N_2	195	167.2	22.5	0.012	13	8	7.1	4.4
Na_2SO_4/air	140	503.2	115	0.037	4.4	4.3	3.8	3.1
Na_2SO_4/N_2	138	163.7	21	0.042	7.7	4.0	4.5	2.0

TABLE IV. Corrosion Current Measurements ($I_{-30}(\mu A)$)/Zn

Solution/Atmosphere	t_{dry}(min)	I^{30}_{max}	I^{30}_{dry}	I^{60}_{max}	I^{90}_{max}	I^{f}_{dry}	Q_{dry}(mCb)
NaCl/air	250	230	0.18	2.4	10.5	0.165	1306.5
NaCl/air + 1 ppm SO_2	183	83	0.07	0.63	6.1	0.05	301.6
NaCl/N_2	162	65	0.41	4.6	27.5	20	333.9
NaCl/N_2 + 1 ppm SO_2	170	180	0.37	3.0	10.0	0.2	812.9
Na_2SO_4/air	192	62	0.11	0.2	0.68	0.17	428.2
Na_2SO_4/air + 1 ppm SO_2	222	64	-0.14	-0.25	2.9	0.003	366.1
Na_2SO_4/N_2	158	140	-0.01	0.01	7.1	-0.01	1098.4
Na_2SO_4/N_2 + 1 ppm SO_2	125	165	0.26	1.9	7.5	0.55	1021.0
HCl/air	short						
HCl/N_2	> 166	51	0.55	1.95	1.6	0.49	154.8
H_2SO_4/air	> 267	310	0.46	0.48	1.25	0.70	517.7
H_2SO_4/N_2	167	230	0.001	0.20	0.50	0.047	593.5

	t_{dry}(min)	I^{30}_{max}	I^{30}_{dry}	I^{90}_{max}	$I^{90,0.1}_{max}$	$I^{90,1.0}_{max}$	I^{90}_{f}	Q_{dry}(mCb)
NaCl/air	233	135	0.03	31	32	30	1.5	595.2
NaCl/N_2	207	52	0.072	24	19.5	13.5	5.9	309.7
Na_2SO_4/air	208	135	-0.07	2.6	2.0	0.9	0.28	605.6
Na_2SO_4/N_2	250	110	0.29	3.0	3.0	2.25	1.2	611.6

in less than two hours. For 0.1N NaCl + 0.1N $NaNO_2$ no rusting occurred, while for a lower $NaNO_2$ concentration the current was initially low but increased sharply after some time when pitting of the steel occurred. $NaNO_2$ was more effective in NaCl than in Na_2SO_4. Dichan inhibited rusting when 3 g/ℓ was added in 0.1N NaCl but not in 0.1N Na_2SO_4 (Fig. 18).

The behavior during drying out in air or air + SO_2 of NaCl or Na_2SO_4 (0.01N) solutions containing 0.01N $NaNO_2$ or 0.01N dichan and the response of the corrosion product films to varying RH-values was also followed with polarization resistance measurements as shown in Fig. 19a-d. The results of these measurements are summarized in Table V . From Fig.19, which shows the results for NaCl, it can be seen that $NaNO_2$ (Fig. 19a) and dichan (Fig. 19b) are similarly effective in reducing corrosion rates. During the drying-out period the inhibition efficiency in NaCl based on the integrated current (Table V) for $NaNO_2$ is 95.5% in air and 96.5% in air + 1 ppm SO_2, while for dichan the corresponding values are 96.5% and 98.4%. An effect of SO_2 is seen at RH = 90%, when current flow is much higher in air + SO_2 than in air. In the initial drying-out period such an effect of SO_2 is not observed.

In Na_2SO_4 solution much higher currents are measured than in NaCl. In Na_2SO_4 + dichan appreciable current flow occurs at RH = 90% in air and air + 1 ppm SO_2 (Fig. 19d), while in Na_2SO_4 + $NaNO_2$ the current flow is much lower (Fig. 19c). According to Table V, the inhibitor efficiency is 91.4% for $NaNO_2$ and 92.1% for dichan in air, but only 68.0% for $NaNO_2$ and 81.9% for dichan in air + 1 ppm SO_2.

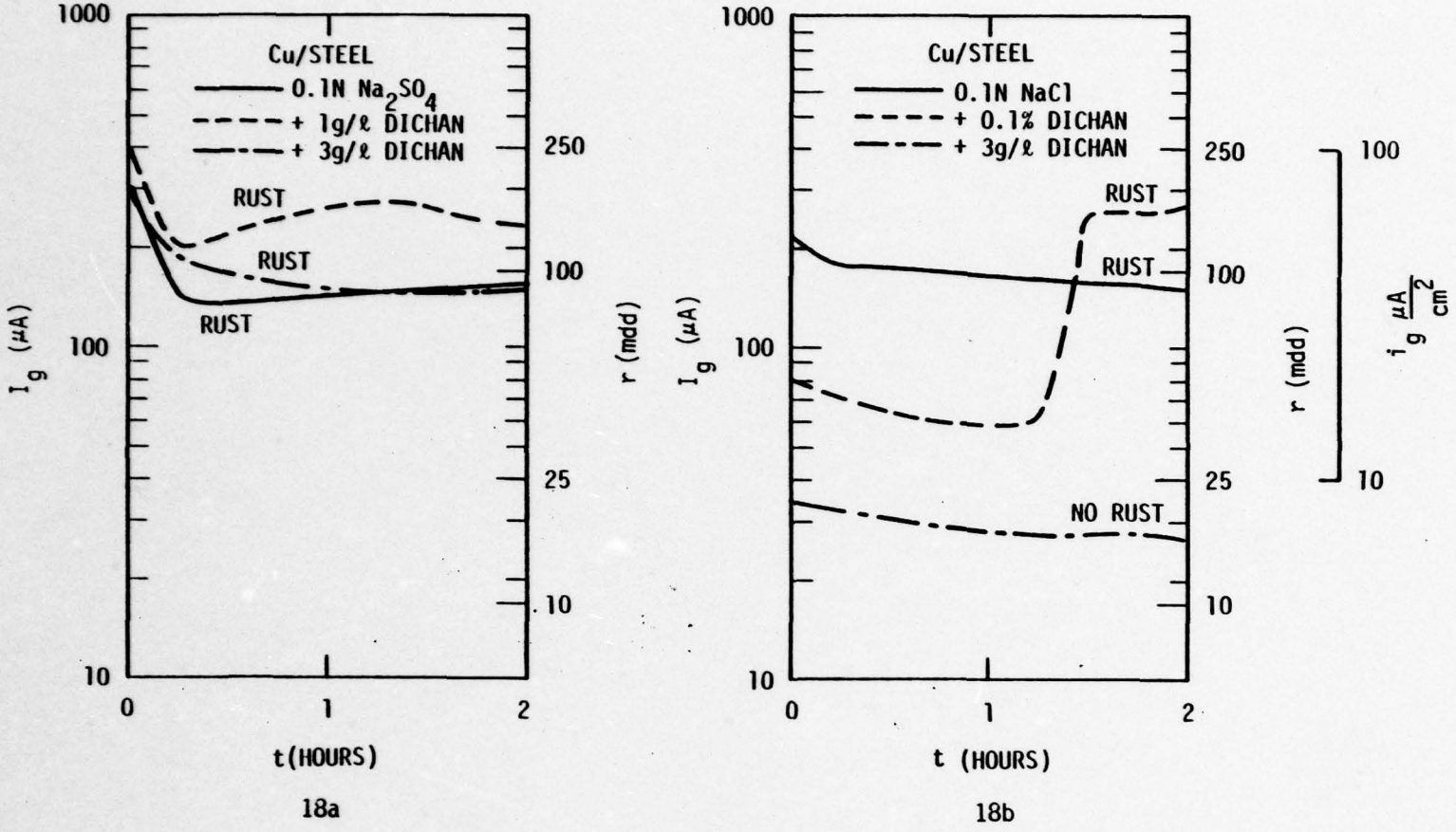

Fig. 18 Current flow in Cu/steel ACMs in 0.1N NaCl (Fig.18a) and 0.1 N Na_2SO_4 (Fig.18b) with additions of dichan.

SC78-625

Rockwell International
Science Center

SC5030.7FR

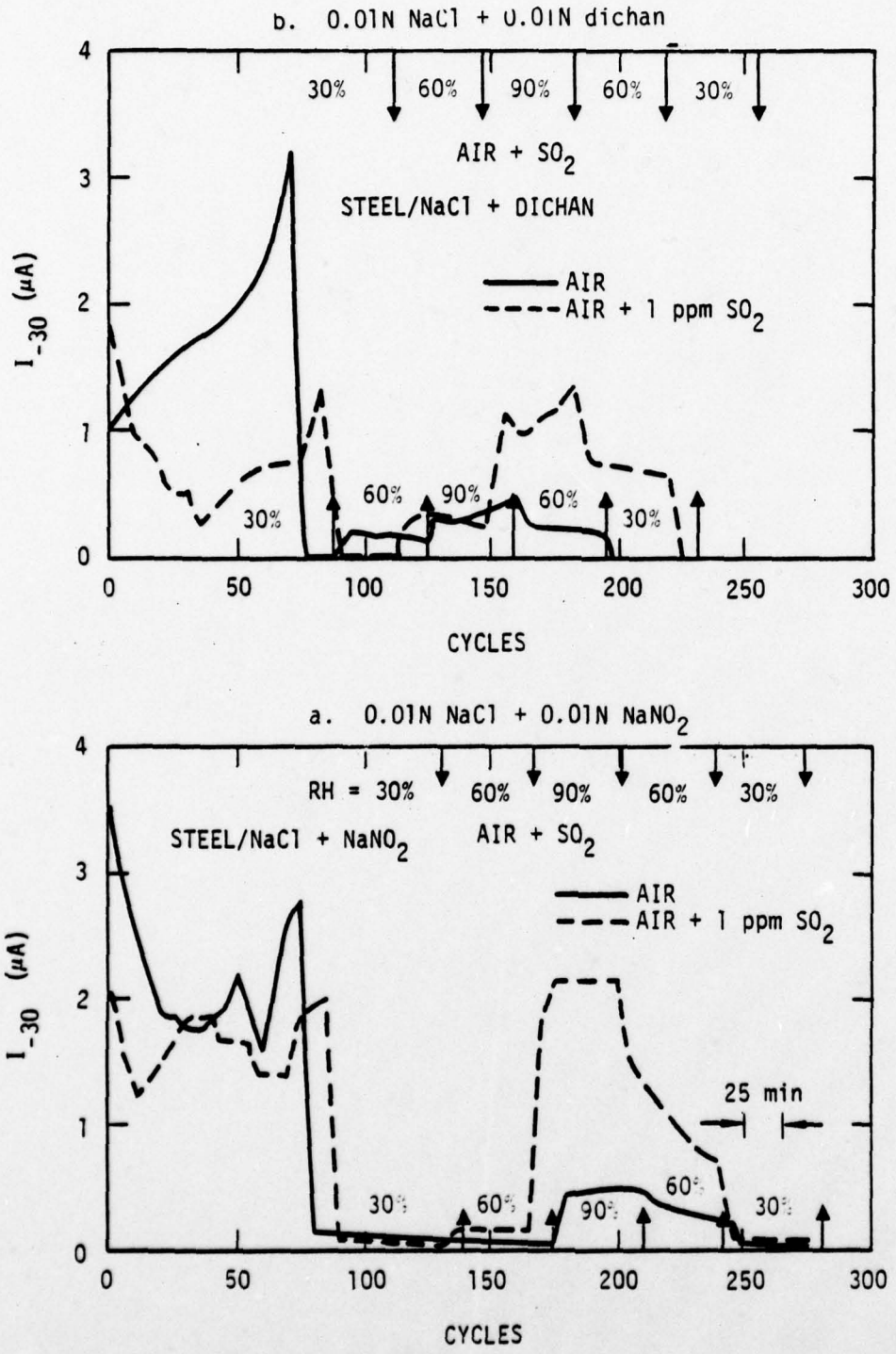

Fig. 19 Current flow for 4130 steel under solutions containing inhibitor exposed to air and air + 1 ppm SO_2 at varying RH.

SC78-642

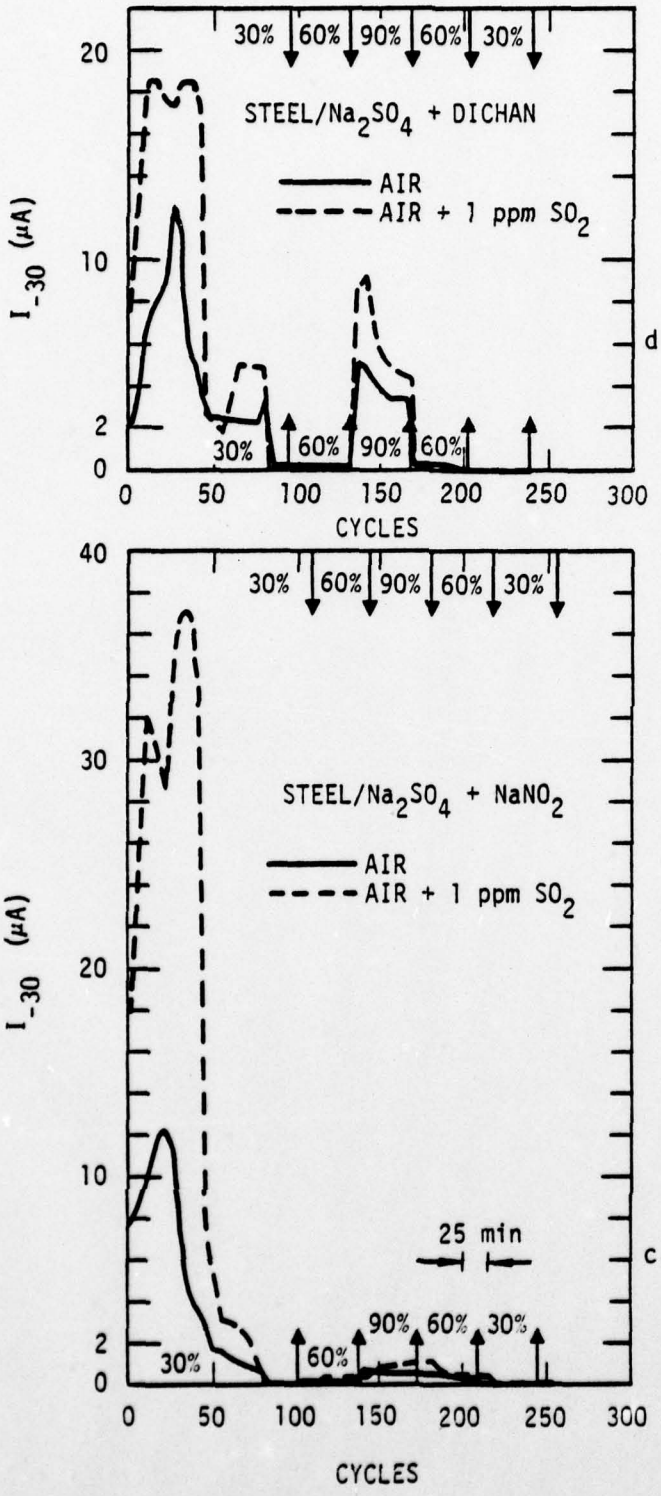

Fig. 19 Current flow for 4130 steel under solutions containing inhibitor exposed to air and air + 1 ppm SO_2 at varying RH.

TABLE V. Corrosion Current Measurements (I_{-30} (μA))/4130 Steel

I, NaCl (0.01N)

Additive/Atmosphere	t_{dry}(min)	Q(mCb)	I^{30}_{max}	I^{30}_{dry}	I^{60}_{max}	I^{90}_{max}	$I^{30,f}_{dry}$
None/air	242	383.9	103	0.073	1.5	2.8	0.115
$NaNO_2$/air	232	17.3	2.7	0.076	0.086	0.51	0.037
Dichan/air	143	13.6	3.2	0.035	0.20	0.46	0.0005
none/air + 1 ppm SO_2	218	421.7	96	0.053	0.58	17.5	0.032
$NaNO_2$	217	14.7	2.0	0.040	0.16	2.5	0.072
Dichan/air + 1 ppm SO_2	185	6.6	1.35	0.028	0.47	1.35	0.0009

II, Na_2SO_4 (0.01N)

None/air	168	485.5	115	0.057	0.30	3.5	0.038
$NaNO_2$/air	167	41.9	12.5	0.062	0.22	0.66	0.052
Dichan/air	157	38.4	12.5	0.026	0.13	5.2	0.010
None/air + 1 ppm SO_2	135	460.5	97	0.033	0.135	2.3	0.0135
$NaNO_2$/air + 1 ppm SO_2	180	147.4	37	0.060	0.28	1.1	0.035
Dichan/air + 1 ppm SO_2	157	83.2	18.5	0.005	0.032	9.5	0.0016

Task 3. Comparison of Weight Loss and Electrochemical Data under Thin Layer Electrolytes

In the previous tasks electrochemical techniques modified for corrosion studies under thin layers have been used. A number of factors which are assumed to influence atmospheric corrosion reactions have been evaluated such as RH, electrolyte and corrosion product composition, effect of SO_2 and nature of the metal. Since the formation and disappearance of electrolyte layers is so important in atmospheric corrosion as will also be discussed in the task on corrosion monitoring, most experiments were related to this phenomena.

While the electrochemical techniques have the advantage of providing a continuous record of the instantaneous corrosion rate, certain assumptions have to be made upon converting the measured electrochemical parameters into corrosion current densities (c.d.). It was, therefore, decided to carry out weight loss measurements and electrochemical experiments under identical conditions and compare the results obtained with both techniques. In order to meet this goal, a new weight loss technique (20) has been developed in which thin layers of electrolyte were placed on horizontal metal plates which were exposed to a controlled environment until the surface layers had dried out. For comparison, weight loss data were also obtained by total immersion in bulk electrolyte for 4 hours which is approximately the time for drying out at RH = 60%.

a. Weight Loss Data

Flat plates (2"x2") of 4130 steel and zinc (99.9%) were exposed horizontally in glass cells through which air or argon at constant RH with or without 1 ppm SO_2 flowing at a rate of 2ℓ/min. A 0.5 mm thick layer of electrolyte was placed on the samples, the unexposed side of the specimen was coated with turco mask. Experiments were carried out at RH = 30, 45, 60, and 75%. The weight loss was determined after removal of the corrosion products in inhibited HCl (steel) and ammonium acetate (zinc) taken into account a correction factor for blank samples. The corrosion product chemistry of similar samples has been determined by scanning Auger microprobe (SAM) analysis as discussed in Task 5. Figures 20-22 show the results obtained in 0.01N solutions of NaCl, Na_2SO_4, H_2SO_4, NCl and in deionized water. For steel (Fig. 20a) additions of 0.01N $NaNO_2$ and 0.01N dichan were made to NaCl and Na_2SO_4 at RH = 60%. Increasing RH increases the weight loss for experiments in air most likely due to the longer time period during which corrosion could occur. SO_2 has an accelerating effect which increases with increasing RH. $NaNO_2$ and dichan have a marked inhibiting effect in NaCl, but only a small effect in Na_2SO_4.

a. air and air + 1 ppm SO_2,

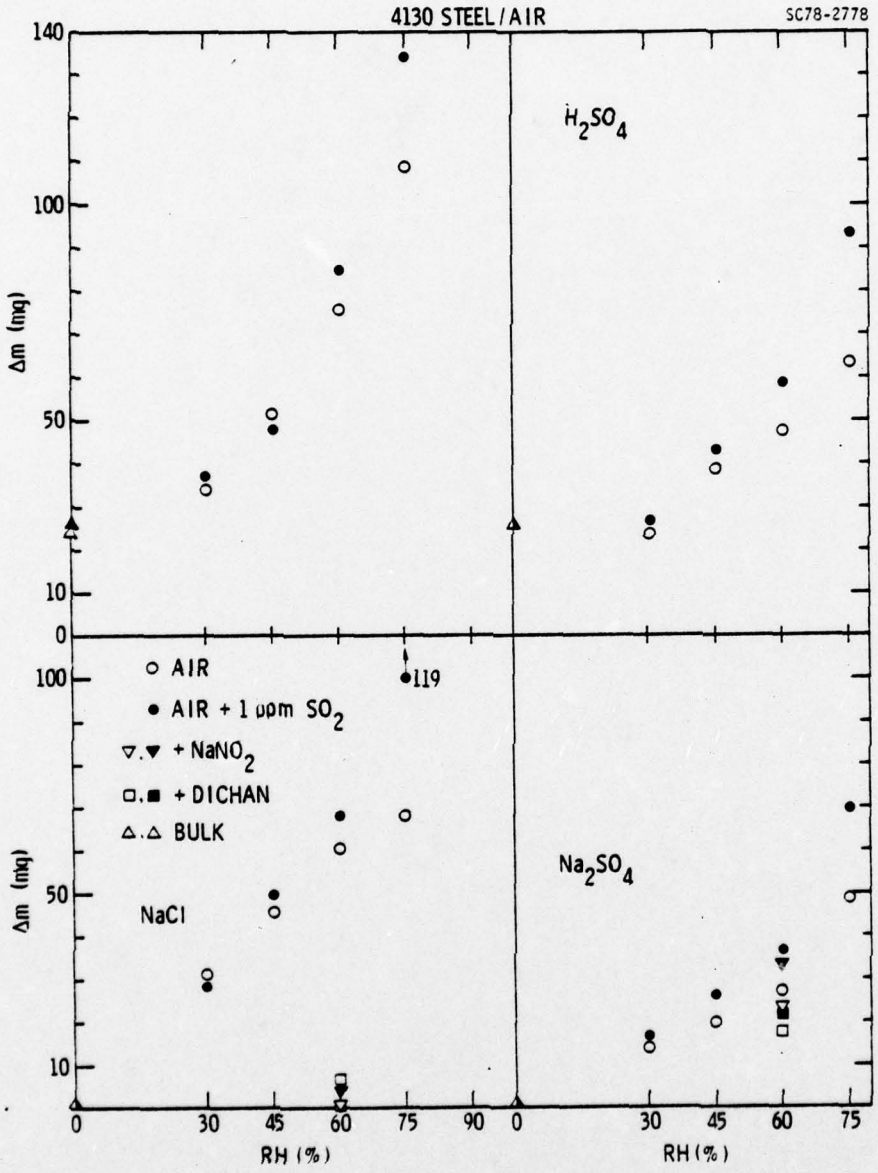

Fig. 20 Weight loss data for 4130 steel in bulk and under thin layer electrolytes.

The experiments in argon (Fig. 20 b), which were carried out in order to obtain more information about the mechanism by which SO_2 affects the corrosion process, showed much lower weight loss, which seemed to be independent of RH in the absence of SO_2. Addition of 1 ppm SO_2 increased the weight loss Δm with increasing RH. However, even the highest Δm values are much lower than those observed in air.

The results for steel in air and air + 1 ppm SO_2 show that exposure to a thin layer of electrolyte leads to much higher corrosion rates than exposure to bulk NaCl or Na_2SO_4. In the case of HCl and H_2SO_4 the effect is not so drastic but increases with increasing RH.

For zinc (Fig. 21) no effect of SO_2 was observed in air for NaCl and Na_2SO_4. For H_2SO_4 surprisingly the weight loss was lower than in the neutral solutions and independent of RH. In HCl a strong effect of RH was found in air, in air + SO_2 the weight loss was much lower than in air and similar to that observed in H_2SO_4. In argon Δm was very low, no definite effects of RH and SO_2 were observed. In NaCl and Na_2SO_4 corrosion rates were much lower in bulk solutions than under thin layers which were drying out during the corrosion process. For HCl and H_2SO_4, on the other hand, corrosion was much higher in the bulk electrolyte (Fig. 21a).

Experiments were also carried out in deionized water to eliminate the possible effect of anions on the action of SO_2. Different effects of SO_2 were observed for steel and zinc (Fig.22): for steel Δm increased with increasing RH and SO_2 accelerated corrosion, while for zinc Δm also increased with RH, but SO_2 had an inhibiting effect.

b. argon and argon + 1 ppm SO_2

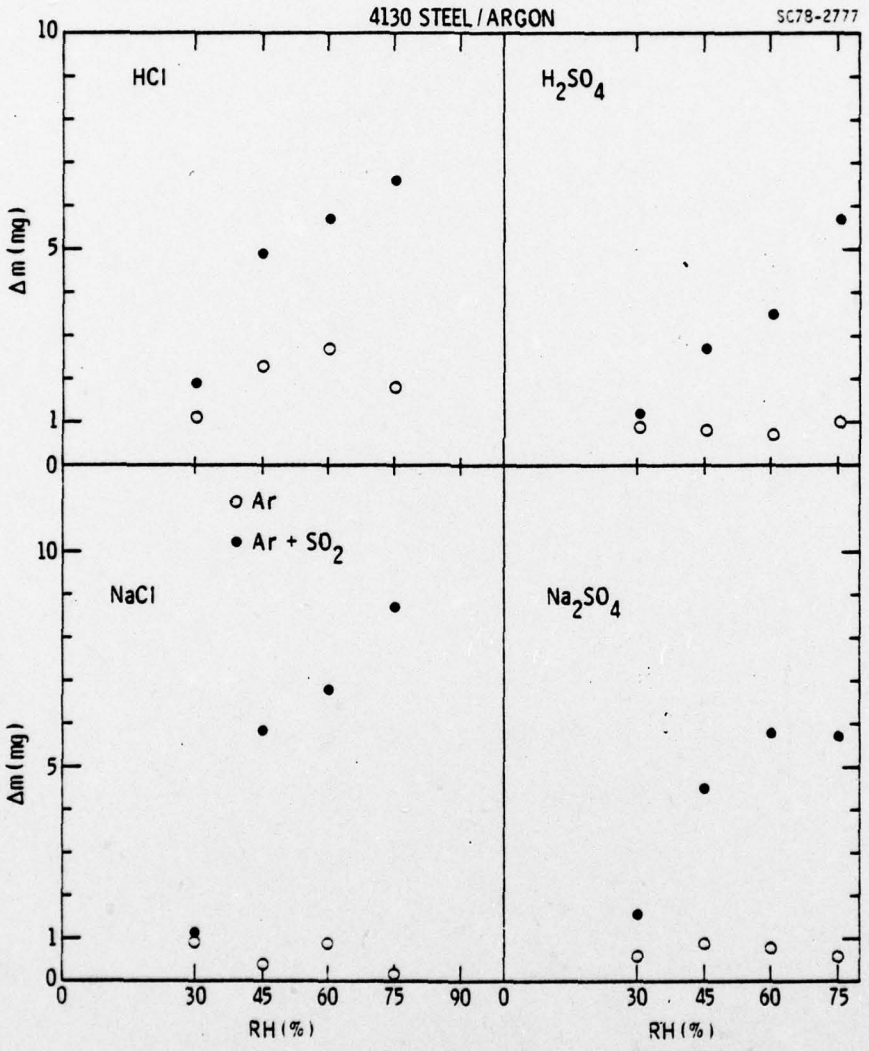

Fig. 20 Weight loss data for 413U steel in bulk and under thin layer electrolytes.

a. air and air + 1 ppm SO_2

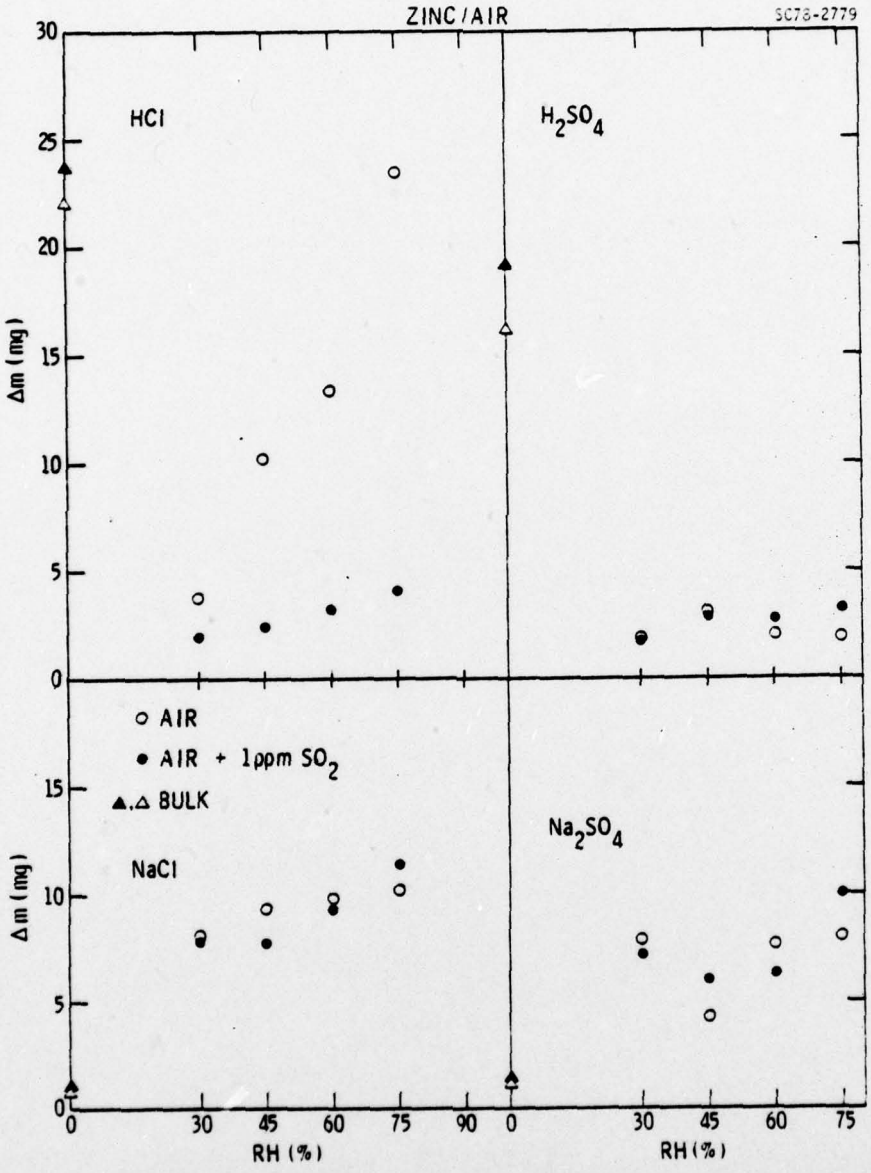

Fig. 21 Weight loss data for zinc in bulk and under thin layer electrolytes.

b. argon and argon + 1 ppm SO_2

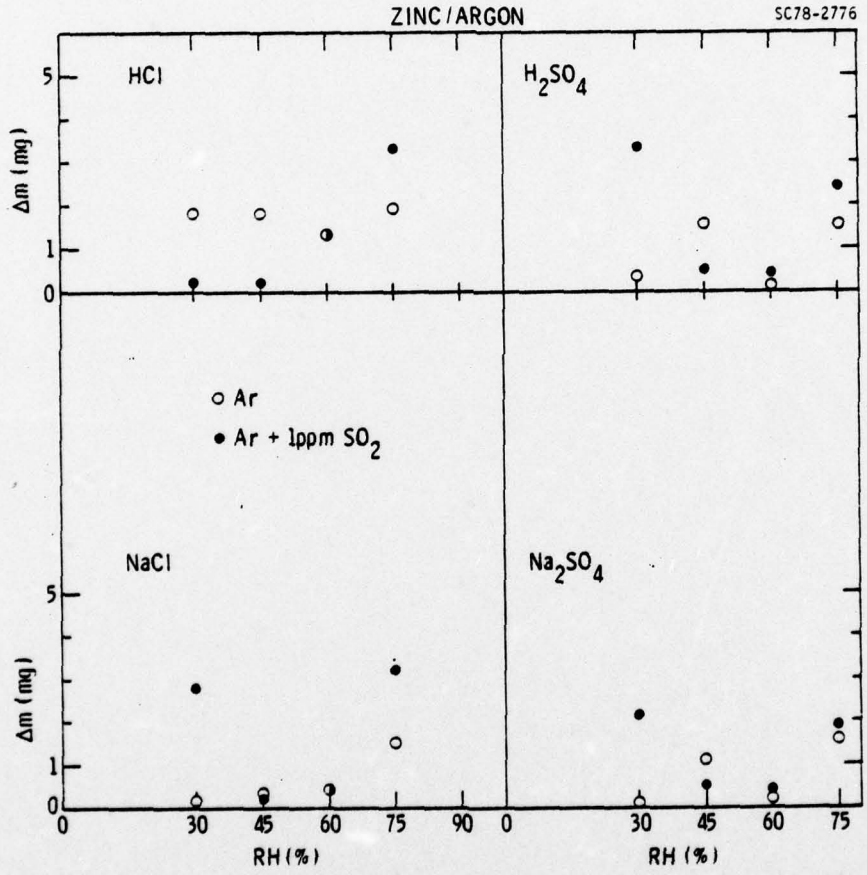

Fig. 21 Weight loss data for zinc in bulk and under thin layer electrolytes.

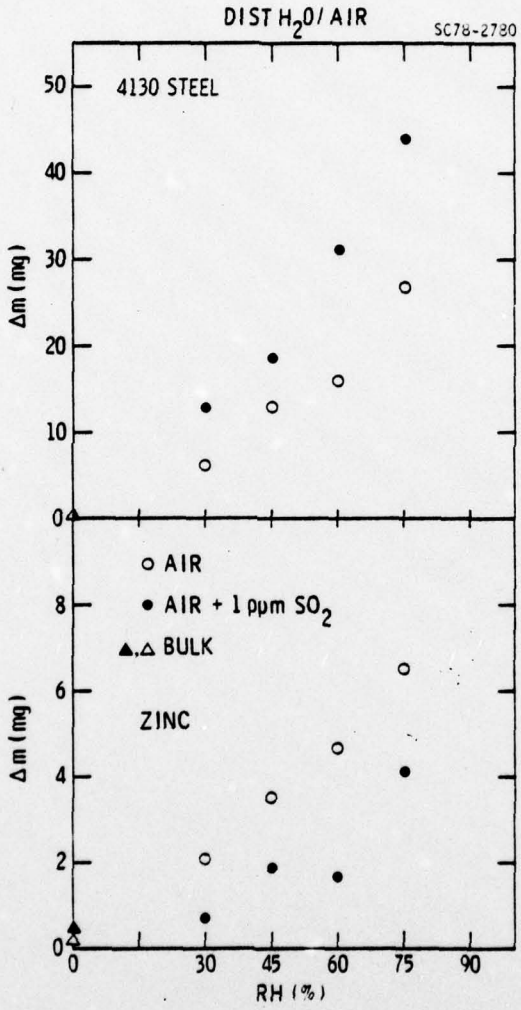

Fig. 22 Weight loss data for 4130 steel and zinc under layers of dist. H_2O in air and air + 1 ppm SO_2.

The effect of electrolyte concentration c on corrosion rates during drying out of thin electrolyte layers was also investigated in Na_2SO_4. For both 4130 steel and zinc an approximately linear increase of the weight loss with log c was observed (Fig. 23). The results obtained for 4130 steel at RH = 60% in air and air + SO_2 are summarized in Table VI which contains also the inhibitor efficiency E for additions of $NaNO_2$ and dichan. The bulk electrolyte data are also listed, the poor inhibitor efficiency in Na_2SO_4 is also observed in bulk solutions. Additional data for iron chlorides and sulfates (0.01N), which might be involved in the atmospheric corrosion process, are also listed in Table VI.

b. Electrochemical Measurements

The electrochemical measurements (20) were carried out with steel or zinc ACMs at an applied potential of $\Delta E = \pm 30$ mV with reversal of polarity after 50 sec as discussed above, and with galvanic cells (Cu/steel and Cu/zinc). The results obtained under a layer of 0.01N Na_2SO_4 at different RH values are shown in Fig.24 for steel, Fig.25 for Cu/steel, Fig.26 for zinc, and Fig.27 for Cu/zinc. The current-time curves for steel and Cu/steel are characterized by a steep increase of the current which is more pronounced when the visible electrolyte layer starts to disappear especially at low RH. For both types of ACMs the time at which the current maximum occurs and at which the current decreases to values less than 1 μA both increase with increasing RH except at RH = 30% and 45%, (Fig. 24 and 25) where the main effect of increasing RH is an increase of the maximum current and total current flow. While significant corrosion occurs for only 2 to 3h at RH = 30% and 45%, this time increases to about 6h at RH = 75% and 9 hr for steel and 13 h for Cu/steel at RH = 90%.

SC78-3180

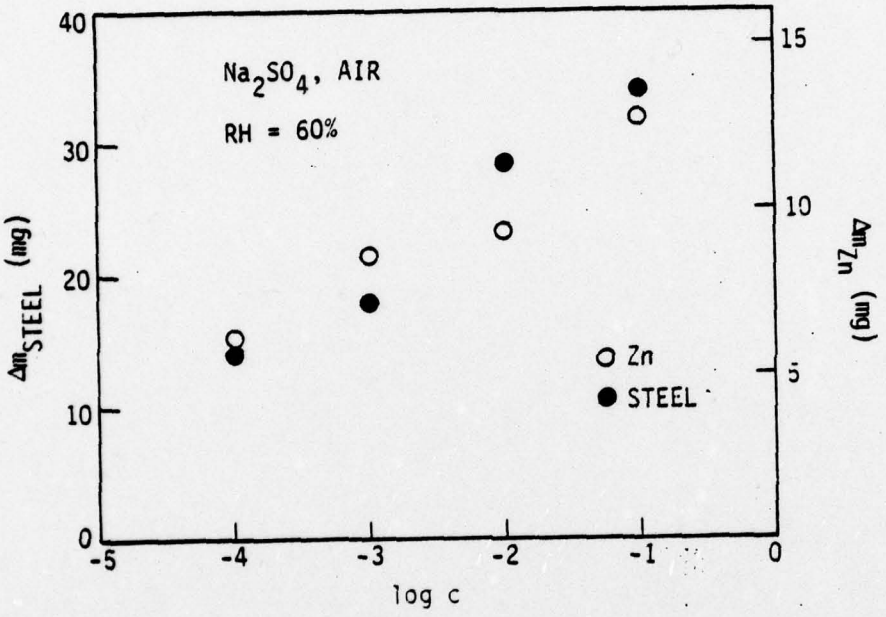

Fig. 23 Weight loss data for 4130 steel and zinc under tnin layers of Na_2SO_4 as a function of concentration. RH = 60%.

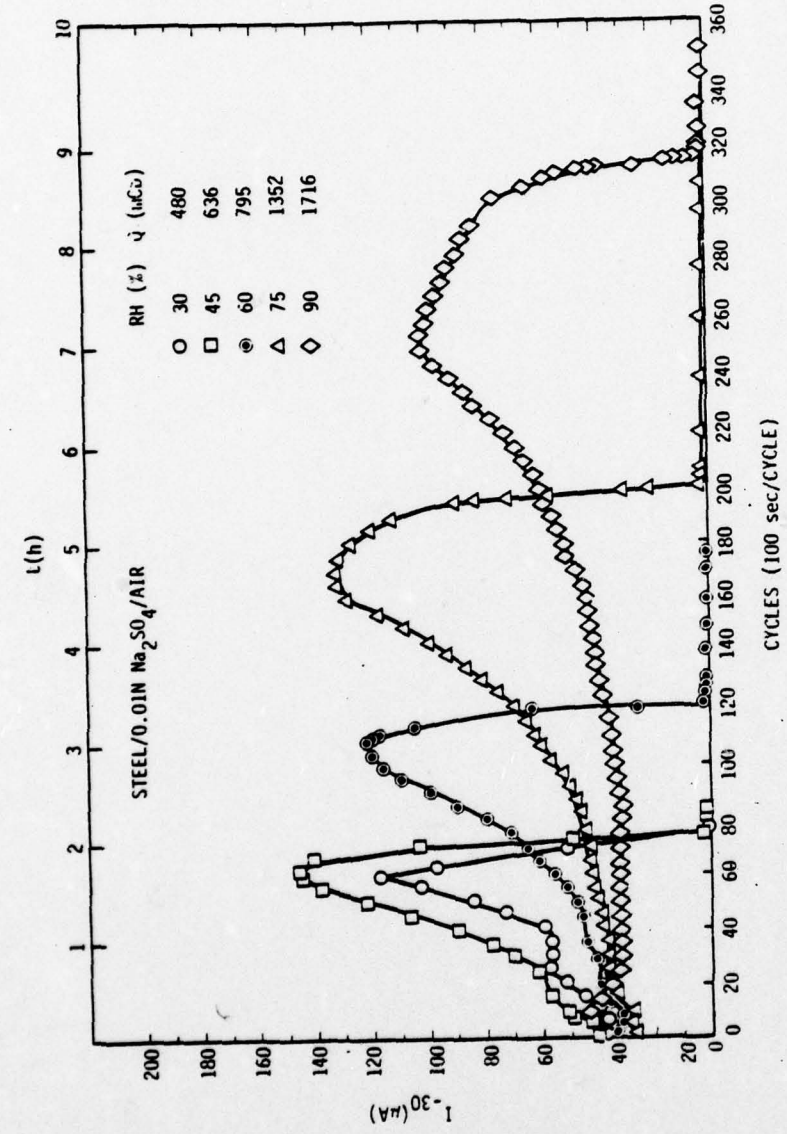

Fig. 24 Current at $\Delta E = \pm 30$ mV for 4130 steel during drying out of 0.01N Na_2SO_4 at different RH values.

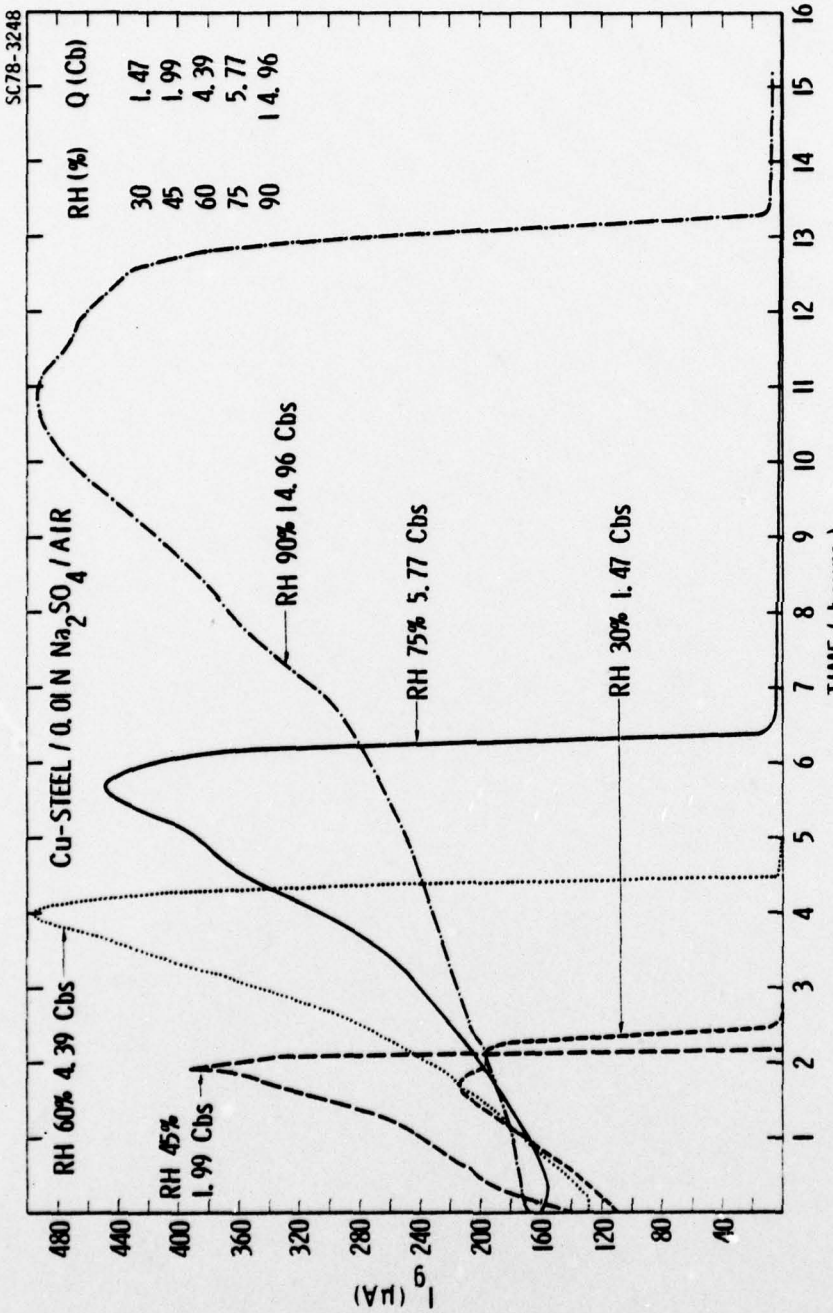

Fig. 25 Current at ΔE = ±30 mV for Cu/steel during drying out of 0.01N Na_2SO_4 at different RH values.

For zinc (Fig. 26) differences in the current-time behavior for different RH values are not so pronounced. The time at which the surface dries out is much shorter than for steel, being less than 3h for RH $\leq$ 75%. At RH = 75% the current decreases slowly from 3 μA to 0.5 μA over a 3h period after the large current drop associated with disappearance of visible electrolyte has occurred. The corrosion loss in this time period as determined by integration of the current-time curve is, however, very small as compared to the initial corrosion period. For Cu/Zn a sharp current maximum is not observed during the drying-out period (Fig. 27), instead the current decreases continuously from high values measured when the electrolyte was placed on the freshly polished ACM surface and dropped sharply when the surface dried out. The results for RH = 30% and 45% are again rather similar. Drying-out occurs after 4h at RH = 75% and about 7.5h at RH = 90%.

In order to evaluate the effects of electrolyte concentration, experiments were performed in which the concentration of Na_2SO_4 was varied from 10^{-1} to 10^{-4} N (Fig.28-31). In both cases the characteristic features for both metals shown in Figs. 24-27 are preserved. With decreasing concentration the current flow decreases. For steel and Cu/steel no clear current maximum is observed at 10^{-4}N. For steel the surface dries out in about 4h at 10^{-1} N and in 3h in 10^{-4} N, for Cu/steel the corresponding times are 6h and 3h. For zinc and Cu/Zn, drying out occurs faster than for steel as observed above (Fig.26 and 27). While the maximum current and the total charge Q increase with RH for both types of sensors, the time for drying out seems to be independent of Na_2SO_4 concentration except for Cu/Zn at C = 0.1N, which is contrary to what was observed for steel and Cu/steel.

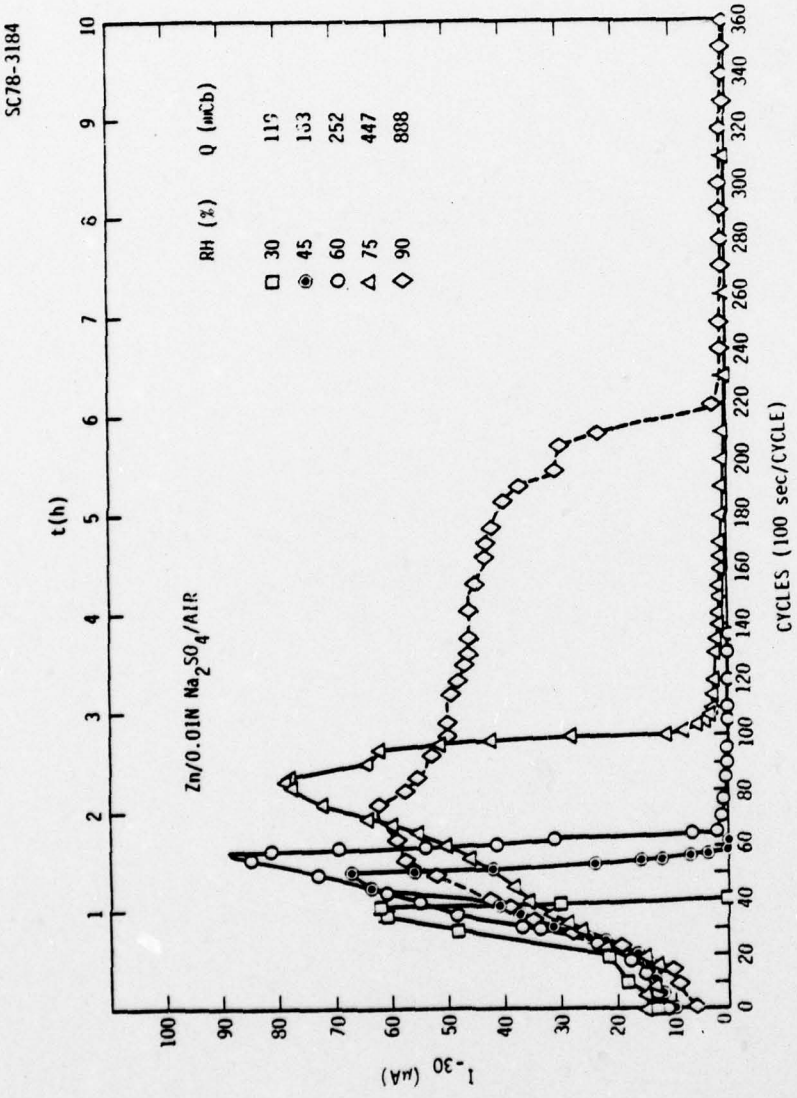

Fig. 26 Current at $\Delta E = \pm 30$ mV for zinc during drying out of 0.01N Na_2SO_4 at different RH values.

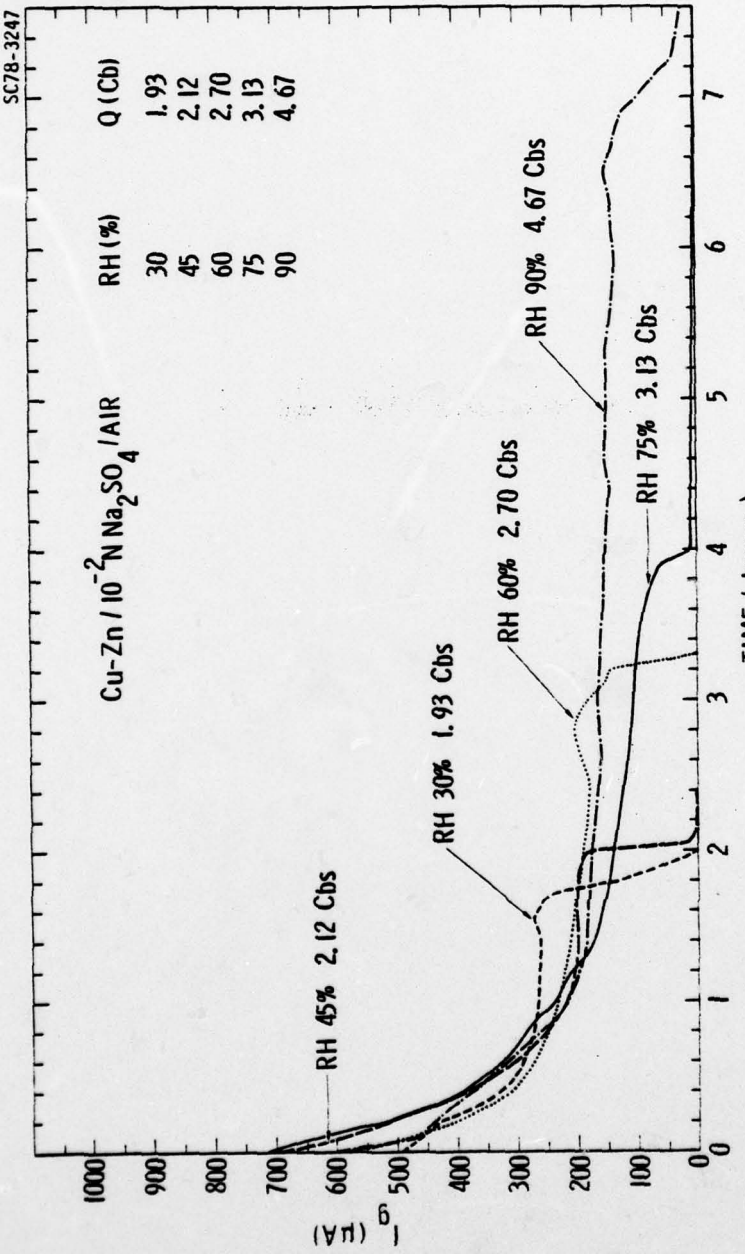

Fig. 27 Current at $\Delta E = \pm 30$ mV for Cu/zinc during drying out of 0.01N Na_2SO_4 at different RH values.

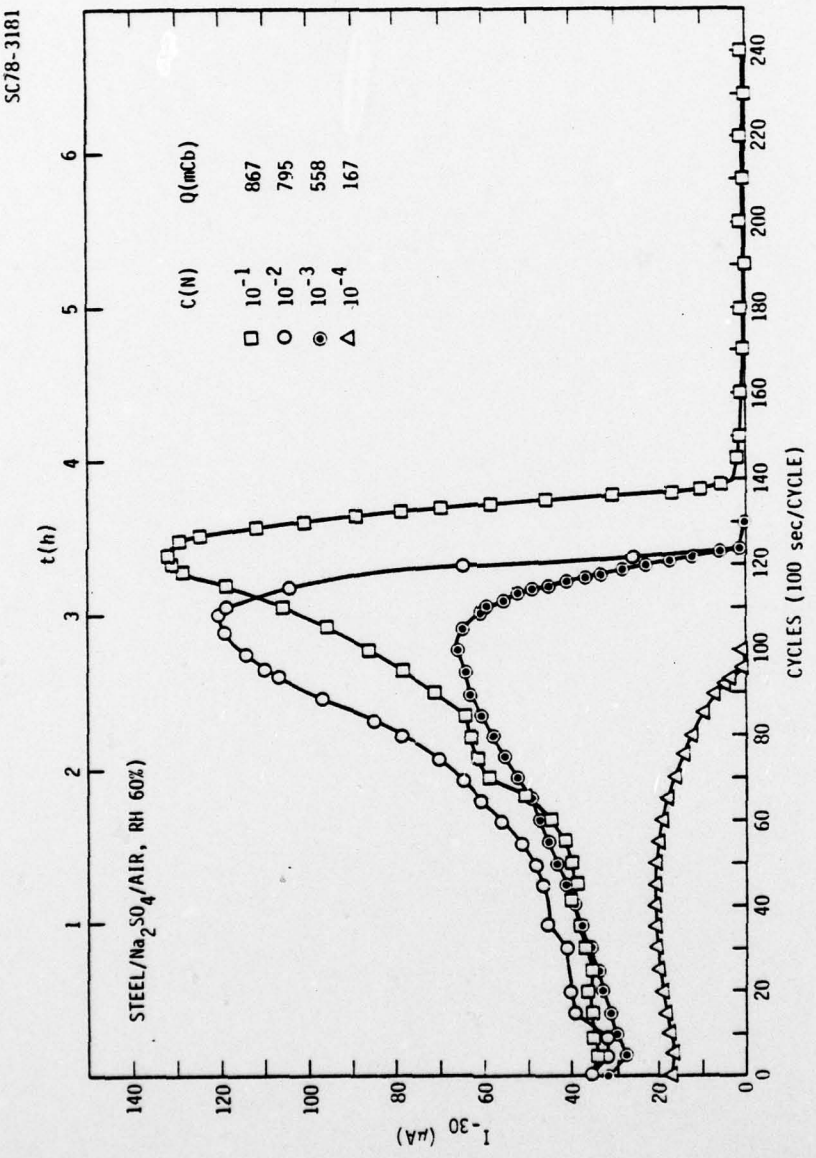

Fig. 28 Current at Δt = ±30 mV for 413U steel during drying out as a function of Na_2SO_4 concentration. RH = 60%, T = 21 ± 1°C.

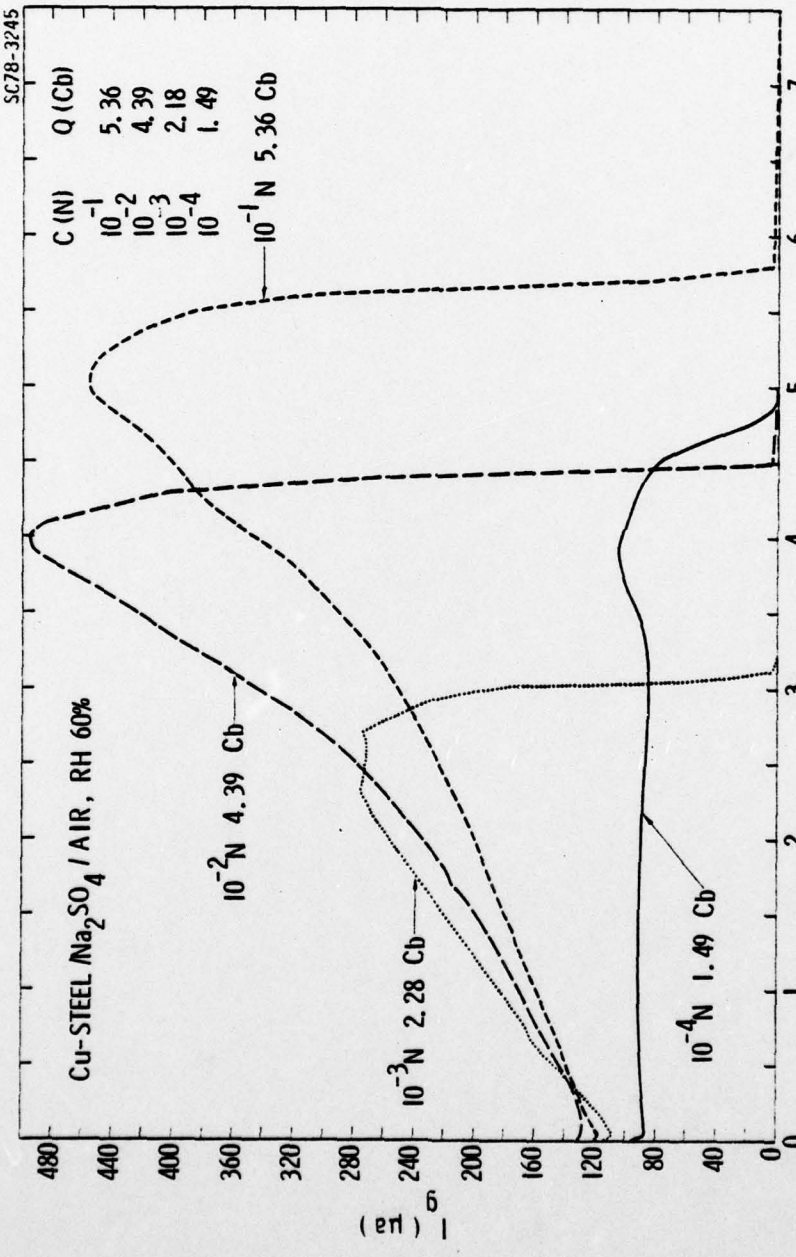

Fig. 29 Current at $\Delta E = \pm 30$ mV for Cu/steel during drying out as a function of Na_2SO_4 concentration. RH = 60%, T = 21 ± 1°C.

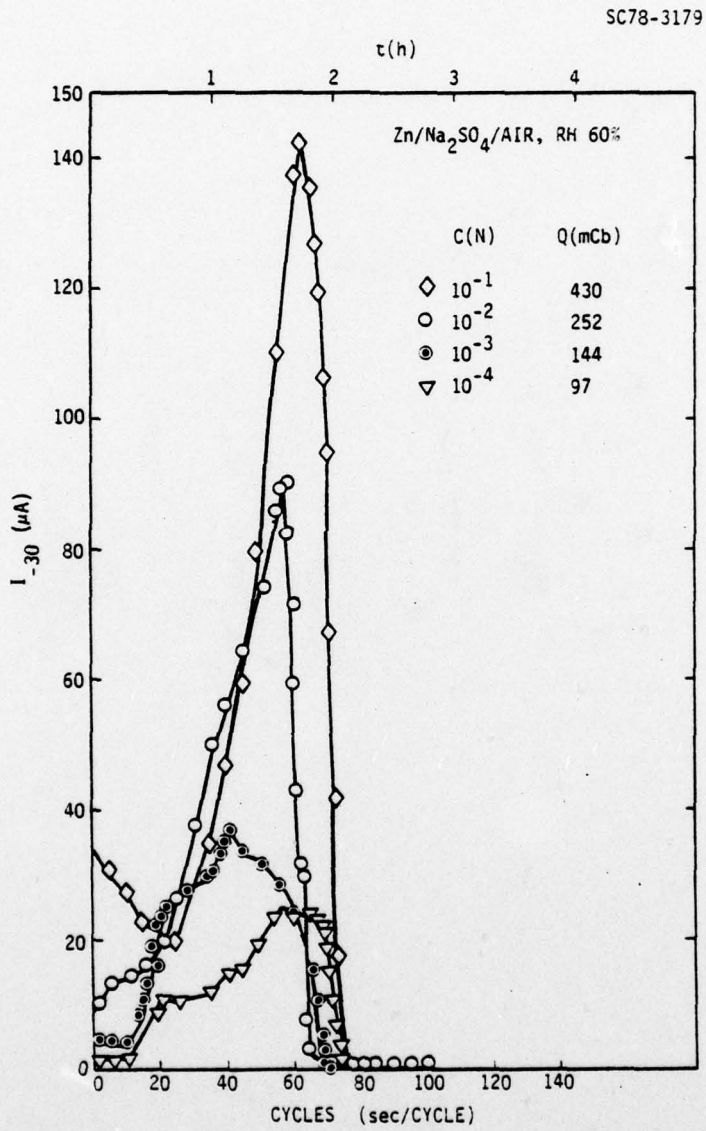

Fig. 30 Current at ΔE = ±30 mV for zinc during drying out as a function of Na_2SO_4 concentration. RH = 60%, T = 21 ± 1°C.

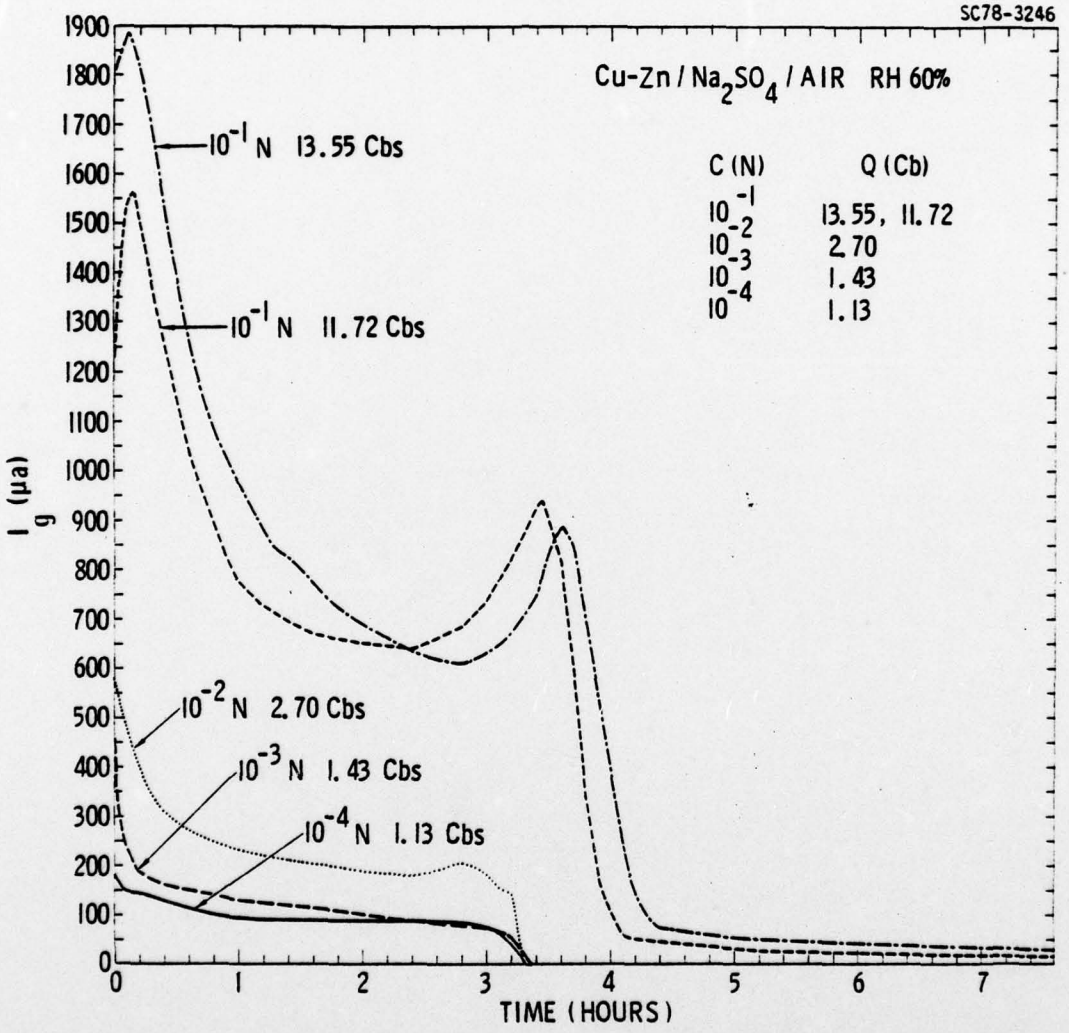

Fig. 31 Current at $\Delta E = \pm 30$ mV for Cu/zinc during drying out as a function of Na_2SO_4 concentration. RH = 60%, T = 21 ± 1°C.

c. Correlations between Weight Loss and Electrochemical Measurements

A correlation between the weight loss data and the electrochemical measurements is important from a mechanistic point of view as well as for interpretation of the data obtained in outdoor exposure of ACMs such as discussed in Task 4. An attempt will be made in the following to establish such correlations by comparing the weight loss Δm with the area under the current-time curve of the electrochemical data. The amount of coulombs Q obtained by graphical integration for steel or zinc ACMs does not correspond exactly to the electrochemical equivalent of the weight loss since the I_{30}-values have not been converted to corrosion currents I_{corr}. The factor k (Eq.15) is not known exactly; moreover, previous results (12) have shown that it changes with time. For a qualitative evaluation of correlations between the two types of measurements (Δm vs. Q), this complication is, however, of minor significance. For the galvanic cells a quantitative relationship should exist provided the corrosion process is diffusion controlled.

The analysis of Cu/steel ACM data for surfaces covered with synthetic rust as prepared or doped with various salts has shown that there is a linear relationship between log I_g and RH [(21),Fig. 12]. The data obtained in the present study show a linear relationship between log Q and RH for the four ACMs under 0.01N Na_2SO_4 in air (Fig. 32) in a form similar to the one discussed above. The slope of the straight line in Fig. 32 is close to +1 except for Cu/steel, where the slope is +1.5.

The dependence of the charge Q on the Na_2SO_4 concentration at RH = 60% is given in Fig. 33 for the two-electrode ACMs (Fig. 33a) and the galvanic ACMs (Fig. 33b). An approximately linear relationship between Q and log c is obtained in both cases; while the charge has similar values for the two galvanic cells, it is about twice as much for the steel ACMs as for the zinc ACMs. The weight loss data obtained for steel and zinc are compared

with the integrated charge in Fig. 34 as a function of RH and in Fig. 35 as a function of electrolyte concentration. For the former case there is a linear relationship with a slope of 3.6 mg/Cb for steel (Fig. 34a) and 1.34 mg/Cb for Cu/steel (Fig. 34b) taking into account the areas of the weight loss sample (25.8 cm^2), the steel ACM (2.3 cm^2) and the Cu/steel ACM (4.6 cm^2)

When weight loss and electrochemical data are compared as a function of Na_2SO_4 concentration, a linear relationship seems to be indicated for zinc with a slope of 1.8 mg/Cb, but not for steel. The dashed line in Fig. 35a corresponds to the slope of the curve for steel in Fig. 24a. A linear relationship is also observed for Cu/steel with a slope of 0.92 mg/Cb.

Due to the scatter of the weight loss data for zinc as a function of RH (Fig. 21a), there is similar scatter in the Δm-Q plots of Fig. 35a.

The comparison of the results obtained with weight loss and electrochemical techniques under identical conditions has shown essentially linear correlations (Fig. 34 and 35). However, the electrochemical data underestimate the corrosion rate - as determined from the weight loss data - to an extent which depends on the type of the measurement and the metal studied. According to Faraday's law a charge density Q = 1 Cb/cm^2 corresponds to 0.29 mg/cm^2 for iron (z=2) and 0.34 mg/cm^2 for zinc (z=2).

The weight loss data have been converted into charge densities Q_{WL} using this conversion factor and are compared in Table VI with the charge densities obtained from the galvanic current (Q_g) and polarization resistance (Q_{30}) measurements. For steel there is a fairly constant ratio Q_g/Q_{WL} of about 0.20 for the RH-dependence and 0.22 for the concentration dependence, which could be called the cell efficiency or "cell factor" as discussed by Kucera (22) who determined in outdoor exposure a cell factor of 15% for steel polarized at ΔE = 100 mV.

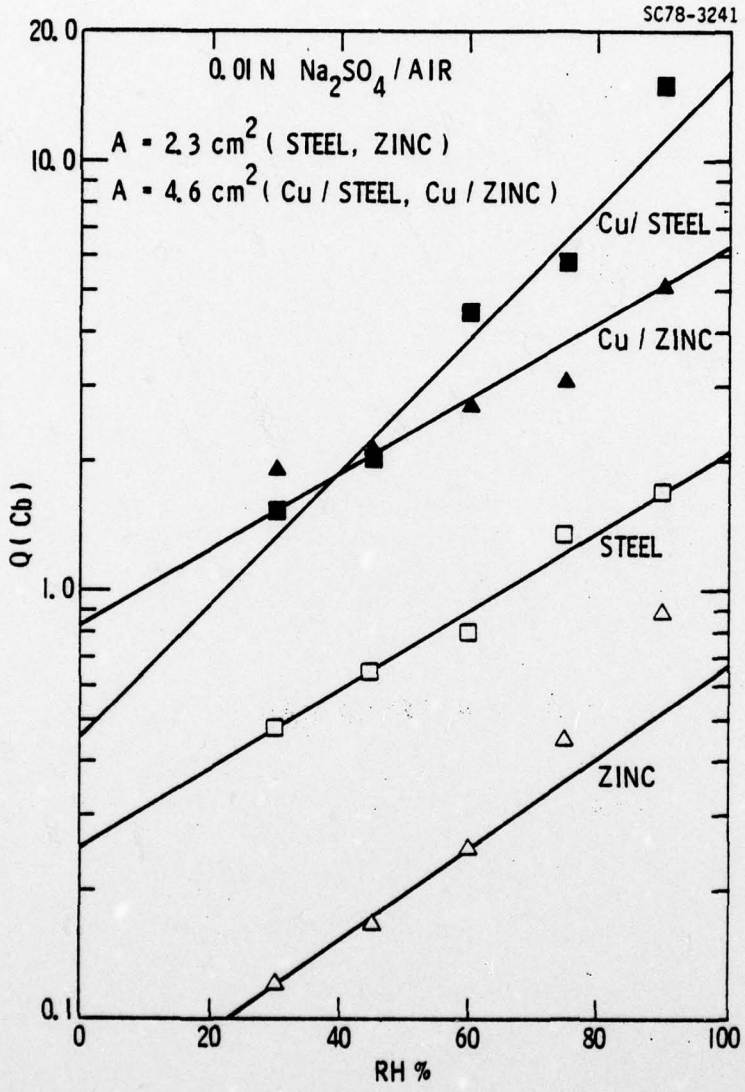

Fig. 32 Integrated current values for steel, Cu/steel, zinc, and Cu/zinc under 0.01N Na_2SO_4 drying out at different RH-values.

SC78-3182

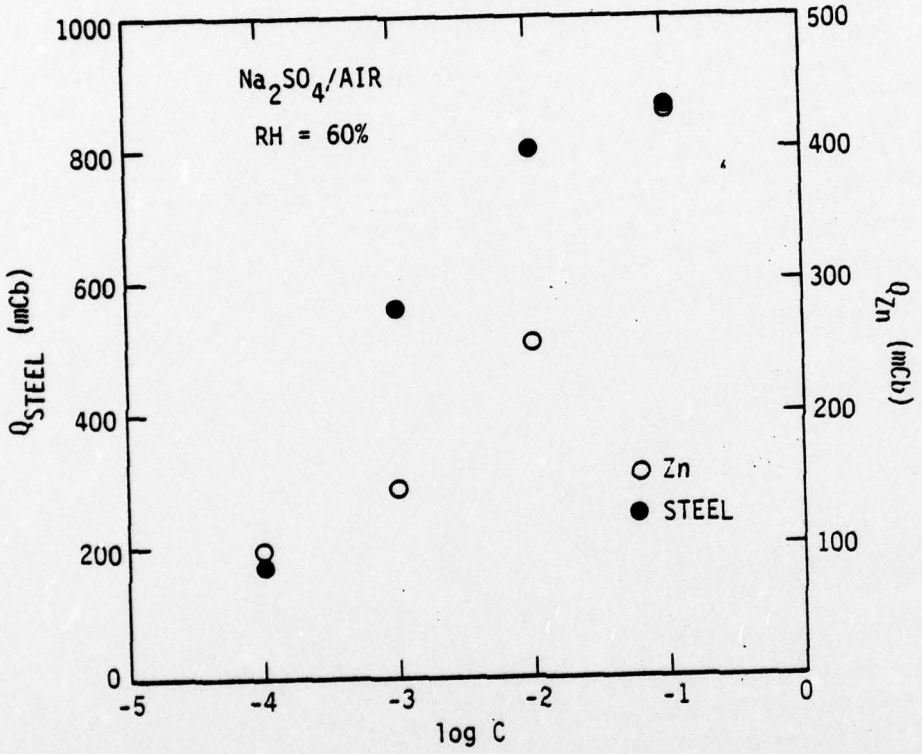

Fig. 33a Integrated current values for steel and zinc (Fig. 33a) and Cu/steel and Cu/Zinc (Fig. 33b) drying out under Na_2SO_4 of different concentration. RH = 60%.

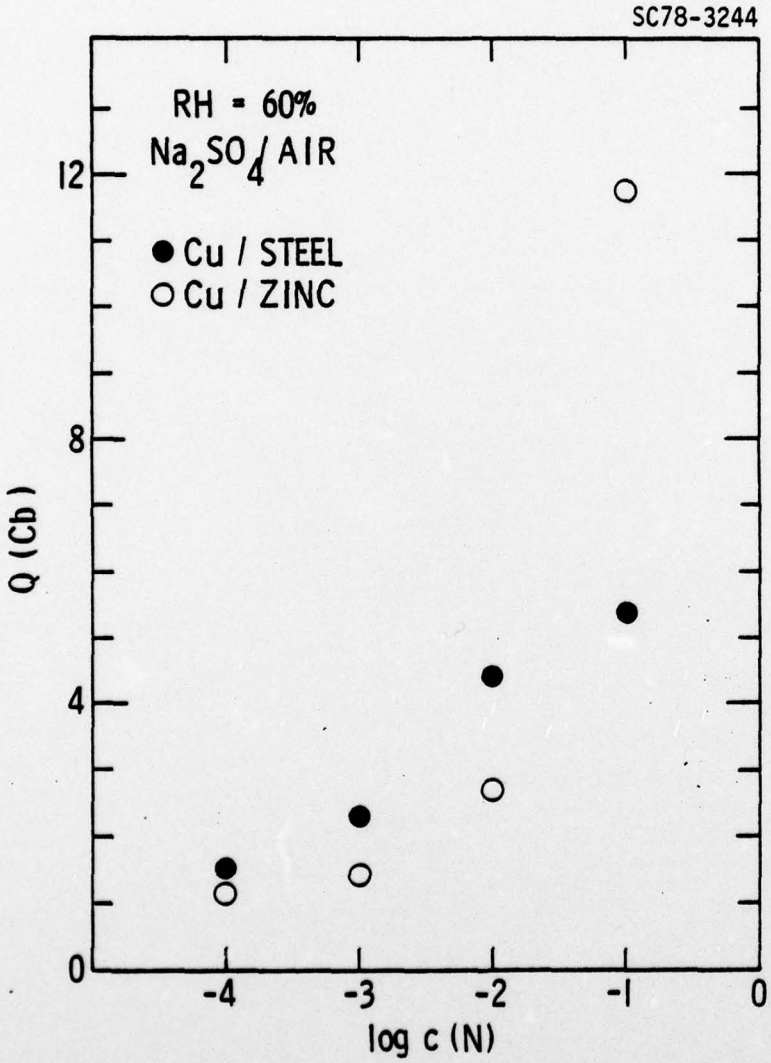

Fig. 33b Integrated current values for steel and zinc (Fig. 33a) and Cu/steel and Cu/Zinc (Fig. 33b) drying out under Na_2SO_4 of different concentration. RH = 60%.

SC78-3178

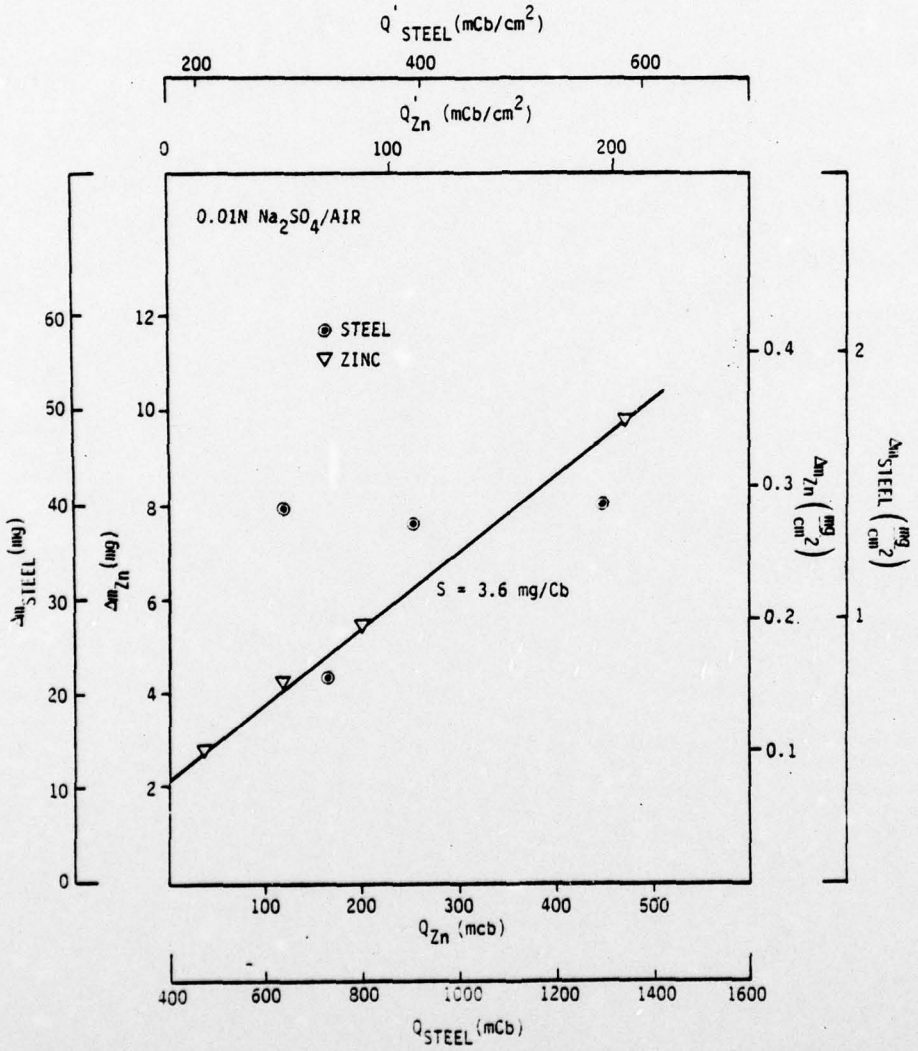

Fig. 34a Correlation between weight loss (Δm) and electrochemical (Q) data for steel and zinc (Fig. 34a) and Cu/steel and Cu/zinc (Fig. 34b) in 0.01N Na_2SO_4 at different RH-values.

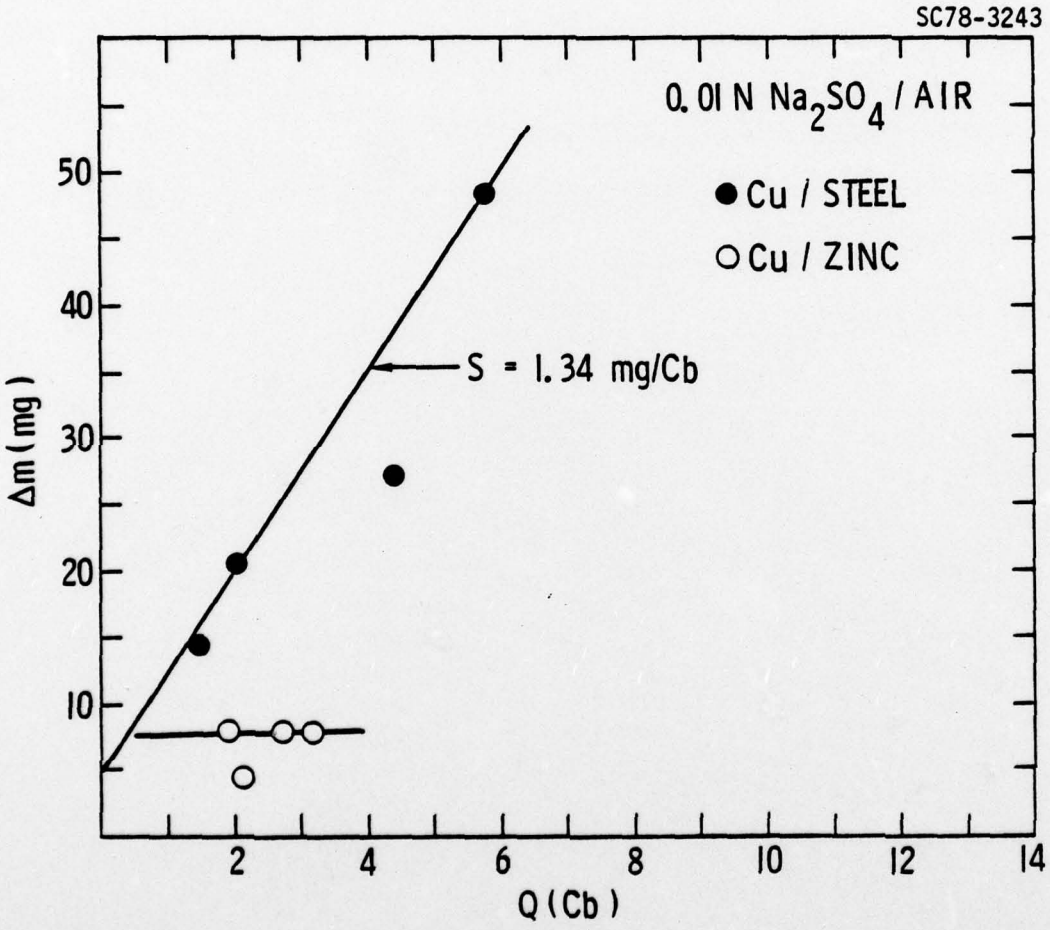

Fig. 34b Correlation between weight loss (Δm) and electrochemical (Q) data for steel and zinc (Fig. 34a) and Cu/steel and Cu/zinc (Fig. 34b) in 0.01N Na_2SO_4 at different RH-values.

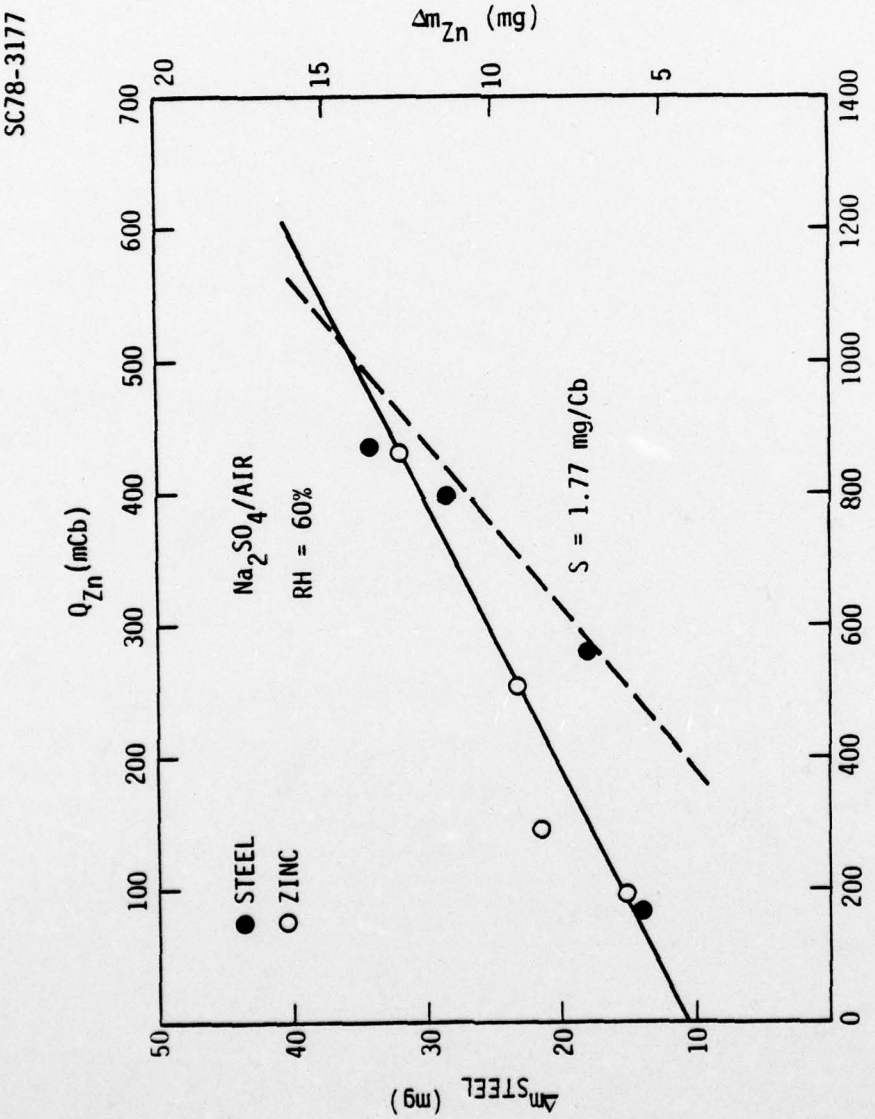

Fig. 35a Correlation between weight loss (Δm) and electrochemical (Q) data for steel and zinc (Fig. 3ba) and Cu/steel and Cu/zinc (Fig. 35b) for different concentrations of Na_2SO_4.

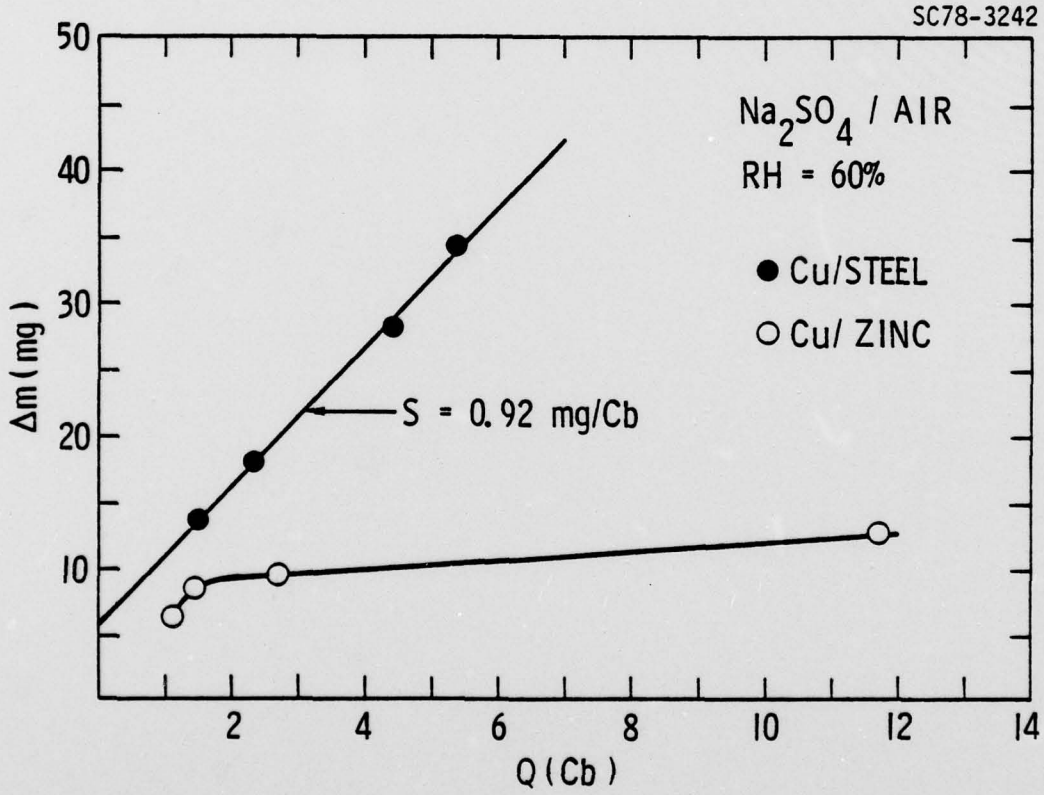

Fig. 35b Correlation between weight loss (Δm) and electrochemical (Q) data for steel and zinc (Fig. 35a) and Cu/steel and Cu/zinc (Fig. 35b) for different concentrations of Na_2SO_4.

AD-A063 922 ROCKWELL INTERNATIONAL THOUSAND OAKS CALIF SCIENCE --ETC F/G 11/6
ELECTROCHEMICAL STUDIES OF ATMOSPHERIC CORROSION.(U)
JAN 79 F B MANSFELD N00014-75-C-0788
UNCLASSIFIED SC5030-7FR NL

2 OF 2
AD
A063922

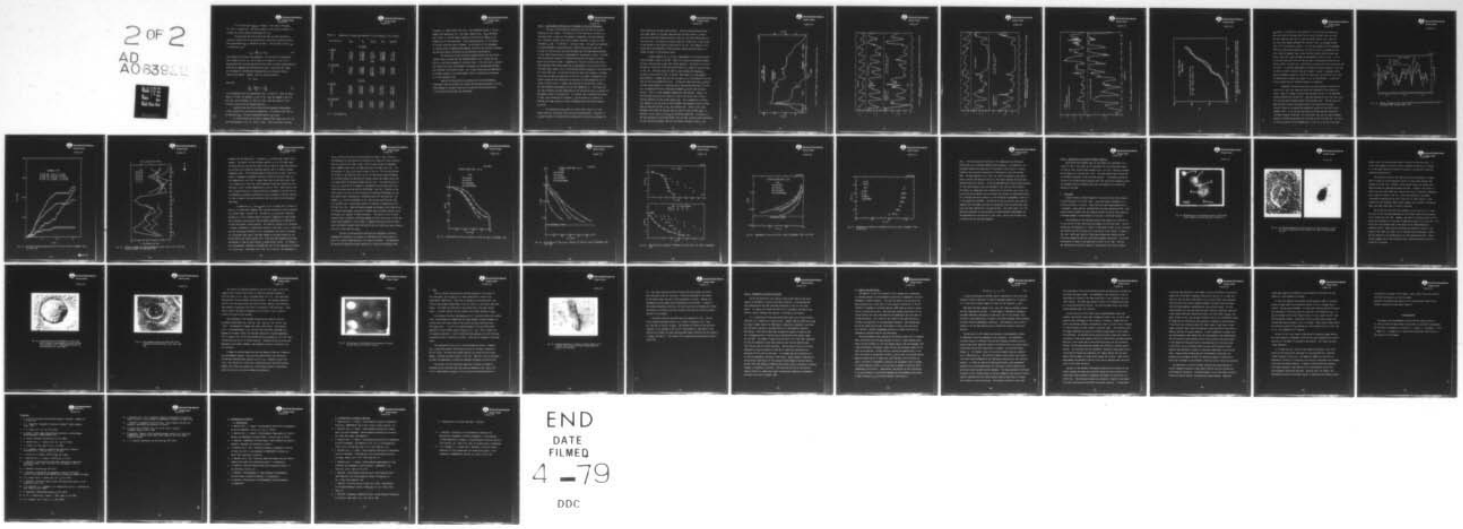

END
DATE
FILMED
4 -79
DDC

For zinc the ratio Q_g/Q_{WL} is larger, in one case (0.1N Na_2SO_4, RH = 60%) it exceeds one. Due to the scatter in the weight loss data, an average cell factor cannot be determined for zinc.

The data obtained with 30 mV pulses have not been converted to corrosion currents due to the uncertainty of the correct conversion factor. The charge density Q_{30} is therefore too small. The corrosion current I_{corr} is related to I_{30} by

$$I_{corr} = \frac{2B}{\Delta E} I_{30} = kI_{30} \qquad (15)$$

The parameter B can have values between B = 6.5 and 52 mV for theoretical Tafel slopes which for ΔE = 30 mV leads to a range of k = 0.43 to 3.47. The Q_{30}-data have to be multiplied with this factor to obtain charge densities which can be compared with the weight loss data. Since the Tafel slopes are not known for the ACM data discussed here, the conversion factor k cannot be calculated. However, since for diffusion control:

$$I_g = I_{corr} \ ,$$

the ratio:

$$\frac{I_g}{I_{30}} = \frac{I_{corr}}{I_{30}} = k = \frac{Q_g}{Q_{30}} \qquad (16)$$

can be determined from the experimental data. As Table VI shows the experimental k'-values fall between 1.5 and 4.4 for steel and between 3 and 13.6 for zinc, which indicates, at least for steel, that the kinetics of the corrosion process show the expected behavior.

Another factor which can affect the electrochemical measurements is the IR-drop due to low solution conductivity. This effect would lead to an effective $\Delta E_{eff} < \Delta E$ and corresponding smaller I_{30} values.

An IR-drop effect can be seen by comparing the weight loss (Fig. 23) and electrochemical (Fig. 33) data for steel. While the weight loss data

TABLE VI. Comparison of Charge Data Obtained in 0.01N Na_2SO_4/air. (Q in Cb/cm^2)

Test Condition	$Q_{W.L.}$	Q_g	$Q_g/Q_{W.L.}$	Q_{30}	$Q_g/Q_{30}=k'$
		A, Steel			
I, RH(%)					
30	1.90	0.320	0.17	0.209	1.53
45	2.75	0.433	0.16	0.276	1.57
60	3.62	0.954	0.26	0.345	2.77
75	6.49	1.254	0.19	0.588	2.13
90	n.d.	3.252		0.746	4.36
			0.20		
II, log c(N)					
-4	1.85	0.324	0.18	0.073	4.44
-3	2.40	0.496	0.21	0.243	2.04
-2	3.81	0.954	0.25	0.346	2.76
-1	4.57	1.165	0.25	0.377	3.09
			0.22		
		B, Zinc			
I, RH (%)					
30	0.89	0.42	0.47	0.05	8.11
45	0.48	0.46	0.96	0.07	6.50
60	0.87	0.59	0.68	0.11	5.36
75	0.90	0.68	0.76	0.19	3.50
90	n.d.	1.14		0.39	2.95
II, log c(N)					
-4	0.70	0.25	0.36	0.04	5.83
-3	0.98	0.31	0.32	0.06	4.97
-2	1.06	0.59	0.56	0.11	5.36
-1	1.45	2.55	1.76	0.19	13.63

n.d. - not determined

increase in a linear fashion with log c, the integrated charge Q decreases steeply with decreasing log c (and lower conductivity). ΔE_{eff} decreases most likely in a similar manner leading to k-values which depend on the conductivity of the electrolyte. A more detailed analysis of the effects of IR-drop cannot be given at present. An evaluation of this phenomenon is planned using AC impedance measurements from which the solution resistance and the polarization resistance can be determined simultaneously.

The discussion of the correlation between weight loss and electrochemical data has shown that the ACM measurements can at present be used only as a qualitative measure of corrosion rates. Since for steel a constant cell factor was found, the necessary corrections can be made when ACM data are converted into corrosion rates. Cell factors should also be determined in outdoor exposure to evaluate whether similar correlations are observed as in the laboratory test.

Despite the uncertainties associated with the electrochemical techniques, they are valuable for research and monitoring purposes to follow large changes of corrosion rates with any desired time resolution which is not possible with weight loss techniques.

Task 4. Electrochemical Monitoring of Atmospheric Corrosion Phenomenon

The task on electrochemical monitoring was initiated at the very beginning of this project. The objective of this task was to collect on a continuous basis a record of the changes of atmospheric corrosion behavior over a period of several years and to analyze these data in terms of time-of-wetness t_w and -- if possible -- corrosion rates. This goal was approached by using atmospheric corrosion monitors (ACM) of the galvanic type (e.g. Cu/steel or Cu/zinc) which have the advantage that the experimental approach is very simple requiring only a measurement of the galvanic current. Provided that the corrosion reaction is diffusion controlled, the galvanic current equals the corrosion current. Integration of the daily current-time curves would represent under these conditions a measurement of the corrosion rate of the anodic metal (steel, zinc) in the ACM and provide a measure of the corrosivity of a given test site. In the work carried out under this contract, corrosion rates have not been calculated due to the lack of a simple, inexpensive integration system and the uncertainty of the exact corrosion mechanism as discussed in Tasks 2 and 3. Instead, the logarithm of the galvanic current I_g has been recorded simultaneously with RH and temperature T. From these data the time-of-wetness has been determined as the time during which I_g exceeds the background current of the amplifier. In addition, for a selected time period in 1978, the distribution of different I_g and RH levels as a function of time has also been obtained in order to determine the relationship between I_g and RH.

The recording of the I_g-data on a daily basis results in a very large variety of information which cannot be reproduced here. Figure 36 is a typical example for formation and disappearance of electrolyte between the

early evening and the early morning hours. Based on the observations made with these sensors it has been concluded that the ACM surface is covered with bulk electrolyte formed from dew in the last five hours before the surface dries out. The drying out process leads to a strong rise in the current as can be seen in the linear I_g-time trace of Fig. 36. This behavior illustrates again the importance of the drying-out process which has been discussed in detail in the previous tasks.

Further examples for I_g, RH and T measurements on the Science Center roof are shown in Figs. 37 and 38. There is an inverse relationship between RH and T, while RH and I_g show very similar behavior. The effect of rain can be seen for 10-30-1975 in Fig. 37a and the effect of a number of very dry days in Fig. 37b. The total hours for which I_g has exceeded the background current are also shown in Figs. 37 and 38. When these early measurements were analyzed, it seemed that the rise and decay of I_g correlated well with the time at which RH exceeded 40% (6,10). It should be noted that both I_g and RH can have large changes in a relatively short time period which makes it difficult to determine the exact relationship between I_g and RH from the daily records. There is close agreement between both time periods; however, as the following discussion will show, RH = 40% is too low for the "critical relative humidity" on the Science Center roof. As an example for a correlation between t_w and the time for which RH $\geq$80%, the cumulative hours for both types of data are plotted in Fig. 39 for March 1977. There is very close agreement which seems to indicate that the time for which an ACM signal is observed is very close to time t_{80} for which RH exceeds 80%. An analysis of the data obtained on the Science Center roof was then initiated which determined for the time period between 1976 and 1978 monthly averages of the t_w- and

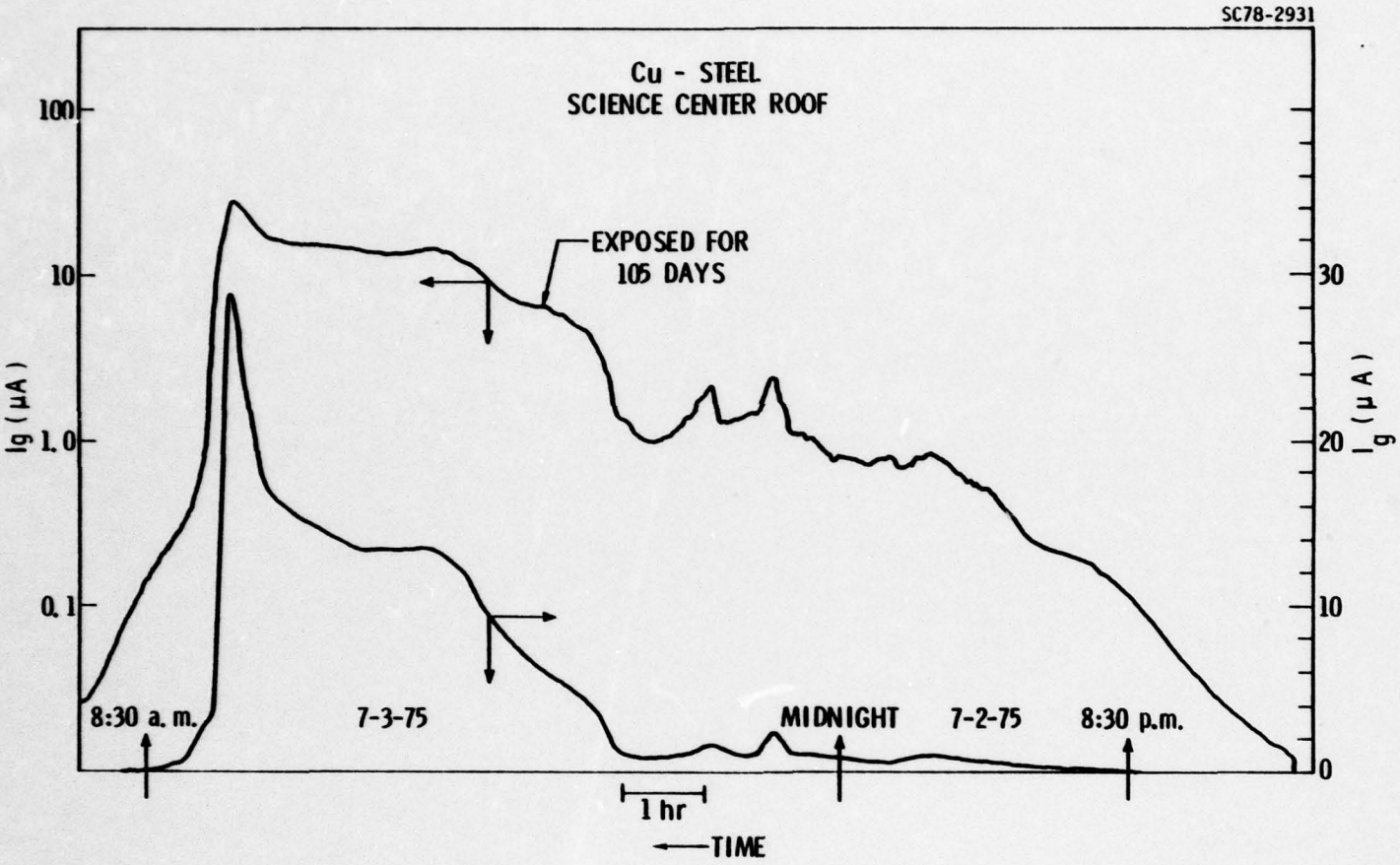

Fig. 36 Typical example for ACM recording on Science Center roof.

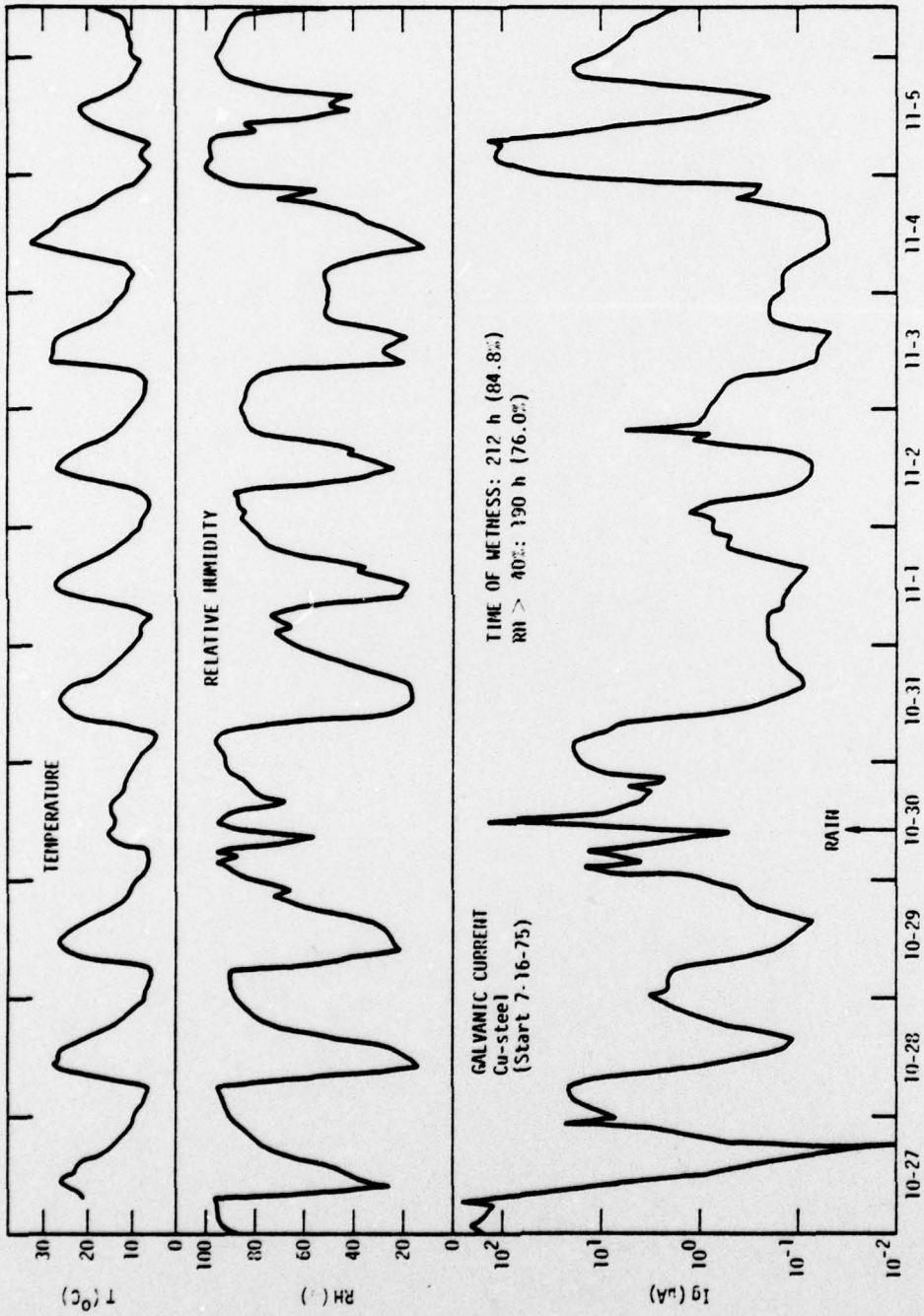

Fig. 37 a Temperature T, relative humidity RH, and ACM output I_g for a 20 period on Science Center roof.

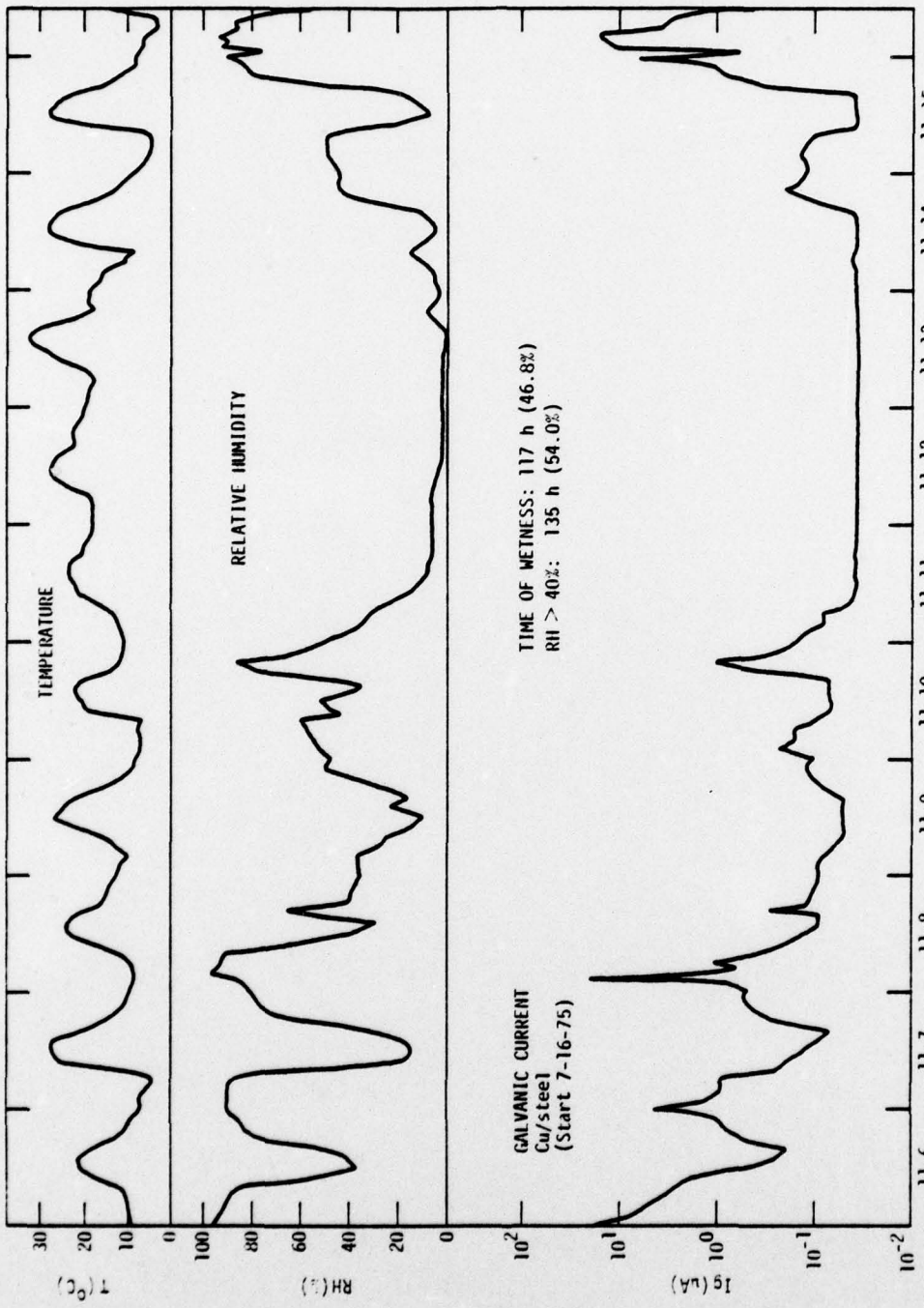

Fig. 37b Temperature T, relative humidity RH, and ACM output Ig for a 20 period on Science Center roof.

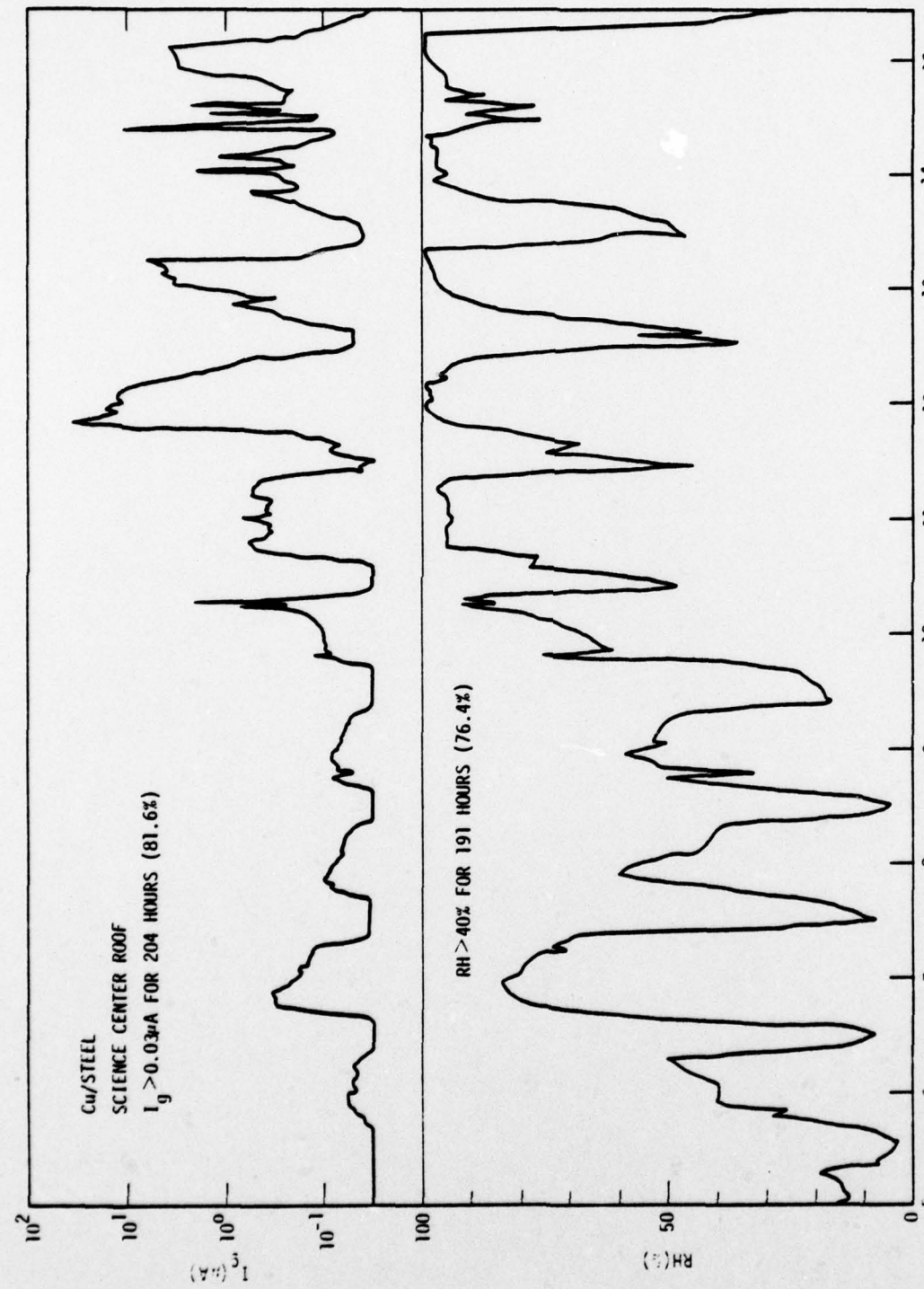

Fig. 38 Further examples for recordings of RH and ACM on Science Center roof.

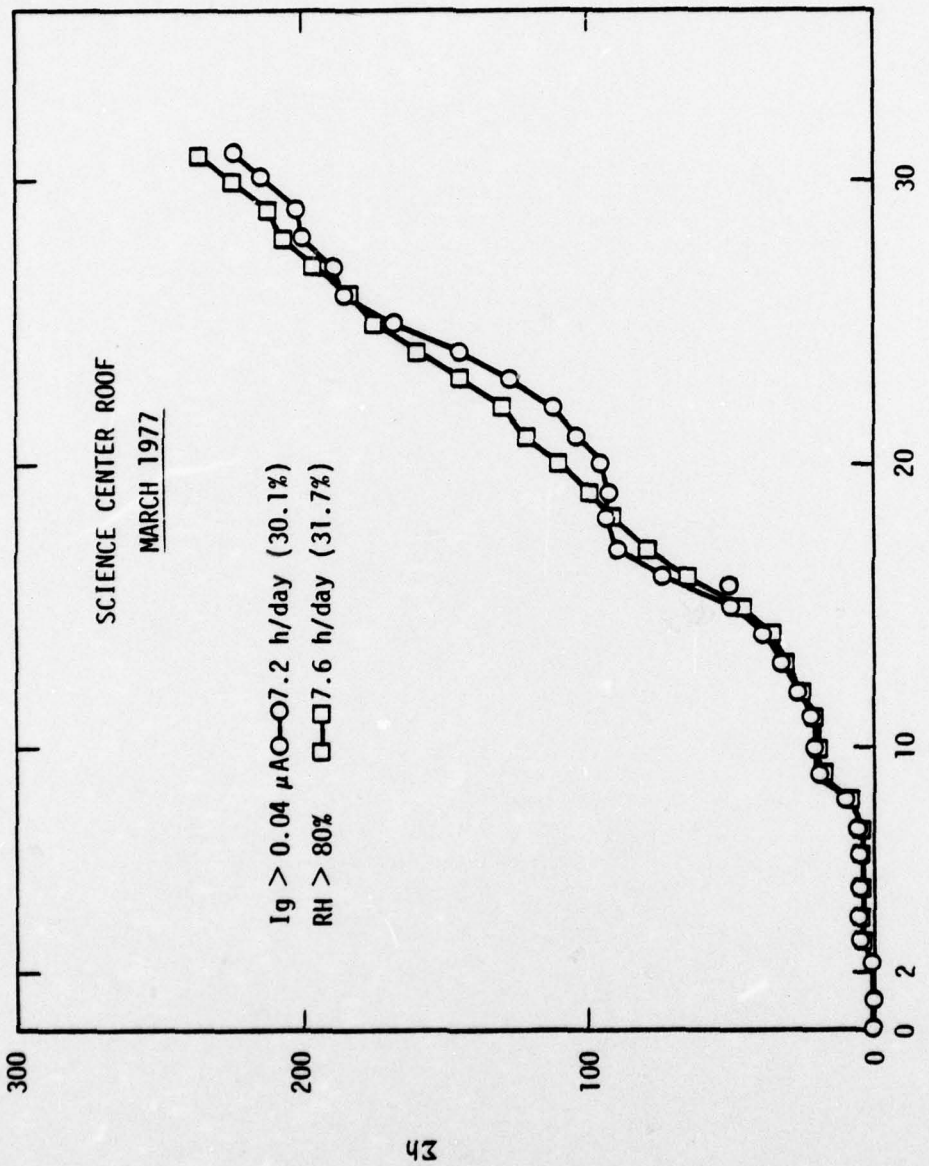

Fig. 39 Cumulative hours for which the galvanic current exceeds the background and RH exceeds 80% for March 1977, Science Center roof.

t_{80}-values. The results of this analysis in Fig. 40 show that average t_w-values as high as 22.8h/day (95%) and as low as 4.5h/day (19%) can occur. For the rather dry year 1977, t_w did not exceed 17h/day (71%), while for the rainy time between December 1977 and April 1978, t_w exceeded 16h/day (67%) for five consecutive months. For the time between June and September 1978 the t_w-data were determined as the time for which I_g exceeded 0.05 μA which leads to somewhat lower values than the previous practice where the time at which the signal exceeded the background current was used. It will be noticed referring to Fig. 36 that for most of the wetness period the corrosion current is rather low; significant corrosion occurs only during the last few hours. It might be advantageous to define the time-of-wetness as the time at which a certain corrosion rate, for example 1μm/year is exceeded, which would correspond to about 0.1 μA/cm^2 for steel and 0.07 μA/cm^2 for zinc. Such an approach would reduce the t_w-data in Fig. 40 considerably. Further discussion concerning this important question is necessary.

Atmospheric corrosion data have also been recorded at several test sites in St. Louis, MO, where the author has conducted a thirty month exposure study of a number of metals and non-metals as part of the RAPS/RAMS program sponsored by the EPA (23). ACMs were exposed at up to four test sites for the time period between October 1975 and March 1977. The ACM signal has been recorded on tape, the present analysis has used hourly averages. Figure 41 shows as an example the cumulative t_w-data for four test sites in December 1976. It can be seen that there are discontinuities reflecting different climatic conditions. For sites #103, 106, and 112 time-of-wetness amounts to 20-30% per day while for site #122 it was less than 10%. In order to relate t_w-data to RH and temperature T, plots of t_w, RH and T have been

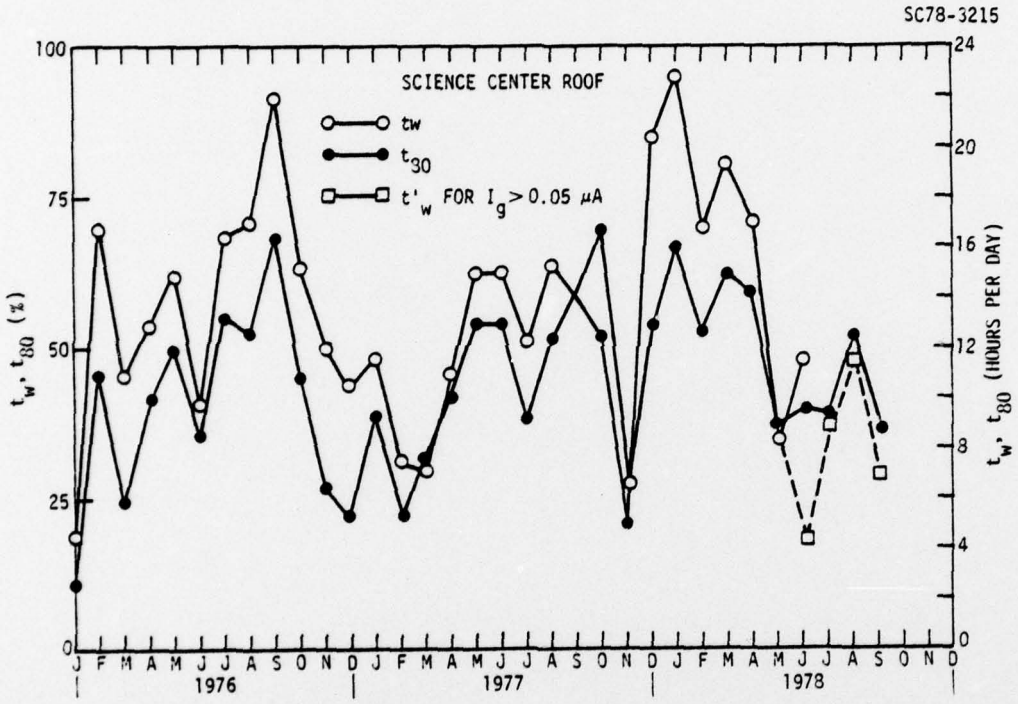

Fig. 40 Monthly averages of the time-of-wetness t_w and the time t_{80} for which RH exceeds 80%, Science Center roof.

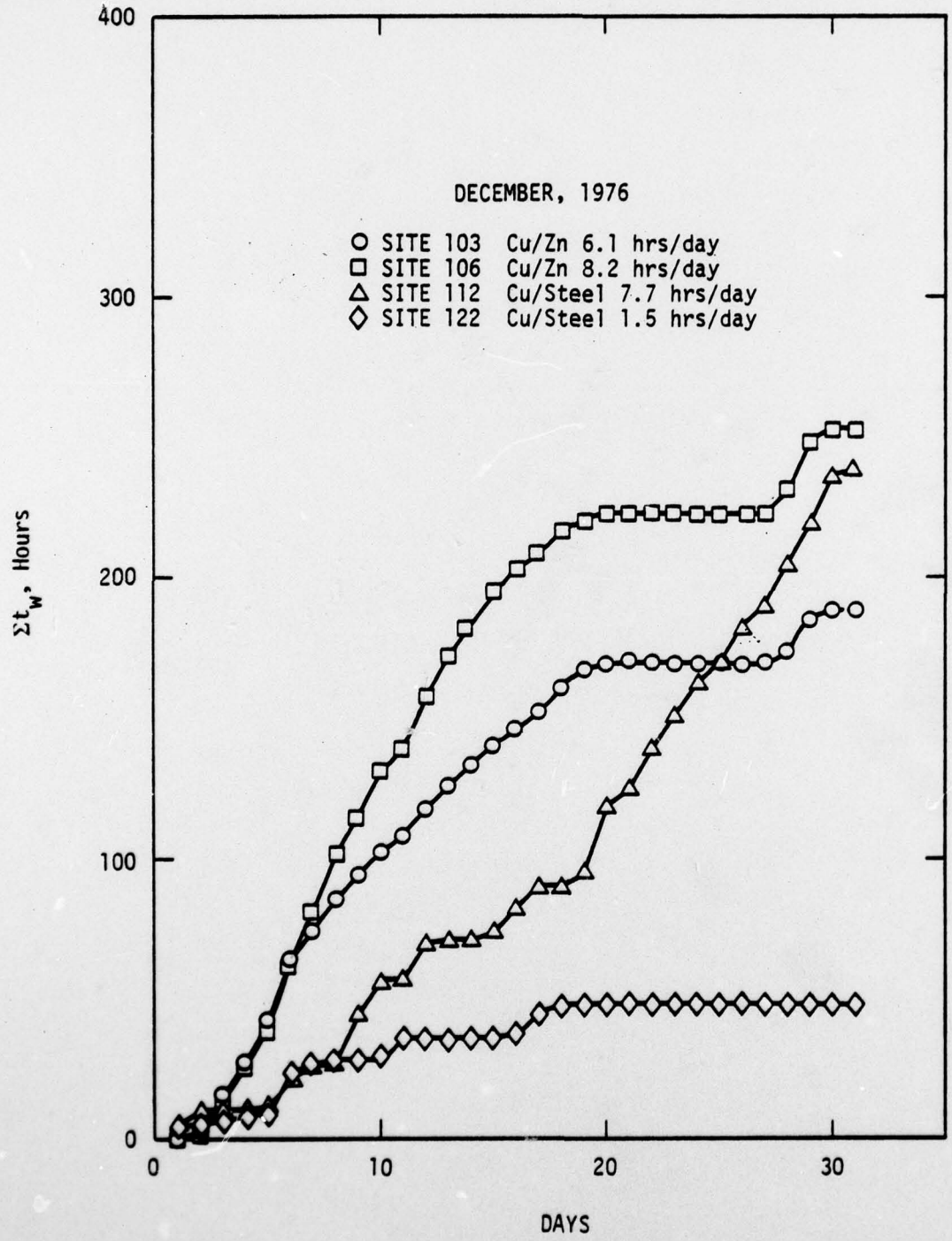

Fig. 41 Cumulative time-of-wetness data for four test sites in December 1976, St. Louis, Mo.

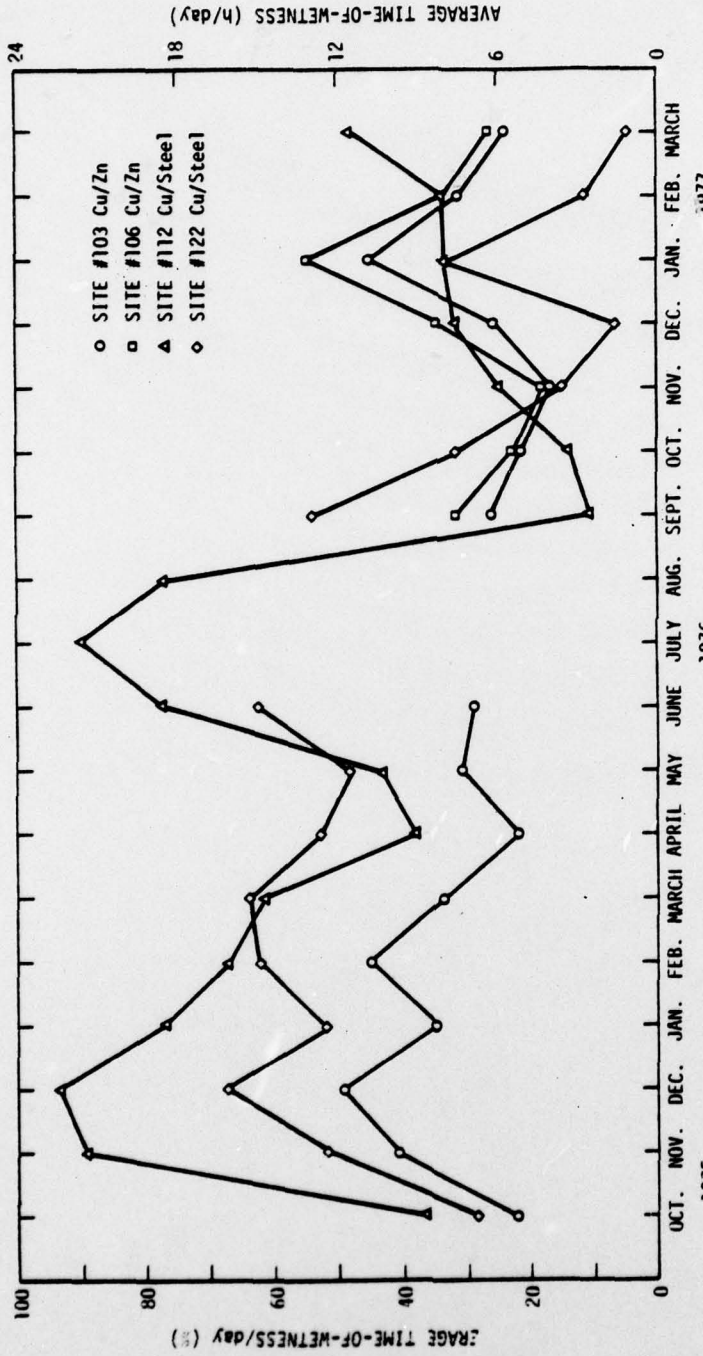

SC78-253

Fig. 42 Monthly averages of time-of-wetness for test sites in St. Louis, Mo. between October 1975 and March 1977.

prepared for the time period. In general, t_w- and RH-values showed similar changes. The reasons for the different behavior at site #112 where some corrosion activity occurred for several days at which no signal was observed at the other sites cannot be explained based on daily or monthly average atmospheric data. This different behavior might be due to small, local variations in atmospheric parameters leading to different periods of dew, etc. The temperature at site #122 is always lower than at the other three sites; it is interesting to note that time-of-wetness values were recorded at site #103 even at daily average temperatures as low as -10°C. These results show that a detailed analysis of factors leading to atmospheric corrosion has to use atmospheric parameters determined as hourly averages or shorter intervals in order to explain the results obtained with the sensitive electrochemical techniques.

A comparison of t_w- and t_{80}-data in Fig. 40 shows that in almost all cases t_w is higher which suggests that a better correlation could be obtained for an even higher "critical" RH. The data for I_g and RH were, therefore, analyzed in a still different manner following a suggestion of Peter Serada, who is heading a task group on time-of-wetness measurements in ASTM G01.04, in which the author is participating. Two identical galvanic cells developed in Sereda's laboratory in Canada which consist of very small (1.20 x 1.25cm) gold and zinc electrodes fabricated like an integrated circuit which are mounted on a galvanized steel panel, have been exposed at the same location as the Cu/zinc ACM on the Science Center roof. Plots have been prepared which show the percent of time for which RH and I_g exceed certain levels. For Sereda's cell the potential difference ΔE between gold and zinc was measured and plotted in a similar way. From these plots (Figs. 43, 44 and 45), the dependence of

log I_g on RH and ΔE on RH can be constructed as shown in Figs. 46 and 47. The RH-percent of time curve has a characteristic shape with almost identical data for June and July 1978, a small shift to lower values for September and a somewhat larger shift to higher RH-values for August (Fig. 43). The distribution of log I_g with time is shown in Fig. 44. For the distribution of ΔE data for the two Au/Zn cells in Fig. 45 relatively large differences for different months are observed with August having the highest values and also some smaller differences between the two cells. The resulting plot of log I_g as a function of RH suggests an exponential relationship with significant corrosion occurring only for RH $\geq$70-90%. (Fig. 46). Contrary to the Au/Zn results (Fig. 47) for which there are no definite differences for the four months under investigation, differences occur for the Cu/Zn ACM. For example, I_g = 0.05 μA corresponds to RH = 82% for July and 93.5% for June. For the Au/Zn cells a measurable potential difference is observed only for RH $\geq$ 90% (Fig. 45). These differences between two designs, which might be due to different measurement principles, different mass, different spacing of the electrodes, etc. deserve further evaluation. The result in Fig. 47 which indicates that a potential difference between Au and Zn exists only in the very narrow range between RH = 90 and 100% is somewhat surprising since the laboratory and outdoor exposure data obtained with galvanic AMCs have shown corrosion activity at much lower RH values.

The task on electrochemical monitoring of atmospheric corrosion phenomena has produced a vast amount of information which can be used as a basis for a better understanding of this type of corrosion. Instrumentation for monitoring purposes has been tested over a time period exceeding three

SC78-3212

SCIENCE CENTER ROOF / Cu-Zn

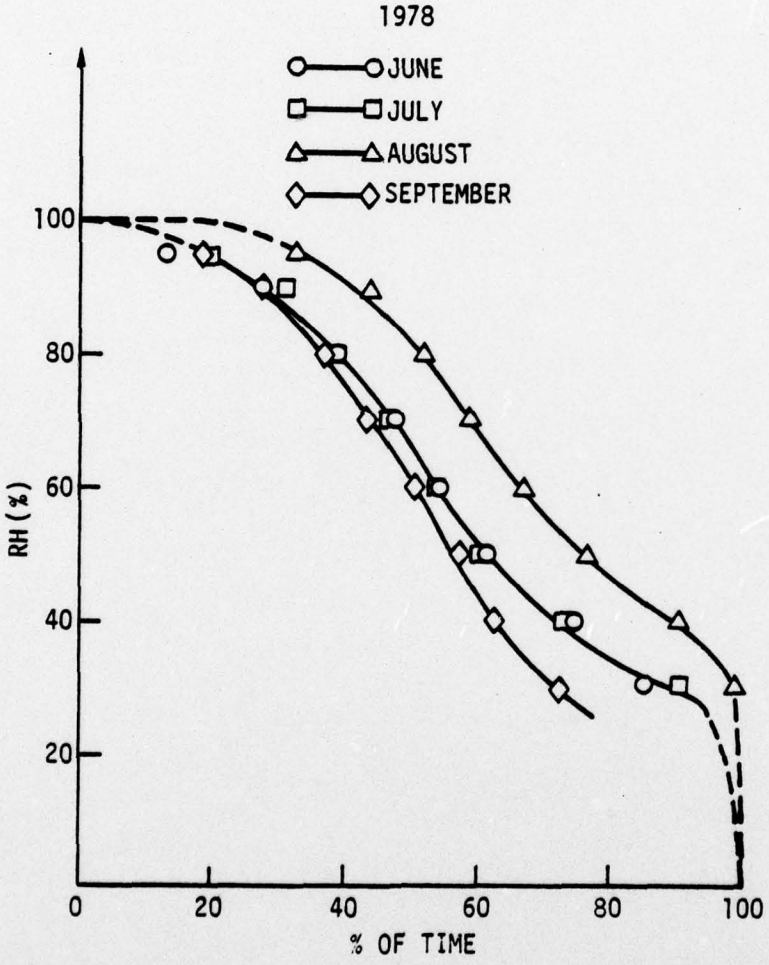

Fig. 43. Distribution of RH as a function of time for June to September 1978.

SC78-3213

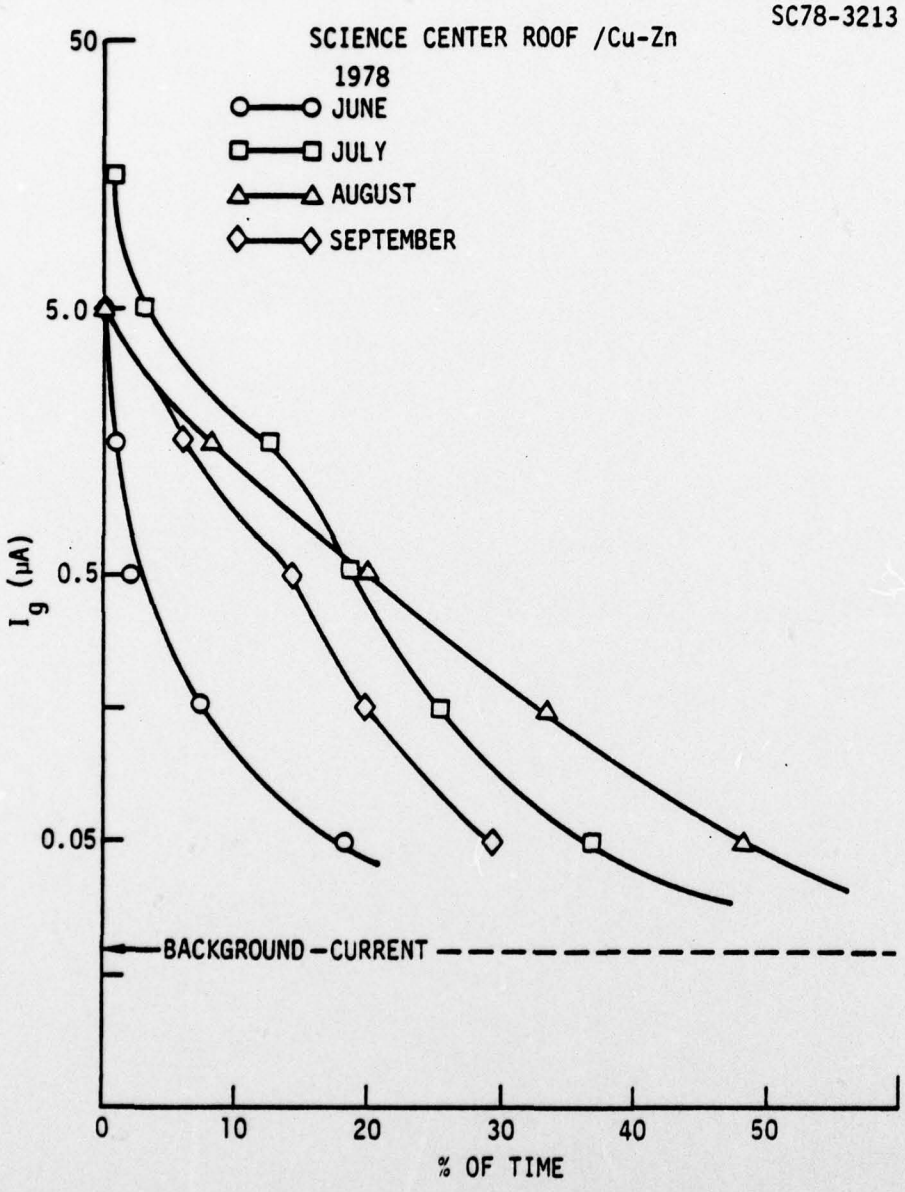

Fig. 44 Distribution of log I_g as a function of time for June to September 1978, Cu-Zn ACM.

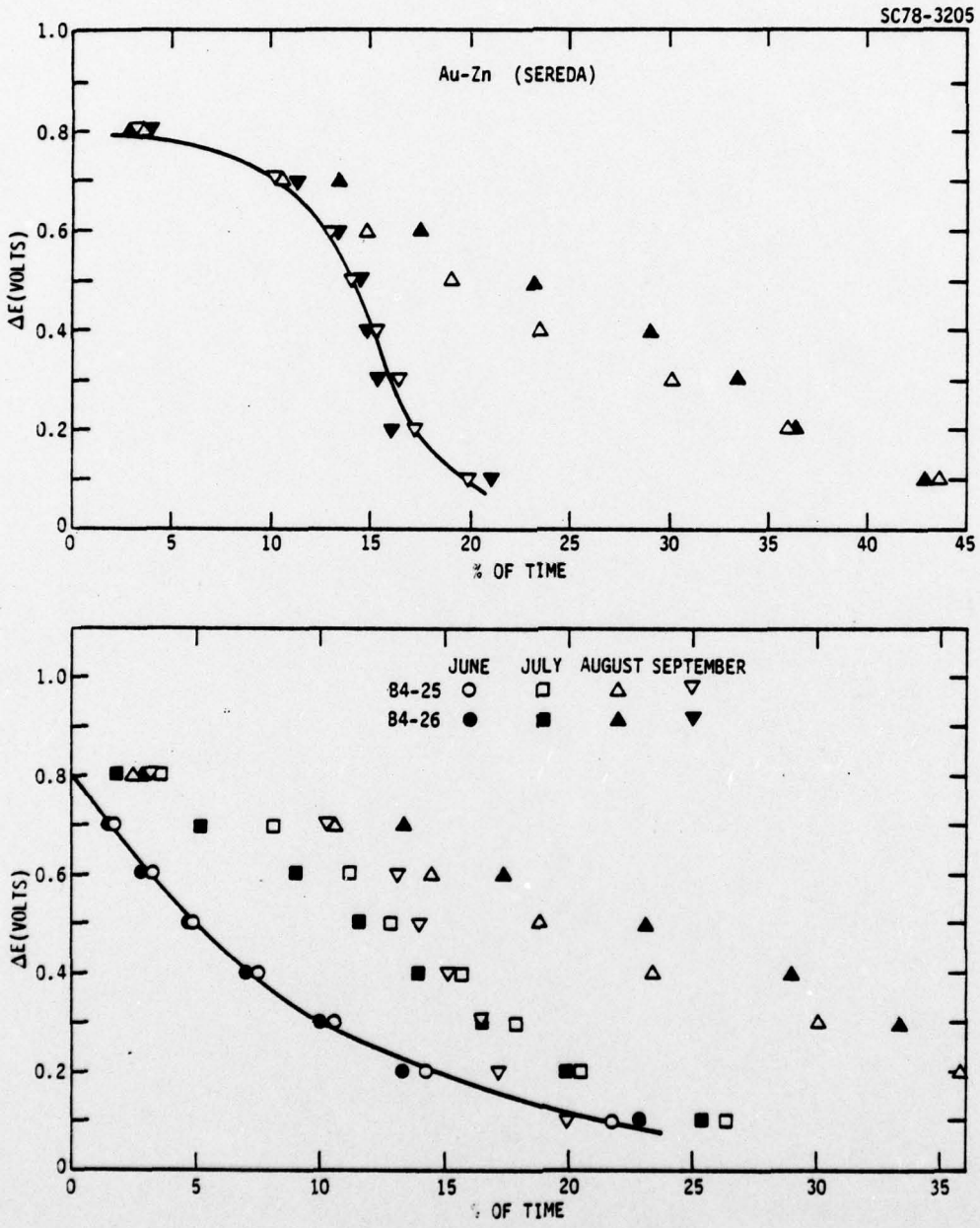

Fig. 45 Distribution of potential difference in Au-Zn cells for June to September 1978.

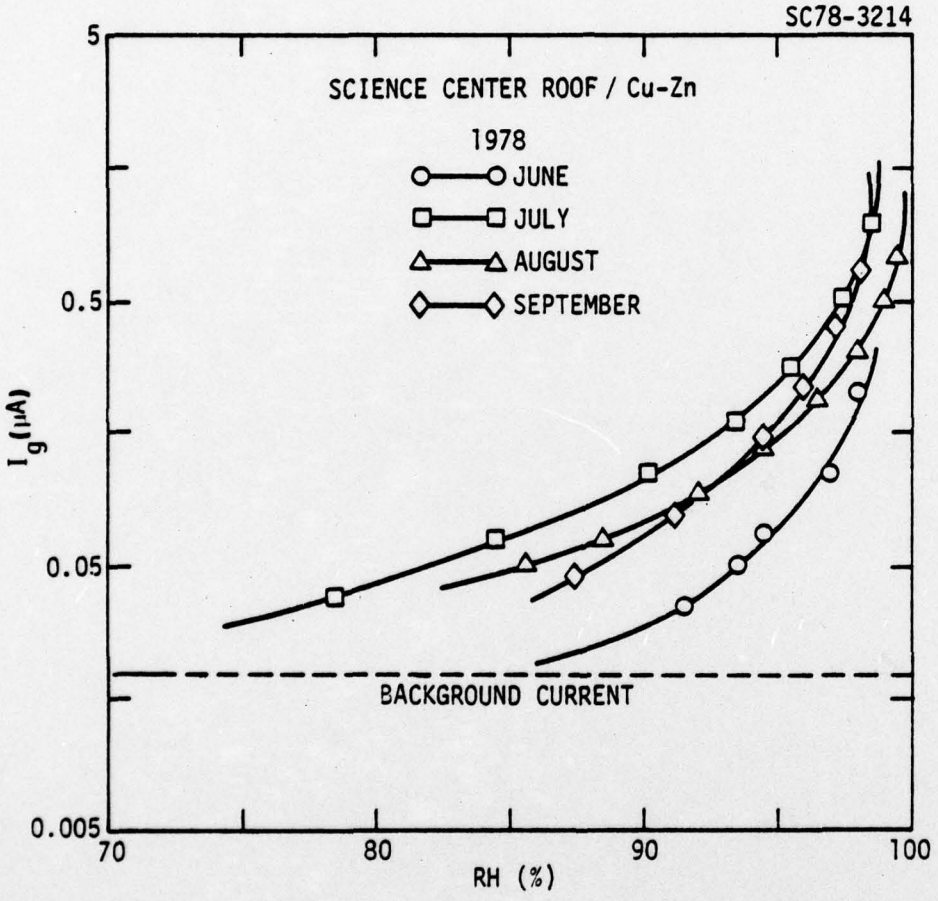

Fig. 46 Dependence of log I_g on RH for June to September 1978, Cu-Zn ACM.

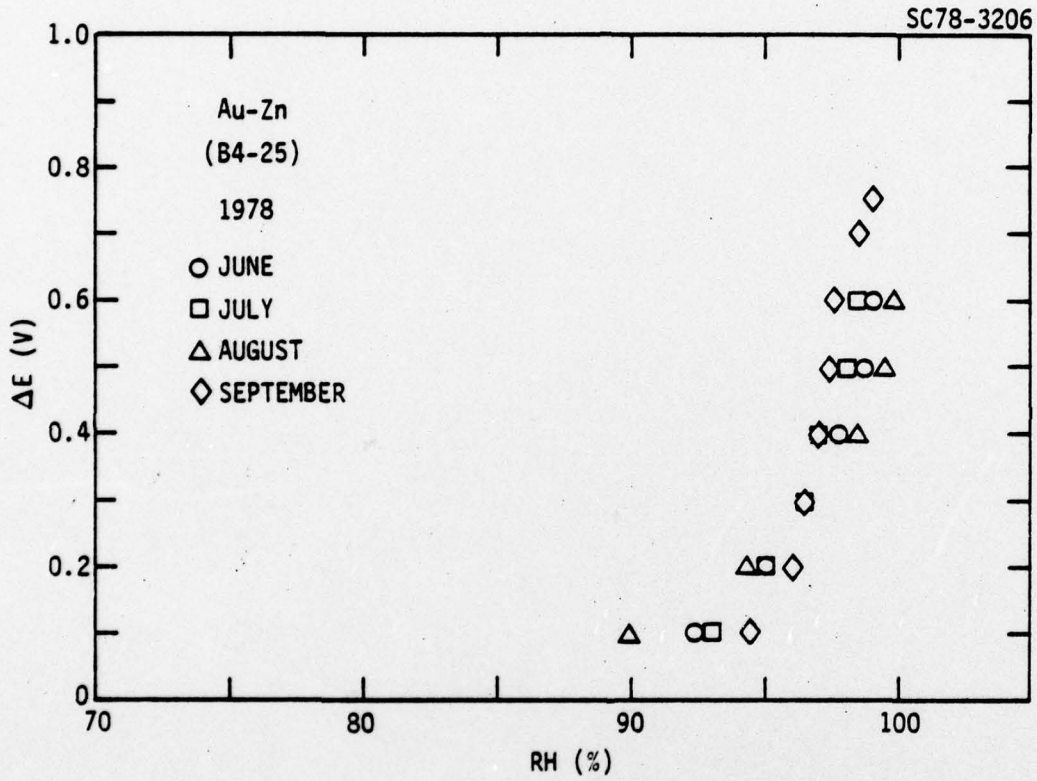

Fig. 47 Dependence of potential difference on RH for June to September 1978, Au-Zn cells.

years. From the continuous recording of RH, temperature and ACM output correlations can be obtained between these parameters. An exponential relationship between the logarithm of the galvanic current, which is closely related to the corrosion rate, and RH is indicated for Cu/Zn and Cu/steel ACMs. The data obtained in St. Louis, Mo. were not analyzed in any detail under a previous EPA contract and only a few time-of-wetness data have been prepared under this contract. Since the RAPS/RAMS data contain minute averages for the electrochemical data and atmospheric data such as wind direction, wind speed, RH, temperature and concentration of pollutants such as SO_2, H_2S, O_3 and particulate matter such as sulfates and nitrates, an opportunity exists for a thorugh statistical analysis of the influence of atmospheric conditions on the response of the ACMs. The results of such an analysis could then be compared with the weight loss data for weathering steel and galvanized steel which have been compiled for a 30 month period. This would result in a very important evaluation of the usefulness of electrochemical measurements for the determination of corrosivity of test sites. Due to lack of funds such an analysis has not yet been prepared.

Task 5. SAM Analysis of Corrosion Product Chemistry

Duplicating the procedure used for the weight loss experiments discussed in Task 2, 4130 steel and Zn specimens with thin electrolyte layers (0.5 mm) on their surfaces were exposed to air, air plus 1 ppm SO_2, nitrogen, and nitrogen plus 1 ppm SO_2 (RH = 75%). The dried samples were transferred to the SAM for analysis of the corrosion products. The exposure period was limited to 30 minutes because exposure until the surface had completely dried out produced corrosion products which were non-conductive as evidence by charging in the SAM.

a. 4130 Steel

Figure 48 shows a photomicrograph of the steel surface after exposure to distilled water in air (RH = 60%). Localized attack originated at inclusions at points 1, 4 and 5. These inclusions were approximately 50 μm in diameter; Auger analysis indicated that they were chromium sulfide. Rust spread radially outward from the chromium sulfide initiation sites reaching a maximum diameter of approximately 0.5 mm after a 30 minute exposure.

The morphology of the attacked surface after exposure to 0.01N HCl in air was similar to that resulting from exposure to distilled water. The difference was the presence of a "crater" in the center of most of the rust spots. The chromium sulfide inclusion was in the center of the "crater" as shown in Fig. 49a. Sulfur was found in a wide region around the chromium sulfide inclusions suggesting that the inclusions underwent dissolution. The sulfur distribution is shown in the Auger map of sulfur in Fig. 49b. Chlorine was detected over the entire region of the bottom of the crater; however,

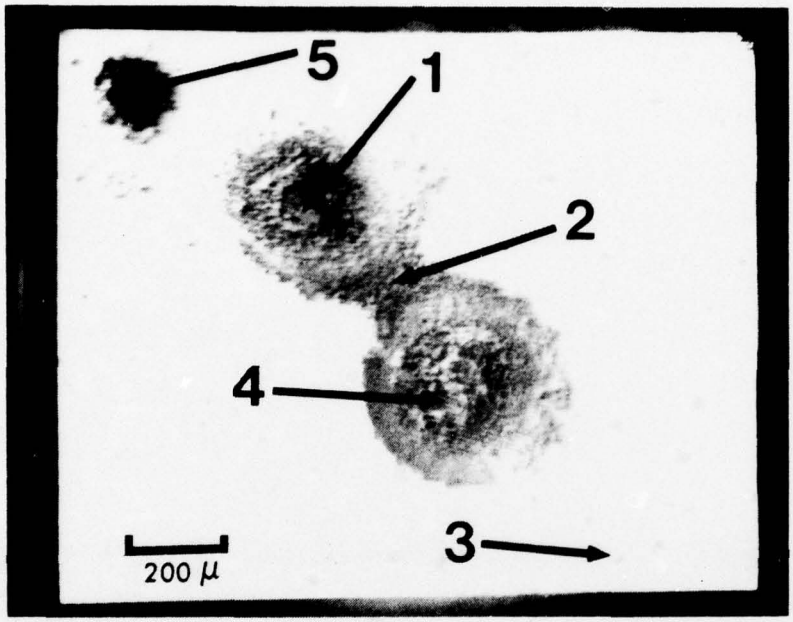

Fig. 48 Morphology of the attacked surface of 4130 steel after exposure to distilled H_2O in humid air.

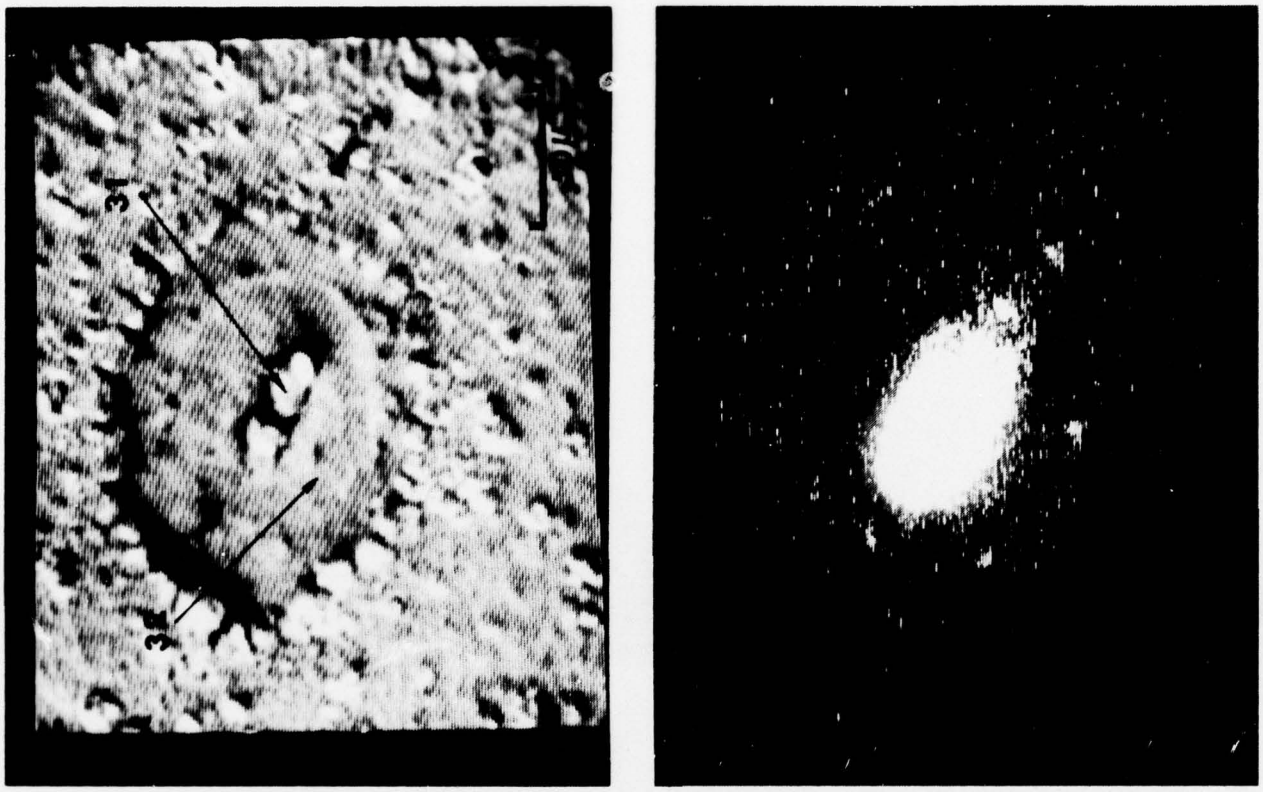

Fig. 49 (a) Photomicrograph of attacked region of 4130 steel with 0.01N HCl layer on the surface, (b) Auger sulfur map of region shown in (a).

neither sulfur nor chlorine were found in regions outside the crater. It is not clear whether the crater results from metal dissolution, or whether it is the region which was originally occupied by the partially dissolved chromium carbide particle.

The attacked surface of the steel resulting from exposure to a H_2SO_4 layer in humid air had an appearance similar to that which resulted from exposure to an HCl film. However, unlike the HCl results no craters were observed where the substrate had been dissolved. Instead in the center of some of the rust spots there was a region which had a "salad bowl" appearance. Such a region is shown in Fig. 50. Sulfur was detected in the bottom (indicated by spectrum 78) but not on the walls of these regions. Since chromium was not observed, these results suggest that corrosion initiated at some sites where there were no sulfide inclusions.

The surface of 4130 steel after exposure to dist. H_2O in air + 1 ppm SO_2 (Fig. 51) has the same appearance as the surface resulting from exposure to air without SO_2 (Fig. 48). However, two types of initiation sites for corrosion were observed as in the case of exposure to H_2SO_4 in air (Fig. 50). The particle in the attacked area in the center of the photomicrograph is chromium sulfide. Auger analysis indicated the presence of sulfur in the center of the other rust spots, but no chromium could be observed. Sulfur was not detected in the mounded area or on the unattacked surface. These results suggest that in the presence of SO_2, sulfide inclusions are not required for initiation.

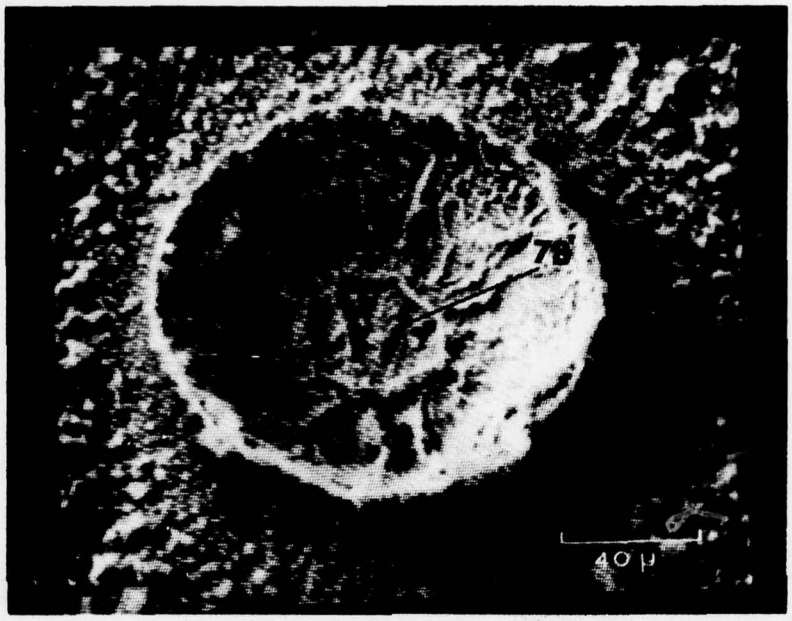

Fig. 50 Unattacked area in the center of a rust spot which resulted from exposure to a thin surface film of H_2SO_4 in air. Note polishing mark at the bottom of the "salad bowl."

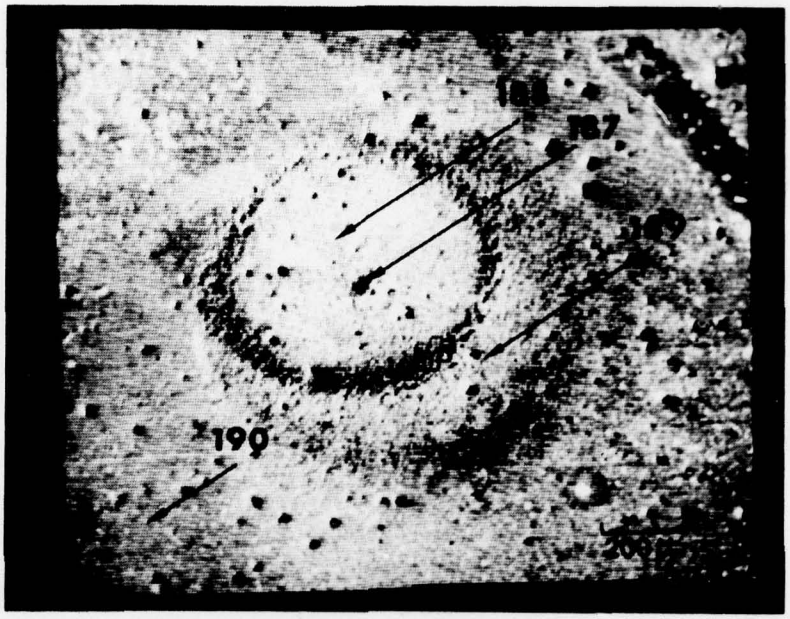

Fig. 51 The attacked surface of 4130 steel after exposure to distilled H_2O in air and 1 ppm SO_2.

The results for specimens exposed to SO_2 with thin layers of HCl and H_2SO_4 on their surfaces were similar to those for specimens exposed to distilled water in air + SO_2 as discussed above (Fig. 51). Rust spots were observed both with and without sulfide inclusions. The specimen exposed to the HCl layer had chlorine over the entire surface; whereas, that which had been exposed to H_2SO_4 had sulfur only in the center of the rust spots. These results differ from those for exposure to acid layers in air in that no craters were found on the surfaces.

The morphology of the attacked surface was the same for the four N_2 exposure experiments (N_2 + H_2O, N_2 + SO_2 + H_2O, N_2 + HCl, and N_2 + SO_2 + HCl). The mounded disc shaped rust spots, which result from exposure to air in the experiments in air, did not occur when steel specimens were exposed to nitrogen; rather, the attacked surface had a stained appearance. This is shown in Fig. 52 for the specimen which was exposed to a thin HCl layer. The particles are ferric or ferrous chloride. Chromium sulfide particles were observed on the surface; however, they apparently were not initiation sites for corrosion.

A change in surface composition occurred whenever there was a change in the environmental species. High chloride concentrations over the entire surface were observed after exposure to HCl in N_2. Exposure to H_2O or HCl in N_2 + SO_2 resulted in a high sulfur concentration over the entire surface. However, the sulfur was present only in the surface layers of the surface oxide film since it was quickly removed by sputtering.

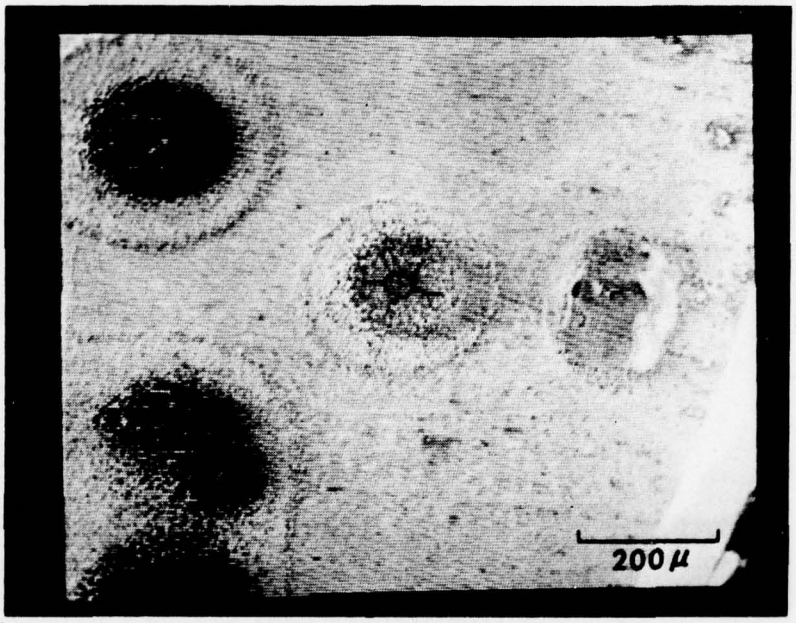

Fig. 52 The surface of 4130 steel after exposure to a thin surface layer of 0.01 N HCl in N_2.

b. Zinc

The zinc (99.9%) specimens which had been exposed to thin layers of distilled water, HCl or H_2SO_4 in air were covered with a uniform film approximately 2000Å thick. There was no evidence of localized attack. The films on the surfaces formed under a thin HCl layer or a thin water layer were oxides. The former had chlorides on the surface and in the near surface layers. A sulfate surface film was formed on the sample exposed to H_2SO_4.

The surfaces resulting from exposure to air + SO_2 had uniform zinc sulfate films. No difference in composition was found between corrosion products resulting from a thin water layer on the surface and that resulting from a thin H_2SO_4 layer. Figure 53 is a photomicrograph of the Zn surface after exposure to a thin surface layer of H_2SO_4 in air + SO_2. This is typical of all exposure conditions. The film resulting from exposure to a thin HCl layer contained chloride in addition to sulfate. There was no evidence of localized attack.

The substitution of N_2 for air did not change the results. Whenever SO_2 or H_2SO_4 were present, the surface film was zinc sulfate; otherwise it was zinc oxide. No attack was evident when HCl was placed on the surface; however, chloride ions were present in the film. When this film was sputtered by argon ion bombardment, chloride was detected throughout the entire film.

The results for 4130 steel have shown that corrosion initiated at chromium sulfide inclusions when the steel was exposed to dist. H_2O or HCl in air. When exposed to H_2SO_4 in air or to any of the three solutions in

Fig. 53 Photomicrograph of a typical surface region of Zn surface after exposure to thin surface layer of H_2SO_4 in air and SO_2.

air + SO_2, both chromium sulfide inclusions and areas without inclusions were initiation sites for corrosion. Sulfate was detected in the center of the latter areas, but not in the surrounding rust areas. Heimler and Vannenberg (24) have made similar observations with the SEM. A repeat of the present experiments with pure iron which would have eliminated the sulfide inclusions as initiation sites for corrosion could not be carried out before the end of this project.

Initiation sites for corrosion were not observed for zinc. The corrosion product contained sulfate in all cases of exposure to air + SO_2, N_2 + SO_2 and, of course, to H_2SO_4. The presence of sulfate in the corrosion products of zinc exposed to HCl in air + SO_2 probably is the reason of the similarity of weight loss data obtained under these conditions and for exposure to H_2SO_4 (see Task 2). The sulfate film is apparently more protective than an oxide film.

Task 6. Atmospheric Corrosion Literature

During the duration of this program, publications dealing with basic aspects of atmospheric corrosion have been collected. A bibliography has been prepared which has been published separately as part of this final report. 171 papers are listed with the title of the paper, the name of the authors, journal reference and abstract if provided by the authors.

It is interesting to note that before 1950 usually only one and before 1960 only 2 or 3 papers are listed per year. Between 1960 and 1969 the average was about 5 papers except for 1968 where a symposium on atmospheric corrosion was held which resulted in the publication of an ASTM Special Technical Publication. From 1970 on more than 10 papers are usually listed per year. This increased activity is mainly due to contributions from Europe, Japan and the USSR. The number of papers from the USA is still very small averaging two per year compared to more than three per year from the USSR and more than five per year from other countries. The low level of activity in basic atmospheric corrosion research in the USA is surprising considering the importance of this form of corrosion. It is hoped that more attention will be paid to atmospheric corrosion in the future. Recent symposia organized by the principal investigator of this project (Electrochemical Society Meeting October 1978, NACE Research Conference March 1979) seem to indicate an increased interest in atmospheric corrosion. The Corrosion Division of the Electrochemical Society is organizing a major international symposium on atmospheric corrosion to be held in October 1980.

D. Summary and Conclusions

The emphasis in the initial phases of this program was on developing an improved approach to electrochemical monitoring of atmospheric corrosion phenomena in outdoor exposure. This work was based on results which had been obtained prior to the start of this project on evaluation of the performance of atmospheric corrosion monitors (ACM) based on galvanic couples such as Cu-steel and Cu-zinc. ACMs have been exposed continuously on the Science Center roof since 1976 where RH and temperature have also been recorded ontinuously. As a result of this effort it has been possible to validate the usefulness of the experimental approach. ASTM Subcommittee G01.04 has asked the principal investigator to lead a task group which will develop a standard recommended practice for outdoor monitoring of atmospheric corrosion based on the ACM concept.

The electrochemical data obtained on the Science Center roof in Thousand Oaks, California have also been analyzed in terms of time-of-wetness data which are now available for the time between January 1976 and September 1978. Large fluctuations from month to month and for the different seasons of the year can be observed. Further analysis involved the determination of the daily variations of the galvanic current I_g and RH over a four months period. Based on these results it seems that a well defined critical RH does not exist, variations in atmospheric conditions can presumably lead to changes in surface chemistry which in turn can lead to changes in the RH at which condensation first occurs. Nevertheless, the analysis of the distribution of I_g and RH leads to a correlation between the two parameters which shows a steep increase of I_g with RH for RH$\geq$70% in the form of:

$$\log \log I_g = c_o + c_1 \cdot RH \qquad (18)$$

It would be desirable to perform similar experiments at test sites with different climatic conditions in order to determine whether Eq. 18 applies in all cases and to obtain numerical values for the constants c_o and c_1.

ACMs have also been exposed in St. Louis, Mo. where an exposure program has been conducted for the EPA. A large number of atmospheric parameters have been monitored continuously at each test site in this project, which provides a unique opportunity to develop correlations between time-of-wetness, corrosion rates and atmospheric conditions. Unfortunately, due to lack of funding it has not been possible yet to perform the necessary statistical analyses.

The main part of this project was devoted to electrochemical studies of atmospheric corrosion phenomena in the laboratory. The atmospheric corrosion process is different from the more frequently studied corrosion process under total immersion insofar as corrosion occurs only during certain time periods during which electrolyte is present - to so-called time-of-wetness t_w. The chemical nature of corrosion products plays an important role in determining t_w. The corrosion reaction occurs within thin electrolyte layers which condensate at RH < 100% due to the action of the corrosion products. In order to study this complicated process a new experimental approach had to be developed which can simulate as close as possible the conditions occurring under natural exposure. The few experimental techniques discussed in the literature have all serious drawbacks, the classical electrochemical technique for thin-layer studies cannot be used since it creates the situation of crevice corrosion. The approach utilized in this study

took advantage of the existing ACM design which was modified to provide two- and three-electrode systems. The advantage of this technique is that all electrodes are located in the same plane which is very important for thin layer studies. Such ACMs were exposed in glass cells through which humid air at any desired RH was flowing. SO_2 could be added using a gas mixing system designed under this contract.

In the first set of thin layer studies potentiodynamic anodic and cathodic polarization curves were recorded for steel, zinc, Cu and Al under layers of NaCl and Na_2SO_4 of 100 to 1000 μm thickness. Normal Tafel behavior was observed contrary to Rosenfeld's results (2) with little influence of layer thickness on Tafel slopes or corrosion rates. The limiting current for oxygen reduction was found to be directly proportional to the inverse film thickness. By determining the corrosion kinetics under thin layers as a function of time using computer analysis of polarization resistance measurements (12) it was found that as the electrolyte layers dry out and become thinner, the corrosion mechanism changes from diffusion to charge transfer control. The corrosion rate can, therefore, increase to some extent during the drying out process but eventually will remain smaller than one would expect from the amount of oxygen which reaches the surface. These kinetic measurements are believed to be the first results reported under the conditions of thin layer corrosion.

Analysis of the ACM data from outdoor exposure and the results of the kinetic studies had shown that corrosion during the drying out period of electrolyte layers presents an important contribution to the overall corrosion loss. The drying-out process was, therefore, studied in more detail using the two-electrode polarization resistance technique. A large amount

of data has been obtained in this manner in which the effects of electrolyte composition (0.01N NaCl or Na_2SO_4), additions of SO_2 (0.1 or 1.0 ppm) and nature of the test metal (4130 steel, zinc, Cu and Al 6061) were evaluated. These data were also used to determine whether corrosion rates calculated from the electrochemical represented the true corrosion rates. For this purpose weight loss data were obtained under identical conditions using horizontal plates which were covered with layers (0.5 mm) of NaCl, Na_2SO_4, HCl, H_2SO_4 (0.01N) or dist. H_2O and were allowed to dry out at different RH values. By comparison with weight loss data obtained in exposure to bulk solutions it was found that corrosion under thin layers leads in most cases to much higher corrosion rates, which confirmed the trends observed by the electrochemical ACM data in outdoor exposure. A direct comparison of weight loss and electrochemical data showed that the electrochemical data underestimate the true corrosion rates probably due to IR-drop effects and uncertainties in the conversion from polarization resistance data into corrosion rates. A cell factor can be calculated which could be used to convert electrochemical data obtained in outdoor or laboratory experiments into corrosion rates. Despite these shortcomings the electrochemical techniques are believed to be extremely valuable for detecting changes in corrosion behavior due to changes in environmental conditions and for monitoring purposes.

The importance of corrosion product chemistry and the usefulness of various compounds proposed as vapor phase inhibitor was also studied with electrochemical techniques. Chlorides present in rust were shown to greatly increase corrosion rates by increasing the time-of-wetness. $NaNO_2$ and

dichan were shown to be effective in the presence of chlorides, but less effective in the presence of sulfates.

In the final phase of this project surface analyses (SAM) of corrosion products formed under thin electrolyte layers in air or nitrogen with or without 1 ppm SO_2 were performed. For 4130 steel chromium sulfide inclusions were observed as initiation sites for corrosion in the absence of SO_2. If SO_2 was present corrosion was found to occur also on a second kind of sites which contained sulfates. Both steel and zinc surfaces were covered with sulfate when SO_2 was present in air or nitrogen. These results might explain the inhibiting effect of SO_2 observed for zinc covered with HCl or dist. H_2O in air + SO_2 compared to air exposure.

As part of this final report a compilation of important papers dealing with basic aspects of atmospheric corrosion has been prepared which contains abstracts of the papers if provided by the authors. This report has been issued separately.

It is hoped that the results of the research discussed in this final report and the publications published or to be published will stimulate further research in this area. The number of symposia on the topic of atmospheric corrosion is increasing, the principal investigator has arranged and chaired two recent symposia. A number of publications have appeared which make reference to the results of our investigations and use the electrochemical techniques developed. Gonzales (24), for example, has performed polarization resistance studies in laboratory and outdoor exposure

using ACMs as discussed in this report. Other authors have used the basic principles discussed in our earlier papers
Release of the unpublished results of this investigation should lead to further discussion and additional research.

ACKNOWLEDGEMENT

The support and encouragement received from the contract monitor Dr. Philip Clarkin and many helpful discussions are gratefully acknowledged. The principal investigator's co-workers J. V. Kenkel, S. Jeanjaquet, S. Tsai, C. Ogden, Dr. J. Lumsden and P. Stocker have contributed significantly to the success of this program.

References

1. H. H. Uhlig, "Corrosion and Corrosion Control", 2nd edit., Chapter 15, J. Wiley, 1971.

2. I. L. Rosenfeld, "Atmospheric Corrosion of Metals", NACE, Houston, Texas, 1972.

3. U. R. Evans, Corr. Sci. 12, 227 (1972).

4. K. Barton, "Schutz gegen atmosphärische Korrosion", Verlag Chemie, Weinheim/Bergstr., West Germany, 1973.

5. H. Kaesche, Werkstoff und Korrosion 5, 379 (1964).

6. F. Mansfeld and J. V. Kenkel, Corr. Sci. 16, 111 (1976).

7. P. Sereda, Ind. Eng. Chem. 52 (2), 157 (1960).

8. N. D. Tomashov, "Theory of Corrosion and Protection of Metals", The MacMillen Co., New York 1967, p. 375-378.

9. V. Kucera and E. Mattson, ASTM STP 435, 223 (1968).

10. F. Mansfeld and J. V. Kenkel, Corrosion 33, 13 (1977).

11. F. Mansfeld, "The Polarization Resistance Technique for Measuring Corrosion Currents", Adv. in Corros. Sci. and Technol., Vol. 6, 163 (1976).

12. F. Mansfeld, Corrosion 29, 397 (1973).

13. F. Mansfeld, "Bibliography fo Atmospheric Corrosion Literature" Task 6 of Final Report to ONR (SC5030.7FR), Contract No. N00014-75-C-0788.

14. S. G. Fishman and C. R. Crowe, Corr. Sci. 17, 27 (1977).

15. F. Mansfeld, "Corrosion Kinetics under Thin Electrolyte Layers", to be submitted to Corr. Sci.

16. A. M. Zinevich, E. I. Sergeeva, Yu N. Mikhailovskii and V. V. Serafimovich, Prot. Metals 6, 310 (1970).

17. A. Bukowiecki, Oberflaeche-Surface 13, 219 (1972).

18. R. St. J. Preston and S. Sanyal, J. Appl. Chem. 6, 26 (1956).

19. K. A. Chandler, Brit. Corros. J. 1, 264 (1966).

20. F. Mansfeld and S. Tsai, "Laboratory Studies of Atmospheric Corrosion of Steel and Zinc", to be presented at CORROSION/79, Atlanta, Ga. March 1979.

21. F. Mansfeld, "Atmospheric Corrosion Rates, Time-of-Wetness and Relative Humidity", Werkstoffe und Korrosion (in press).

22. V. Kucera and E. Mattson, Proc. 7th Scand. Corros. Congress, Trondheim, Norway, 1975, p. 202.

23. F. Mansfeld, "Results of Thirty Months Exposure Study in St. Louis, Mo", CORROSION/78, Houston, Texas, March 1978, Paper No. 88; Final Report to EPA (in press).

24. J. A. Gonzales, Werkstoffe und Korrosion 29, 556 (1978).

F. Documentation of Results

a. Publications

1. F. Mansfeld and J. V. Kenkel, "Electrochemical Monitoring of Atmospheric Corrosion Phenomena", Corros. Sci. 16, 111 (1976).
2. F. Mansfeld and J. V. Kenkel, "Electrochemical Measurements of Time-of-Wetness and Atmospheric Corrosion Rates", Corrosion 33, 13 (1977).
3. F. Mansfeld, "Atmospheric Corrosion Rates, Time-of-Wetness and Relative Humidity", Werkstoff und Korrosion (in press).
4. F. Mansfeld and S. Tsai, "Laboratory Studies of Atmospheric Corrosion of Steel and Zinc", to be presented at CORROSION/79, Atlanta, Ga. March 1979, submitted to Corrosion.
5. F. Mansfeld and S. Tsai, "Corrosion Rates from Weight Loss and Electrochemical Data Under Thin Electrolyte Layers", in preparation.
6. F. Mansfeld, "Corrosion Kinetics Under Thin Electrolyte Layers", to be submitted to Corros. Sci.
7. F. Mansfeld, "The Dependence of Time-of-Wetness and Atmospheric Corrosion Rates on Relative Humidity", in preparation.
8. F. Mansfeld, "Applications of the Atmospheric Corrosion Monitor", in preparation.

b. Presentations at Technical Meetings

1. F. Mansfeld and J. V. Kenkel, "Electrochemical Studies of Atmospheric Corrosion", CORROSION/75, April 1975, Toronto, Canda, paper No. 161.
2. F. Mansfeld and J. V. Kenkel, "Electrochemical Monitoring of Atmospheric Corrosion Phenomena", Gordon Research Conference on Corrosion, July 1976, New London, New Hampshire.
3. F. Mansfeld and J. V. Kenkel, "Electrochemical Monitoring of Atmospheric Corrosion Phenomena", 27th Meeting of Int. Soc. of Electrochemistry (ISE), Zurich, Switzerland, Sept. 6-11, 1976, paper No. 163.
4. F. Mansfeld and J. V. Kenkel, "Electrochemical Monitoring of Atmospheric Corrosion Phenomena", 150th Meeting of the Electrochemical Society, Las Vegas, Nevada, Oct. 17-22, 1976, paper No. 95.
5. F. Mansfeld and J. V. Kenkel, "Electrochemical Measurements of Time-of-Wetness and Atmospheric Corrosion Rates", CORROSION/77, San Francisco, Calif., March 14-18, 1977.
6. F. Mansfeld, "Electrochemical Monitoring of Time-of-Wetness Data", 154th Meeting of the Electrochemical Society, Pittsburgh, Pa. Oct. 15-20, 1978, paper No. 119.
7. F. Mansfeld, "Corrosion Kinetics Under Thin Films", 154th Meeting of the Electrochemical Society, Pittsburgh, Pa. Oct. 15-20, 1978, paper 121.
8. F. Mansfeld, "Atmospheric Weathering Tests", Gordon Research Conference on Corrosion, New London, N.H., July 10-14, 1978.

b. Presentations at Technical Meetings - continued

9. F. Mansfeld, "Evaluation of Electrochemical Techniques for Monitoring of Atmospheric Corrosion Phenomena", to be presented at ASTM Symposium on "Progress in Electrochemical Corrosion Testing", San Francisco, Cal., May 21-23, 1979, to be published in Proceedings.
10. J. B. Lumsden, P. J. Stocker and F. Mansfeld, "Corrosion Product Chemistry of Films Formed under Thin Electrolyte Layers", to be presented at CORROSION/79, Atlanta, Ga., March 12-16, 1979.